

**THE INTERACTION OF STRONG HYDROGEN-  
BONDING MOLECULES WITH  
THE SURFACE OF ICE  
NANOCRYSTALS**

**By**

**LANCE DEAN DELZEIT**

**Bachelor of Science**

**St. Mary of the Plains**

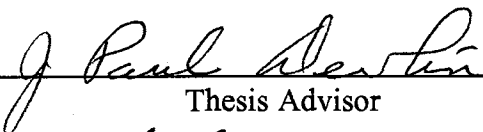
**Dodge City, Kansas**

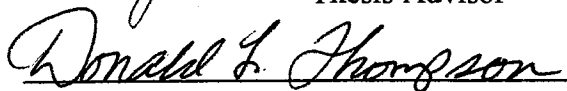
**1991**

**Submitted to the Faculty of the  
Graduate College of the  
Oklahoma State University  
in partial fulfillment of  
the requirements for  
the Degree of  
DOCTOR OF PHILOSOPHY  
May, 1997**


**THE INTERACTION OF STRONG HYDROGEN-  
BONDING MOLECULES WITH  
THE SURFACE OF ICE  
NANOCRYSTALS**

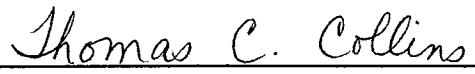
Thesis Approved:

  
\_\_\_\_\_  
Thesis Advisor

  
\_\_\_\_\_

  
\_\_\_\_\_

  
\_\_\_\_\_

  
\_\_\_\_\_  
Dean of the Graduate College

## PREFACE

This study was undertaken in order to increase the knowledge of the adsorbate-ice surface interaction. Specifically, the interaction of strong hydrogen-bonding adsorbates with the surface of microporous amorphous ice and crystalline nanoclusters was investigated. In this study, it was found that the strong hydrogen-bonding adsorbates needed to be divided into three classes defined by how they interact with and affect the surface: a) nonordering, b) ordering, and c) ordering and reactive. Further, this study allowed for the unambiguous identification of the symmetric stretch of the dangling-hydrogen molecule and led to the identification of the subsurface spectrum.

I would like to express my sincere appreciation to Dr. Devlin for his guidance, understanding, patience, and financial support. Next, I would like to thank Brad Rowland for his friendship and many hours of "discussions" which we engaged in, and also Mark Fisher for his invaluable assistance. Diane Arbuthnot and Shelly Long for their friendship. Finally my parents for always encouraging and supporting me.

## TABLE OF CONTENTS

### Chapter

I. LITERATURE REVIEW.....	1
Introduction .....	1
Description of the Ice Nanocluster Surface .....	3
Introduction .....	3
Experimental Evidence for the Structure of the Ice Nanocluster surface ..	3
Theoretical Description and Structure of the Cluster Surface .....	6
Ordering of the Ice Surface by an Amphiphilic Monolayer .....	19
H <sub>2</sub> O Complexes .....	25
HCl .....	25
Thin Films .....	25
Matrix Isolation .....	48
Theoretical .....	60
HCN .....	64
Matrix Isolation .....	64
Thin Film .....	71
H <sub>2</sub> S .....	74
SO <sub>3</sub> .....	74
Matrix Isolation .....	77
Theoretical .....	77
SO <sub>2</sub> .....	79
II. EXPERIMENTAL .....	84
Introduction .....	84
Equipment .....	84
Introduction .....	84
Vacuum System .....	85
Cryogenic System .....	85
Cryogenic Cells .....	86
FT-IR Instrument and Computer .....	88
Procedure .....	89
Thin Films .....	89
Clusters .....	89
Difference Spectra .....	90

III. ACID COATED THIN FILMS AND CLUSTERS .....	92
General .....	92
H <sub>3</sub> O <sup>+</sup> .....	93
Thin Films .....	94
Introduction .....	94
HCl .....	95
DCl .....	101
HBr .....	104
DBr .....	106
Clusters .....	106
Introduction .....	106
HCl .....	107
DCl .....	114
HBr .....	117
Conclusions .....	120
IV. STRONG HYDROGEN-BONDING ADSORBATES .....	123
General .....	123
Nonordering .....	125
Ordering .....	129
Introduction .....	129
H <sub>2</sub> S .....	131
Acetylene and SO <sub>2</sub> .....	134
Ordering and Reactive .....	137
Introduction .....	137
NH <sub>3</sub> .....	137
Tri-Methyl Amine (TMA) .....	141
SO <sub>3</sub> .....	141
HCl, DCl, and HBr .....	143
Conclusions .....	149
V. COMPARISON OF C <sub>2</sub> H <sub>6</sub> , C <sub>2</sub> H <sub>4</sub> , AND C <sub>2</sub> H <sub>2</sub> .....	151
VI. DISCUSSION AND CONCLUSIONS .....	154
Literature Review .....	154
Strong Hydrogen-Bonding Adsorbates .....	155
HCl Coated Clusters .....	158
Comparison of C <sub>2</sub> H <sub>6</sub> , C <sub>2</sub> H <sub>4</sub> , AND C <sub>2</sub> H <sub>2</sub> .....	159
REFERENCES .....	161
BIBLIOGRAPHY .....	167

APPENDIX A .....	172
The Subsurface .....	172

## LIST OF TABLES

### Table

1. Translational and rotational order parameters .....	11
2. Vibrational frequencies in oxonium salts .....	30
3. Frequencies of HCl, DCl, and HBr on Alkali Halide Surfaces .....	44
4. Absorption frequencies and optical densities of water and hydrochloric acid mixtures .....	50
5. HX absorption frequencies of H <sub>2</sub> O/HX mixtures .....	55
6. HX (DX) frequencies (cm <sup>-1</sup> ) of (HX) <sub>m</sub> (H <sub>2</sub> O) <sub>n</sub> aggregates .....	58
7. Summary of normal coordinate calculations .....	68
8. HCN dimer-monomer shifts .....	69
9. Monomer and open chain dimer bands of HCN and DCN .....	70

## LIST OF FIGURES

### Figure

1. Torchet's Radial Distribution Function of diffraction patterns.....	4
2. Hanson's Theoretical Surface .....	7
3. Drawing of the Surface Groups of Ice .....	10
4. Density Profile of Kroe's 190 K Ice Slab .....	12
5. Surface Layer of Kroe's 190 K Ice Slab .....	14
6. Surface Layer of Kroe's 230 K Ice Slab .....	15
7. Buch's Simulated Spectra of D <sub>2</sub> O .....	17
8. Surface Layer of Buch's Ice Slabs .....	18
9. Density Profile of Buch's S1 and S3 Ice Slabs .....	20
10. Graph of Freezing Points for Amphiphile Covered Water .....	21
11. Superimposed Lattices of Water and C <sub>31</sub> H <sub>63</sub> OH .....	23
12. IR Spectra of D <sub>2</sub> O Coated -CH <sub>3</sub> and -OH Terminated Substrates .....	26
13. IRAS Spectra of D <sub>2</sub> O Coated -CH <sub>3</sub> and -OH Terminated Substrates .....	27
14. Schematic Drawing of SAMs .....	28
15. Infrared Spectra of Oxonium Slats .....	29
16. Spectra of HCl Amorphous Hydrates .....	32
17. Spectra of HCl and HBr Crystalline Hydrates .....	33
18. Spectra of HCl Exposed Gas-Phase Clusters .....	34



19. TPD of HCl Exposed Water .....	35
20. Graph of $\alpha$ - and $\beta$ -HCl vs. Film Thickness .....	37
21. Comparison of TPD from Amorphous and Crystalline Ice Films .....	38
22. Comparison of TPD from Amorphous and Crystalline Ice Films as a Function of HCl Exposure .....	40
23. Graph of HCl Yield vs. HCl Exposure for Amorphous and Crystalline Ice Films .....	41
24. Spectra of HCl on NaCl .....	43
25. Spectra of HCl on NaCl with Preadsorbed Water .....	46
26. Spectra of HCl and HBr on LiF .....	47
27. Spectra of $\text{H}_2\text{O}:\text{HCl}:\text{N}_2$ and $\text{D}_2\text{O}:\text{DCl}:\text{N}_2$ .....	49
28. Structures for $\text{H}_2\text{O}:\text{HCl}$ Complex .....	51
29. Spectra of $\text{H}_2\text{O}:\text{HCl}:\text{Ar}$ .....	53
30. Structures for $\text{H}_2\text{O}(\text{HCl})_2$ .....	56
31. Structures for $(\text{H}_2\text{O})_m(\text{HCl})_n$ .....	59
32. Geometry of HCl with an ideal (0001) Ice Surface .....	61
33. Structures for $\text{H}_2\text{O}-\text{HCl}$ , $(\text{H}_2\text{O})_2\text{HCl}$ , and $(\text{H}_2\text{O})_3\text{HCl}$ .....	63
34. Inertial Axis System for $\text{H}_2\text{O}-\text{HCN}$ Dimer .....	65
35. CH-Stretching Region of HCN .....	66
36. Spectra of HCN on NaCl .....	72
37. Spectra of $\text{H}_2\text{S}$ on Alumina .....	75
38. Structure of $\text{H}_2\text{O}-\text{SO}_3$ .....	76
39. Potential Energy Profile for $\text{H}_2\text{O}-\text{SO}_3$ .....	78
40. Potential Energy Profile for $\text{H}_2\text{O}-\text{SO}_3$ and $(\text{H}_2\text{O})_2\text{SO}_3$ .....	80

41. Optimized Geometries for $\text{H}_2\text{O-SO}_3$ and $(\text{H}_2\text{O})_2\text{SO}_3$ .....	81
42. Structure for $\text{H}_2\text{O-SO}_2$ .....	83
43. Drawing of Mini Cluster Cell .....	87
44. Spectra of HCl Coated Thin Film as It is Warmed .....	97
45. Spectra of HCl Coated Thin Film as It is Held at 45 K .....	100
46. Comparison of HCl and DCl Coated Amorphous Ice .....	102
47. Spectra of DCl Coated Amorphous Ice .....	103
48. Spectra of HBr Coated Amorphous Ice .....	105
49. Difference Spectra of HCl Coated Clusters .....	108
50. Spectra of HCl as It Coats a Cluster Surface .....	109
51. Spectra of HCl Coated Clusters as the Sample is Warmed .....	111
52. Spectra of a $\text{HCl:CH}_4$ Coated Clusters .....	113
53. Spectra of HCl on Highly (140 K) Annealed Clusters .....	115
54. Spectra of DCl Coated Clusters as the Sample is Warmed .....	116
55. Spectra of $\text{DCl:N}_2$ Coated Clusters .....	118
56. Spectra of HBr Coated Clusters as the Sample is Warmed .....	119
57. Spectra of $\text{HBr:CH}_4$ Coated Clusters .....	121
58. Spectra of HCN Coated Clusters .....	126
59. Comparison of HCN Coated Clusters and Amorphous Ice .....	130
60. Spectra of $\text{H}_2\text{S}$ Coated Clusters .....	132
61. Comparison of $\text{H}_2\text{S}$ and HCN Coated Clusters .....	133
62. Comparison of $\text{H}_2\text{S}$ Coated Clusters and Crystalline Clusters .....	135
63. Comparison of $\text{H}_2\text{S}$ , $\text{SO}_2$ , and Acetylene Coated Clusters .....	136

64. Spectra of NH <sub>3</sub> on H <sub>2</sub> O Clusters .....	138
65. Spectra of NH <sub>3</sub> on D <sub>2</sub> O Clusters .....	140
66. Spectra of TMA Coated Clusters .....	142
67. Spectrum of Cluster Surface Converted to Dihydrate .....	144
68. Spectra of HCl Coated Clusters as the Sample is Warmed .....	145
69. Spectra of HCl:N <sub>2</sub> Coated Clusters as the Sample is Warmed .....	147
70. Spectra of the OH-Stretching Region for HCl and HBr Coated Clusters .....	148
71. Comparison of C <sub>2</sub> H <sub>6</sub> , C <sub>2</sub> H <sub>4</sub> , and C <sub>2</sub> H <sub>2</sub> Coated Clusters .....	152
72. Subsurface Spectrum Obtained from HCN Coated Clusters .....	172
73. Subsurface Spectrum Obtained from Bare Annealed Clusters .....	176
74. Comparison of Surface, Subsurface, and Interior Spectra .....	177

## NOMENCLATURE

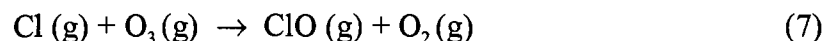
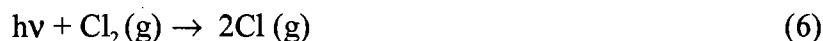
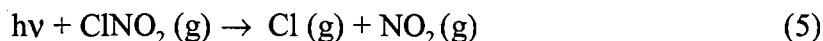
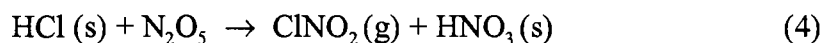
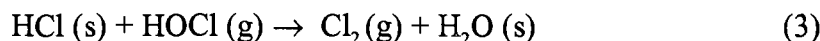
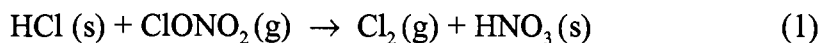
IR	infrared
TMA	Trimethylamine
$I_h$	hexagonal ice
d-H	dangling-hydrogen
d-O	dangling-oxygen
S-4	surface four coordinated
$S_R$	rotational order parameter
$S_T$	translational order parameter
Pa·s	the product of pressure times time
$\alpha$ -HCl	the HCl which precedes H <sub>2</sub> O desorption in Robert's TPD experiments, presumable physisorbed to the surface
$\beta$ -HCl	the HCl which desorbes with the H <sub>2</sub> O in Robert's TPD experiments, presumable from the HCl hexahydrate
TPD	temperture programmed desorption
FWHH	full width at half height
TS	transition state
sym d-H	the symmetric stretch of the d-H molecule, or altenatively the OH-stretch of the bonded hydrogen of the d-H molecule

## CHAPTER I

### LITERATURE REVIEW

#### Introduction

This study of the interactions of strong hydrogen-bonding molecules with the surface of ice nanocrystals was the result of an inquiry into a more practical question, how does HCl interact with the surface of atmospheric ice clusters. The significance of this question stems from the fact that HCl is one of the components which is believed to lead to the depletion of ozone. A few of the reactions that produce chemically active forms of chlorine that catalyze the depletion of ozone are:<sup>1-5</sup>



It is further believed that it is the heterogeneous reaction on the surface of polar atmospheric cloud particles which plays a crucial role in the polar ozone depletion.<sup>2-6</sup>

These reactions are very slow in the gas phase, but are catalyzed by the ice surface.<sup>4-6</sup>

Further, it has been proposed that if these reactions are taking place on the surface of polar stratospheric ice particles, they must also involve an ionic mechanism due to the ionization of the HCl.<sup>7</sup>

For these reasons, an investigation into the adsorption of HCl onto an ice surface at cryogenic temperatures was undertaken. The experiments were monitored by using infrared spectroscopy, and not only the infrared adsorption bands of the adsorbate but also those of the ice surface were followed.

The IR spectrum of the modes associated with the adsorbed HCl could be followed. However, the behavior of the OH-stretch of the surface water molecules is too complicated to be interpreted. The reason for this difficulty is the reactivity of the HCl with the ice surface and a general lack of understanding of any adsorbate interactions with an ice surface beyond simply weak hydrogen-bonding. This meant that less reactive strong hydrogen-bonding adsorbates needed to be studied in order to understand the changes in the ice OH-stretching modes associated with the adsorption of a strong hydrogen-bonding adsorbate and specifically the adsorption of HCl. The alternative adsorbates which have been used were H<sub>2</sub>S, HCN, SO<sub>2</sub>, SO<sub>3</sub>, NH<sub>3</sub>, trimethylamine (TMA), acetylene, ethylene, and ethane. Of these, H<sub>2</sub>S and HCN provided the most information about the behavior of the OH-stretch of the ice surface. The results for acetylene and SO<sub>2</sub> experiments gave good support to the ideas developed from the H<sub>2</sub>S and HCN experiments. The adsorption of NH<sub>3</sub> and TMA were very interesting cases in that they both are reactive with the surface of the ice, although less reactive than HCl, but the study of them did add support to the picture that was developed in the study of H<sub>2</sub>S

and HCN. Ethane and ethylene were used along with acetylene in studies of the effects of adding electron donating and electron accepting groups to an adsorbate.

## **Description of the Ice Nanocluster Surface**

### **Introduction**

The initial experiments were carried out on thin film amorphous ice. However, this surface quickly proved to have many drawbacks. For this reason, and due to the development of a "mini" cluster cell, the ice surface was changed to that of an ice cluster deposit. Additionally, several reports pertaining to the experimental and theoretical description of cluster surfaces are also available.

### **Experimental Evidence for the Structure of the Ice Nanocluster Surface**

Torchet *et al.*<sup>8</sup> investigated the electron diffraction of clusters produced in a free jet expansion of water vapor over a range of inlet jet vapor pressures ranging from 1 to 5 bar. They observed the densitograms, radial intensity distributions, at pressures of 600 torr and 1, 2, 3, 4, and 5 bar (see Fig. 1). They then compared these to the calculated patterns for H<sub>2</sub>O monomer, cubic ice, and a molecular dynamics calculation for a set of 20 H<sub>2</sub>O molecules. Comparison of the densitogram for 600 torr expansion to the calculated pattern of the H<sub>2</sub>O monomer showed that the beam was composed mainly of free molecules. At an inlet jet pressure of 1 bar, oscillations appeared in the radial intensity distributions which indicated the presence of clusters in the beam. When the

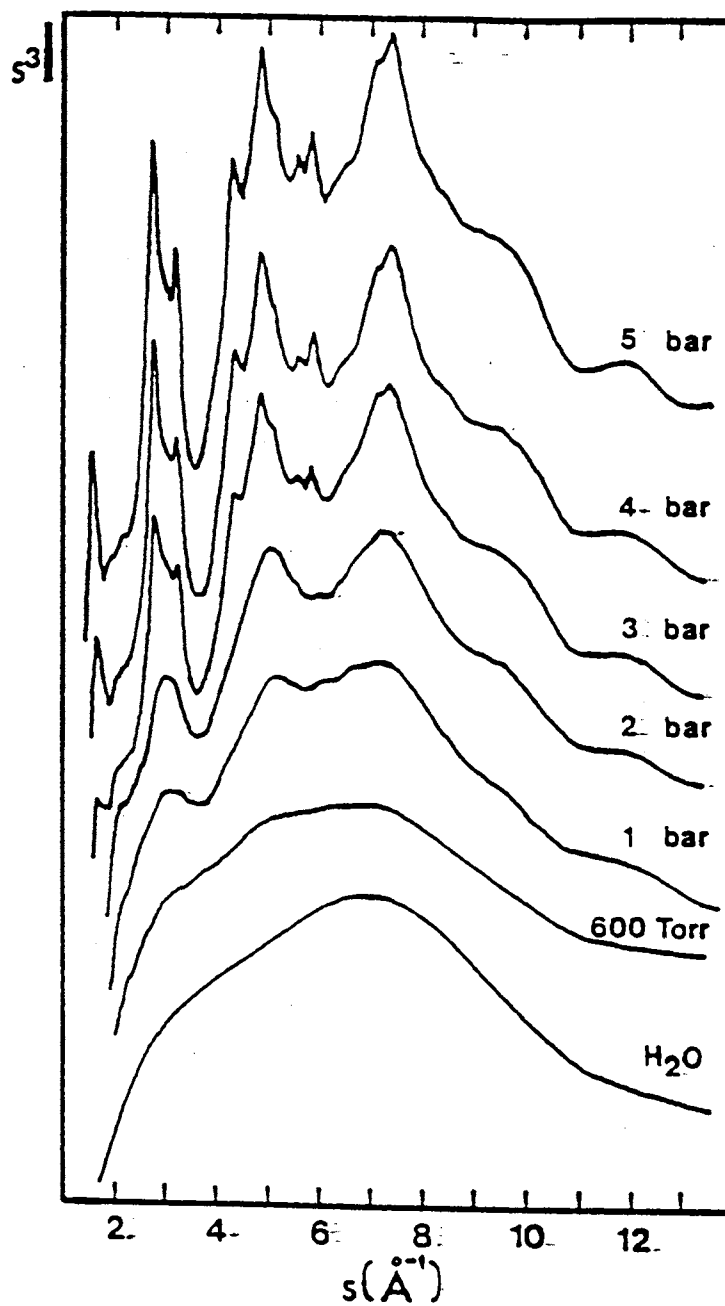


Fig. 1 Radial distribution function of diffraction patterns recorded with several inlet pressures. Lower Curve: Calculated diffraction function of  $\text{H}_2\text{O}$  monomer. Taken from Ref. 8



pressure was increased to 2 bar, the interference pattern was amplified indicating that the mean cluster size in the beam had increased. At an inlet jet pressure of 3 bar, lines emerged from the densitogram which indicated the start of a crystalline phase. When the inlet pressure was increased above 3 bar, the crystalline lines became better resolved and narrower, but the lines still emerged from an oscillating background. From this, they concluded that the smaller clusters have a noncrystalline structure. As the clusters become larger, they begin to develop a crystalline phase, presumably at the center of the clusters with a noncrystalline phase at the surface.

Torchet *et al.*<sup>8</sup> calculated the average number of water molecules per cluster to be 5000, 2200, 900, 230, and 20 for inlet pressures of 5, 4, 3, 2, and 1 bar, respectively. They also gave a mean diameter for their 5-bar clusters of about 45 Å. If you assume a spherical shape, this gives a volume per molecule of approximately 3 Å<sup>3</sup>. From this, the mean radii of the clusters formed at 2 and 3 bar can be calculated, the results are 8.0 and 12.7 Å, respectively. This suggests that the thickness of the noncrystalline phase at the surface of the clusters is between 8.0 and 12.7 Å.

Huang and Bartell<sup>9</sup> also reported electron diffraction patterns for ice clusters generated in a jet expansion which included a disordered component, possibly originating from a disordered surface layer.

In two investigations,<sup>10</sup> both of which directly examined the surface of ice, it was found that the surface of ice terminated in a strongly vibrating and disordered layer. The first of these two investigations used glancing-angle X-ray scattering in order to investigate the premelting of ice surfaces.<sup>10a</sup> This study found that a disordered layer formed on the surface of ice at ~260 K. This disordered layer then grew in thickness as

the temperature was increased and the bulk melting of the ice occurred. At 250 K, the thickness of this layer was found to be  $0 \pm 5$  Å. Thus, they could not detect a disordered layer on the ice surface at 250 K, however, a single bilayer could have been present within the error of their measurement. This will be shown in the following section.

Materer *et al.*<sup>10b</sup> studied the surface of a thin film of  $I_h$  (0001) using low-energy electron diffraction at 90 K. They then compared these results to the results of Hartree-Fock calculations and molecular dynamics simulations. From this, they concluded that the ice (0001) surface terminated with strongly vibrating or otherwise disordered molecules in the top half of a full-bilayer (see Fig. 2).

### **Theoretical Description and Structure of Cluster Surfaces**

Several theoretical calculations<sup>11-17</sup> have been performed in an attempt to better understand the surface of ice clusters. Zhang and Buch<sup>11</sup> performed classical trajectory simulations of 100-300 water molecules in order to understand the condensation dynamics and structure at low temperature, <100 K, amorphous ice. A water molecule is capable of forming four hydrogen bonds (two via the oxygen and two via the two hydrogens) with four other  $H_2O$  molecules in a tetrahedral arrangement. However, a new water molecule landing on the surface typically formed only two bonds, with significantly smaller probabilities for one, three, or four bonds. Quite strikingly, however, whenever two bonds were formed, they were almost always asymmetric, i.e., one bond is via the O atom of the new molecule, and the other is via one of its H atoms.

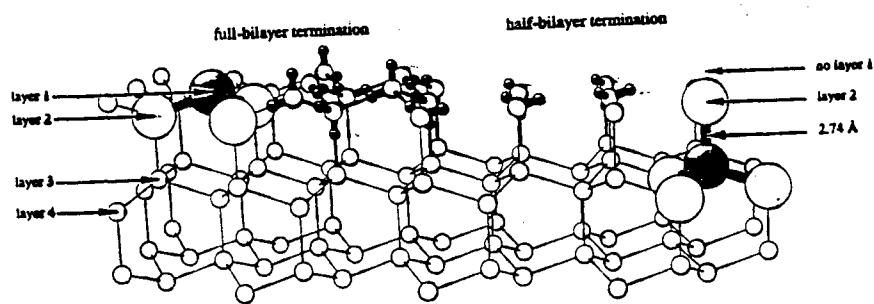


Fig. 2 Perspective grazing view of the Ice  $I_h$  (0001) surface, showing two ideal terminations on top: Full-bilayer termination at left (layers 1 and 2) and half-bilayer termination at right (layer 2 only). Middle-sized atoms are oxygens, with some hydrogens included as small atoms with assumed "bulk like" positions and randomness to for  $H_2O$  molecules (covalent bonds are drawn medium thick and hydrogen-bonds medium thin). Large spheres represent complete  $H_2O$  molecules, emphasizing their tetrahedral "bulk like" bonding arrangement. Layers 3 and 4 (and each subsequent 2 layers) also make up a bilayer. Taken from Ref. 10b

Upon addition of a new molecule, there were two distinct populations of trajectories. A "simple" trajectory in which a new molecule was attached to the surface without disrupting any of the preexisting hydrogen bonds, and a "complex" trajectory in which additional changes (bond breaking or formation) took place within the hydrogen network, in addition to the attachment of the new molecule. The complex trajectories accounted for 60-70% of the overall number of trajectories, changed up to 10 hydrogen bonds, and influenced an area as large as 20 Å across.

These two types of trajectories could also be separated using the final potential energy of the newly attached molecule. The molecules of "simple" trajectories had a mean potential energy of -9.5 kcal/mol with a range from -7 to -13 kcal/mol. The "complex" trajectories gave a mean value of -14.8 kcal/mol with a range from -9 to -21 kcal/mol. Since there was a significant overlap of the two distributions in the -11 to -13 kcal/mol range, the dynamics must play an important role in determining the "complexity" of a trajectory in this range.

Finally, the average coordination (average number of bonds per water molecule) depended upon how long the molecule had been on the surface. The ten last molecules attached to the surface had an average coordination of 2.4 hydrogen bonds. The molecules attached 10-40 collisions ago had an average of ~2.9 hydrogen bonds. Finally, the "older" molecules had an average of ~3.7 hydrogen bonds per molecule.

Later, Buch<sup>12</sup> studied the formation of a larger cluster containing 450 water molecules in a molecular dynamics simulation and obtained very similar results. Looking at the coordination of each water molecule as its trajectory was run, 64% of the impinging molecules were initially hooked to the surface via a single bond, via a H or an

O atom, and 30% were hooked via two bonds in an asymmetric geometry as described earlier. Over the course of the trajectories, a large majority of the newly bonded 1-coordinated molecules acquired additional hydrogen bonds. Thus, looking at the coordination at the end of each of the trajectories, 63% of the new molecules were 2-coordinated in an asymmetric fashion, and 27% were 3-coordinated to the surface. If the 3-coordinated molecule was missing the bond to one of its hydrogens, it is termed a dangling-hydrogen (d-H) molecule. If the missing hydrogen-bond was to the oxygen, it is termed a dangling-oxygen (d-O) molecule (see Fig. 3). Also seen in Fig. 3 is the surface 4-coordinated molecules (S-4). These molecules, which are fully 4-coordinated but are found at the surface, are accessible to adsorbate molecules, and can be identified spectroscopically as being different from the ordered interior of the cluster.

In the final  $(\text{H}_2\text{O})_{450}$  cluster, it was seen that the 20 molecules which arrived last had an average of 2.45 hydrogen bonds per molecule, and that the average coordination increased gradually towards 4 as the "age" of the molecules in the cluster increased. Also, there was a clear preference (2:1) for the formation of d-O as opposed to d-H molecules.

Kroes<sup>13</sup> investigated a (0001) ice slab composed of 480 water molecules in six bilayers (see Fig 2 for a description of a bilayer). The simulated surface was then heated to 190, 210, 230, and 250 K. It was found that at 190 and 210 K, the surface remained solid-like. This can be seen in Table 1 where the translational order parameter  $S_T$  and the rotational order parameter  $S_R$  ( $S_T$  and  $S_R$  equal 1 for a perfectly ordered solid and  $S_T=1/30$  and  $S_R=0$  for a liquid, respectively) remain large. The vertical disorder for the 190 K surface is shown in Fig. 4. It could be seen that the first bilayer was still distinct,

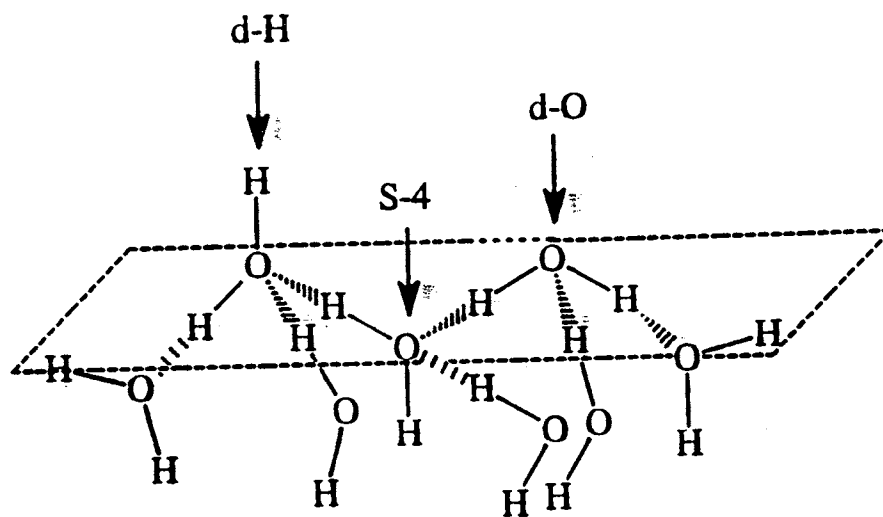


Fig. 3 Drawing showing the three surface groups on the surface of ice. They are: dangling-hydrogen (d-H), dangling-oxygen (d-O), and surface four coordinated (S-4) molecules.

Table 1

The translational and rotational order parameters for the six upper layers of the surface.  
Modified from Ref. 13

Translational order parameters  $S_T$

Layer	$T$ (K)			
	190	210	230	250
1	0.45	0.09	0.03	0.04
2	0.58	0.25	0.03	0.03
3	0.88	0.86	0.65	0.04
4	0.88	0.86	0.65	0.03
5	0.90	0.88	0.85	0.80
6	0.89	0.88	0.85	0.81

Rotational order parameters  $S_R$

Layer	$T$ (K)			
	190	210	230	250
1	0.28	0.22	0.02	0.07
2	0.55	0.30	0.06	0.01
3	0.73	0.69	0.53	0.03
4	0.78	0.75	0.61	-0.04
5	0.79	0.76	0.72	0.61
6	0.80	0.77	0.73	0.68

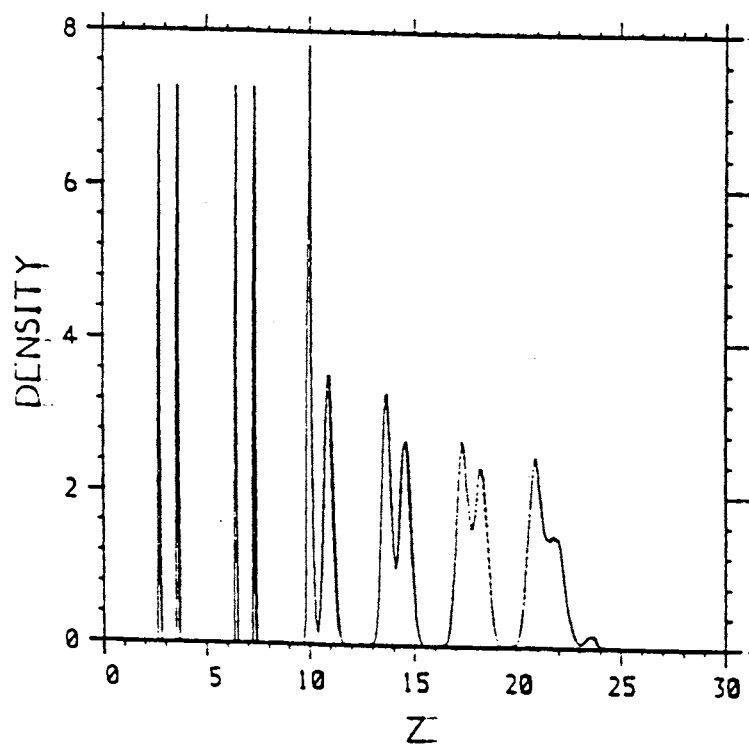


Fig. 4 Density profile along the direction perpendicular to the surface at  $T = 190$  K. The density is in a.u. and has been divided by a factor of 2.5 in the fixed layers. The  $z$  coordinate is in  $\text{\AA}$ . Taken from Ref. 13



although much more scrambling of the molecules of this bilayer had occurred than for the subsequent bilayers. The top bilayer for the 190 K surface can be seen in Fig. 5. The 230 K surface, as seen in Fig. 6 and in Table 1, had a higher degree of disorder than the 190 K surface. Finally, the 250 K surface showed complete melting of the top two bilayers.

Buch<sup>14-17</sup> also studied a 6 bilayer thick slab of water. However, where Kroes<sup>13</sup> was interested in the surface melting of the slab, Buch was more interested in finding a surface which mimicked the surface properties of a crystalline ice surface at lower temperatures. She followed a procedure similar to Kroes except that she recooled her surface after annealing it at a higher temperature. This way, she could allow the surface to relax and induce the disorder into the surface as Kroes had found, while still having a surface which was a solid rather than to a liquid.

In a molecular dynamics simulation, where the surface was relaxed at 197 K,<sup>15</sup> she found that the relaxation proceeded towards elimination of some of the 3-coordinated molecules and an increase in the number of 4-coordinated molecules. The number of four-coordinated molecules increased from 80 in the unrelaxed surface to 102 in the relaxed surface. The number of three-coordinated molecules with d-O was reduced from 40 to 30 and the number of three-coordinated molecules with a d-H was reduced from 40 to 26. Thus, the total number of three-coordinated molecules decreased from 80 to 56. With this increase in coordination, there was a loss of hexagonal order, and a significant distortion of the oxygen's perfect tetrahedral network of the unrelaxed surface. However, despite the relaxation, considerable order was retained in the direction perpendicular to the surface.

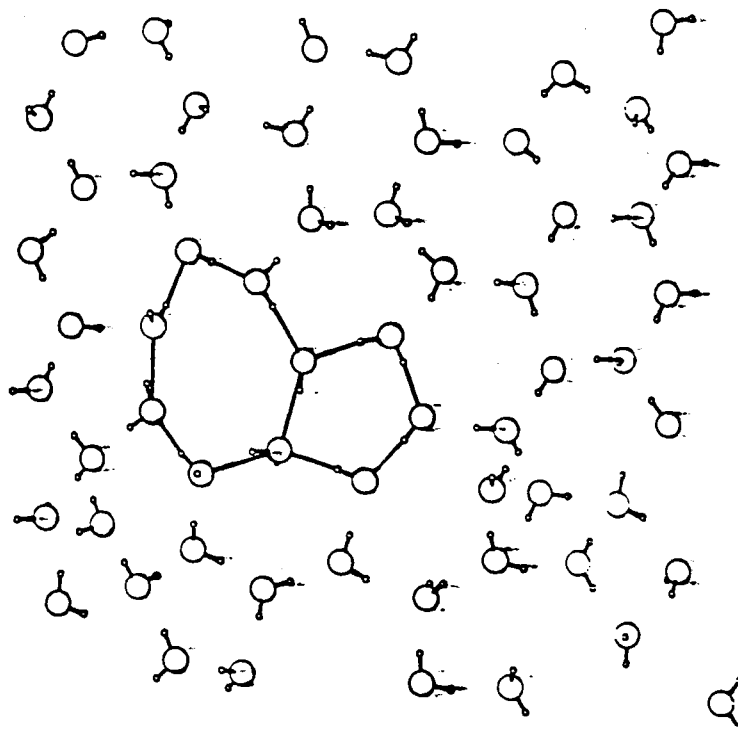


Fig. 5 Top view of a (0001) ice surface at  $T = 190$  K. Though hexagonal order is still present, pentagons and heptagons (one of each drawn in) have started to appear. Taken from Ref. 13

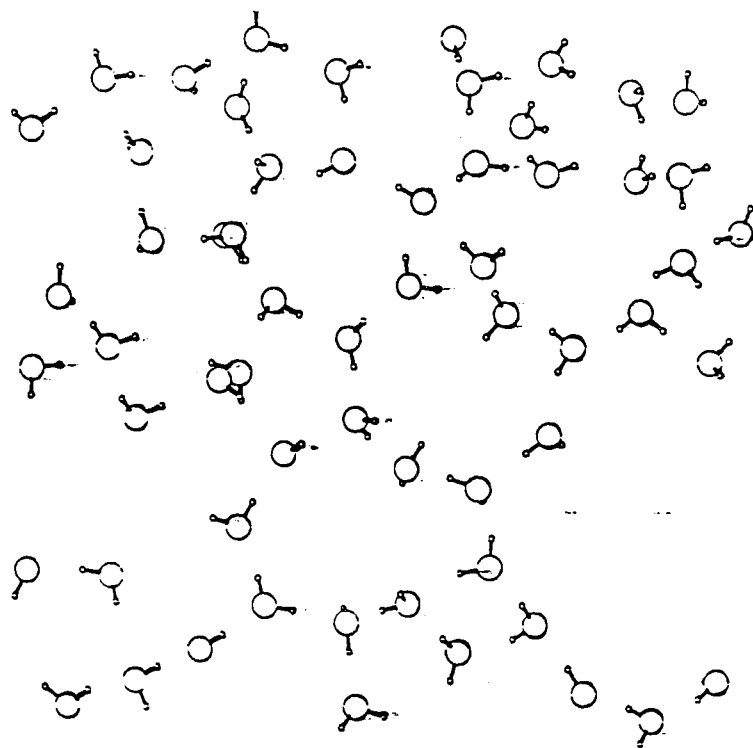


Fig. 6 Top view of a (0001) ice surface at  $T = 230$  K. Taken from Ref. 13

Buch<sup>15</sup> also calculated the spectrum of the top three bilayers of her simulated slab and the contributions of special categories of molecules of these top three bilayers (see Fig. 7). All of the intensity above 2500 cm<sup>-1</sup> is seen to be due to molecules found on the surface, while the majority of the intensity below 2500 cm<sup>-1</sup> is due to four-coordinated molecules found in the second and third bilayer. The contribution due to the d-O and d-H molecules can also be seen. Only the frame with the contribution due to the d-H molecule clearly shows the presence of two separate band complexes, one due to the symmetric and the other due to the antisymmetric stretch of the d-H molecules.

The extent of delocalization of vibrational excitations on and near the surface was also examined. Extensive delocalization was observed for the excited states of the molecules which had vibrational excitation near the maxima of the calculated band. This delocalization spread over several tens up to several hundreds of bonds. The excitation of the surface molecules was much more localized. The number of bonds contributing significantly to any given state was less than 22, and typically less than 10. The excitation corresponding to the nonbonded hydrogen of the d-H molecule was localized on the OH bond of the nonbonded hydrogen.

Buch<sup>16-17</sup> then simulated a number of surfaces relaxed at progressively higher temperatures. In order to evaluate the validity of each of these surfaces, she simulated the adsorption of CF<sub>4</sub> at a variety of different pressures which she then compared the results to experimental data.<sup>16</sup> In this way, she was able to determine the surface that most closely represented the surface of an ice cluster. She found that the surface which most closely mimicked the experimental surfaces was one which was heated to 250 K and allowed to relax at this temperature before being recooled (see Fig. 8). The cr(111)

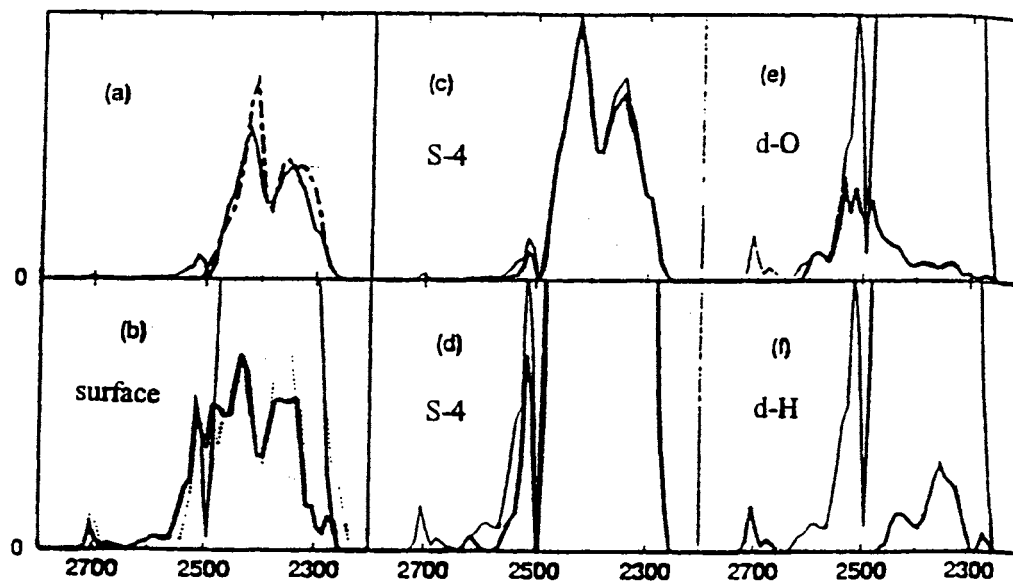
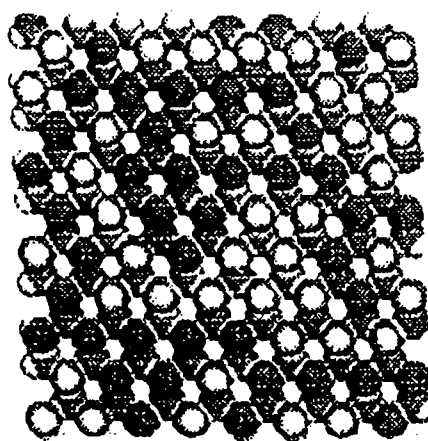
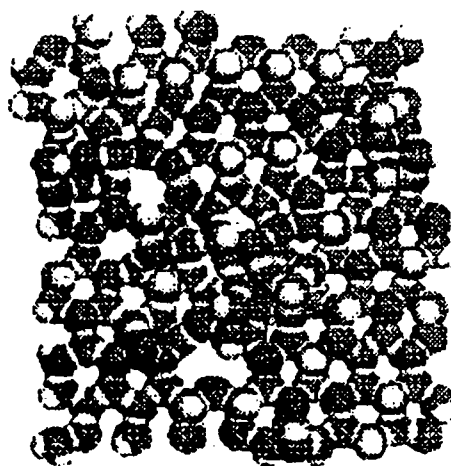


Fig. 7 Calculated OD-stretch spectrum of 100%  $D_2O$  at 27 K. The spectrum of the top three bilayers of the relaxed surface is denoted by a thick solid line in (a), and a thin solid line in (b) - (f). The thick line in (b) - (f) denotes contributions of special categories of molecules to the spectrum of the top three bilayers, as explained below: (a) dot-dashed: the bulk spectrum of the three top layers of the unrelaxed surface; (b) contribution of the topmost bilayer to the spectrum of the relaxed (thick line) and unrelaxed (dotted line) surfaces; (c) - (f) contributions of molecules of different hydrogen-bond coordinations to the spectrum of the relaxed surface, in (d) - (f) the y-scale was expanded; (c), (d) contribution of four-coordinated molecules in the top three bilayers, (e) three-coordinated molecules with a dangling-O atom, (f) three-coordinated molecules with a dangling-D. Taken From Ref. 16

C(111)



S1



S3



Fig. 8 Topmost bilayer (160 molecules) of a model crystalline cubic ice surface (111) and of the S1 and S3 disordered surface models at 83 K. The S1 model was the surface of minimum energy, while the S3 model yielded the best agreement with experimental data. Taken from Ref. 16

surface was an ordered cubic surface, the S1 surface was found to be the surface with the minimum energy, and the S3 surface, although higher in energy than either the cr(111) or the S1 surface, was found to give the closest match to the experimental data. This is believed to be an appropriate surface because, even though the energy of this surface is higher than the S1 surface, its free energy is believed to be lower due to the entropy. This disorder, which is the greatest at the surface, also extends into the subsurface layers of the slab as seen in Fig. 9.<sup>17</sup>

### **Ordering of the Ice Surface by an Amphiphilic Monolayer**

It has been long known that a monolayer of an amphiphilic alcohol ( $C_nH_{2n+1}OH$ ) on the surface of liquid water would form a 2-dimensional crystal.<sup>18-23</sup> The question is, how does this overlayer affect the ordering of the ice surface after the water has crystallized.

Gavish *et al.*<sup>18</sup> found that a monolayer of aliphatic chain alcohols on the surface of a drop of water would nucleate ice at a higher temperature than in the absence of the alcohol. The freezing point of a drop of pure water ranges from -20 to -25 °C. In the presence of an aliphatic alcohol, this freezing point increases asymptotically to a value approaching 0°C for alcohols with odd numbers of carbons, and to a plateau temperature of -8°C for even numbered carbon chains as the length of the carbon chain increased (see Fig 10). This increase in the freezing point was attributed to a suitable matching between the *ab* lattice parameters for hexagonal ice and the *ab* lattices of the alcohols. The lattice parameters for hexagonal ice are  $a = b = 4.5\text{\AA}$  and  $\gamma = 120^\circ$  at -50°C.

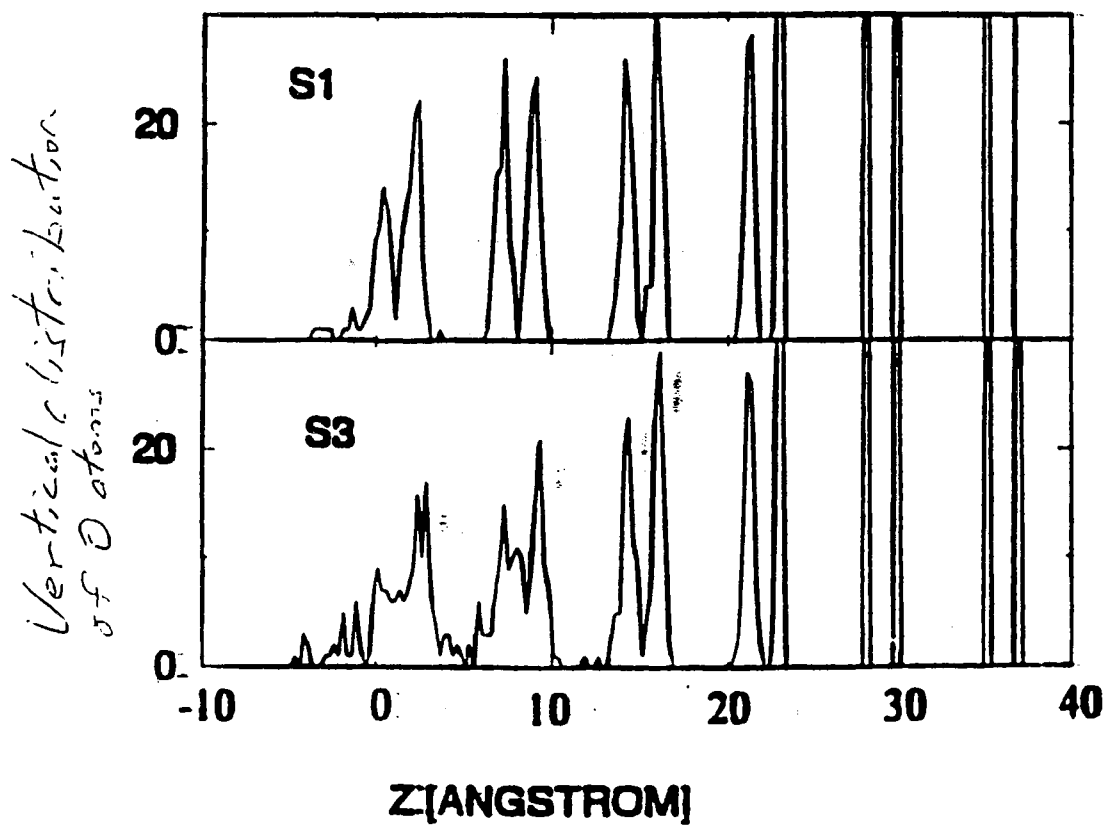


Fig. 9 Simulated vertical distribution of O atoms in models S1 and S3 at 83 K (in the simulation, the bottom two bilayers of a six-bilayer slab were frozen at crystalline positions). Taken from Ref. 17



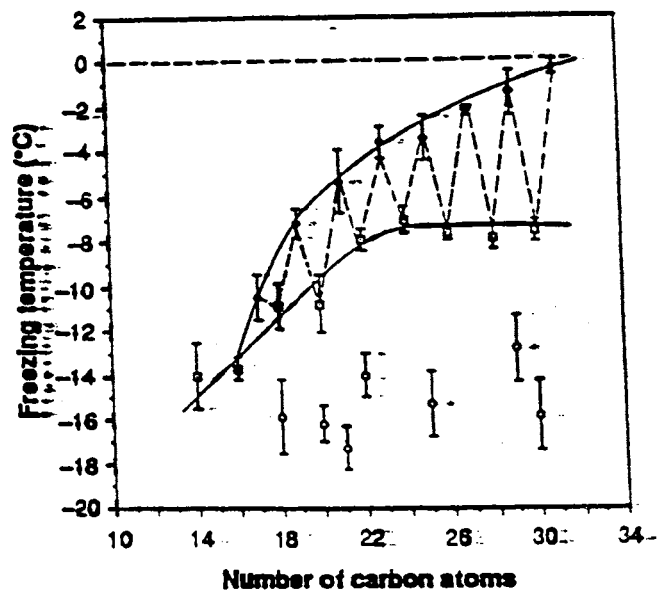


Fig. 10 Freezing points of drops of supercooled water covered by monolayers of alcohols  $C_nH_{2n+1}OH$  ( $n$  even,  $\square$ , and  $n$  odd,  $\bullet$ ) and carboxylic acids  $C_nH_{2n+1}CO_2H$  ( $\circ$ ). Freezing point curves are drawn separately for alcohols with  $n$  even and  $n$  odd. Taken from Ref. 18

The lattice parameters for the longer aliphatic alcohols are  $a = b$  being 4.54 Å for  $n = 23$  ( $n$  is the number of carbon atoms in the alcohol) to 4.52 Å for  $n = 31$  with  $\gamma \approx 113^\circ$ . Thus, as the length of the carbon chain increases, the area per molecule,  $ab \sin \gamma$ , of the aliphatic alcohols approaches that of hexagonal ice. The area per molecule for the aliphatic alcohols with  $n = 23, 30,$  and  $31$  and hexagonal ice are 19.0, 18.7, 18.8, and 17.5 Å<sup>2</sup>, respectively. Just to compare to some very similar systems, long-chain carboxylic acids have an area per molecule of  $\sim 20.7$  Å<sup>2</sup> and cause the substrate water to freeze at  $\sim -15^\circ\text{C}$  (see Fig. 10), and by inserting an amide group into an  $n = 22$  alcohol,  $\text{C}_{11}\text{H}_{23}\text{CONHC}_{11}\text{H}_{22}\text{OH}$ , increases the area per molecule from 20 Å<sup>2</sup> to 24 Å<sup>2</sup> and induces freezing in the substrate water at  $-12^\circ\text{C}$  rather than  $-8^\circ\text{C}$ . The significance of these findings is that alcohols may act not only as antifreeze agents when present in solution, but, when constrained to the water surface, form self-assembled clusters that are highly efficient ice nucleators by virtue of a structural fit with that of ice (see Fig. 11).

Electron diffraction studies of monolayers of amphiphilic molecules on vitreous and hexagonal ice have also been performed. In these studies, the alcohol was found to maintain a 2-dimensional crystalline structure after nucleating hexagonal ice at the monolayer-water interface. In fact, according to electron diffraction data, the underlying ice surface is ordered.<sup>19</sup> Also, grazing incidence X-ray diffraction showed that the ice directly under the monolayer is composed of ice crystals oriented with a (0,0,1) face normal to the amphiphilic monolayer at temperatures just below 0 °C.<sup>20</sup> This is significant since, in light of the previous section, the surface of ice is normally considered to be disordered at these temperatures. This would imply that adsorbing the

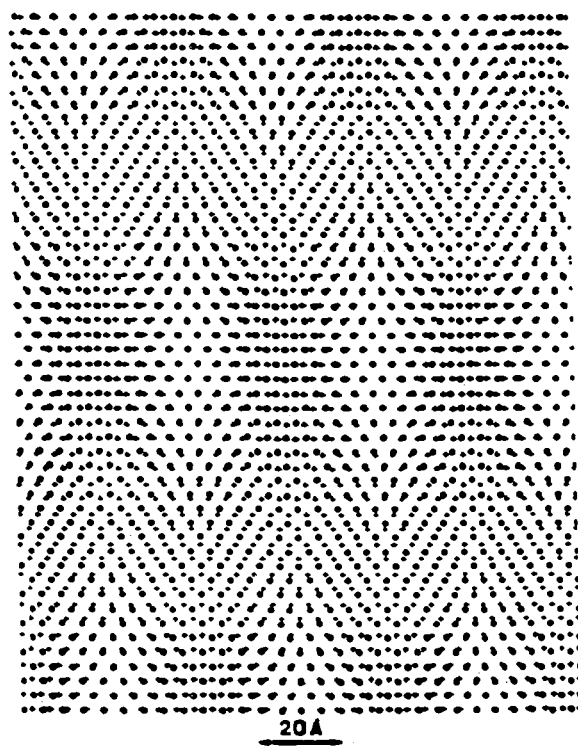


Fig. 11 Superimposed lattices of the oxygen positions within the *ab* layer of hexagonal ice (labeled as "+") and the oxygen positions in a monolayer of  $C_{31}H_{63}OH$  (labeled as "●"). Note the 25 - 30 Å extent of a match between the two lattices. Taken from Ref. 18

right adsorbates onto the surface of ice might induce order into the otherwise disordered ice surface.

Bell and Rice<sup>21</sup> performed a molecular dynamics study of the ordering of a long chain aliphatic acid,  $n = 16$ , on an ordered, rigid ice surface. They found that there is an epitaxial relationship between the overlayer and the ordered ice surface. Although they acknowledged the deficiency in their model with respect to the disordering of the ice surface, their results are still important. Since self assembled carboxylic acids and alcohols have been shown to self assemble into 2-D crystals and that the underlying ice surface beneath one of these monolayers is ordered, their model helps to substantiate that induced order exists at the monolayer-water interface.

Engquist *et al.*<sup>22</sup> studied D<sub>2</sub>O ice on self-assembled alkanethiolate monolayers. They found that amorphous-like ice was formed at sufficiently low temperatures (<100 K) on all mixed self-assembled monolayers [HS(CH<sub>2</sub>)<sub>16</sub>OH and HS(CH<sub>2</sub>)<sub>16</sub>CH<sub>3</sub> mixed monolayers], regardless of the wettability of the monolayer. A structural transition of the D<sub>2</sub>O ice from amorphous-like to polycrystalline-like was observed above 100 K. The exact onset of the transition was strongly dependent on the wettability and varied from 110 K on the extremely hydrophobic (CH<sub>3</sub> terminated) substrate to ~150 K on the hydrophilic (OH terminated) substrate. Although this may at first seem counter intuitive to the epitaxial ordering induced by the monolayer, it actually is not. The epitaxial ordering was seen at much higher temperatures where the ice surface has the mobility to rearrange. Here, the temperature and hence surface mobility is much lower, so surface ordering would not necessarily be expected to be seen. However, what would be expected is the difference in the strength of the interaction between the ice surface and

the monolayer. This interaction with the hydrophilic surface would be expected to be much stronger than the interaction with the hydrophobic surface, and was reflected in the temperature at which the ice layer becomes sufficiently mobile to crystallize (see Fig. 12 and 13). Finally, the shape of the water overlayer was strongly dependent on the wettability of the monolayer. The water formed a 2-dimensional cluster that spread out to cover the entire top of the hydrophilic monolayer, as opposed to the 3-dimensional clustering of the water on the hydrophobic monolayer as is illustrated in Fig. 14.

## H<sub>2</sub>O Complexes

### HCl

#### Thin Films

Ferriso and Hornig<sup>24</sup> investigated the amorphous monohydrate of HCl, DCl, HBr, HF, and HI in order to observe the infrared spectrum of the hydronium ion (H<sub>3</sub>O<sup>+</sup>).<sup>24b</sup> The monohydrate of the hydrogen halides was chosen since the hydronium ion of the monohydrate is the only species in these systems which produces an infrared absorption. They observed four infrared-active fundamentals associated with the hydronium ion (see Fig. 15 and Table 2). These were interpreted in terms of a pyramidal structure for the hydronium ion, consisting of two bending modes and two stretching modes. The lowest frequency peak near 1100 cm<sup>-1</sup> was assigned to the symmetric bend,  $\nu_2$ , of the hydronium ion. The 1700 cm<sup>-1</sup> peak was assigned to the doubly degenerate bend,  $\nu_4$ . The symmetric stretch,  $\nu_1$ , and the doubly degenerate stretch,  $\nu_3$ , in the OH-stretching region are both

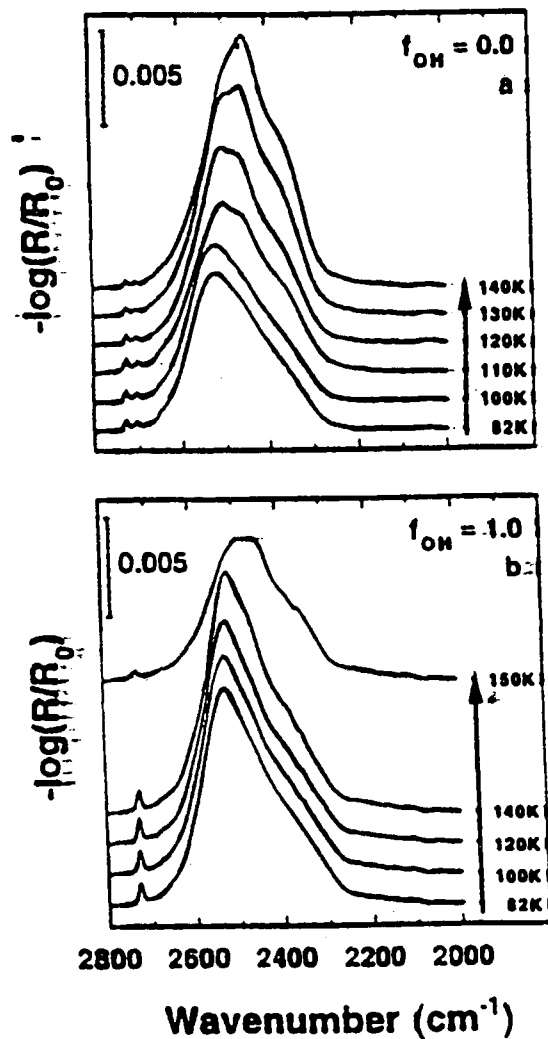


Fig. 12 Infrared spectra of amorphous solid  $\text{D}_2\text{O}$  (7 langmuirs) deposited on  $-\text{CH}_3$  and  $-\text{OH}$  terminated substrates at 82 K and thereafter annealed at successively higher temperatures. Taken from Ref. 22

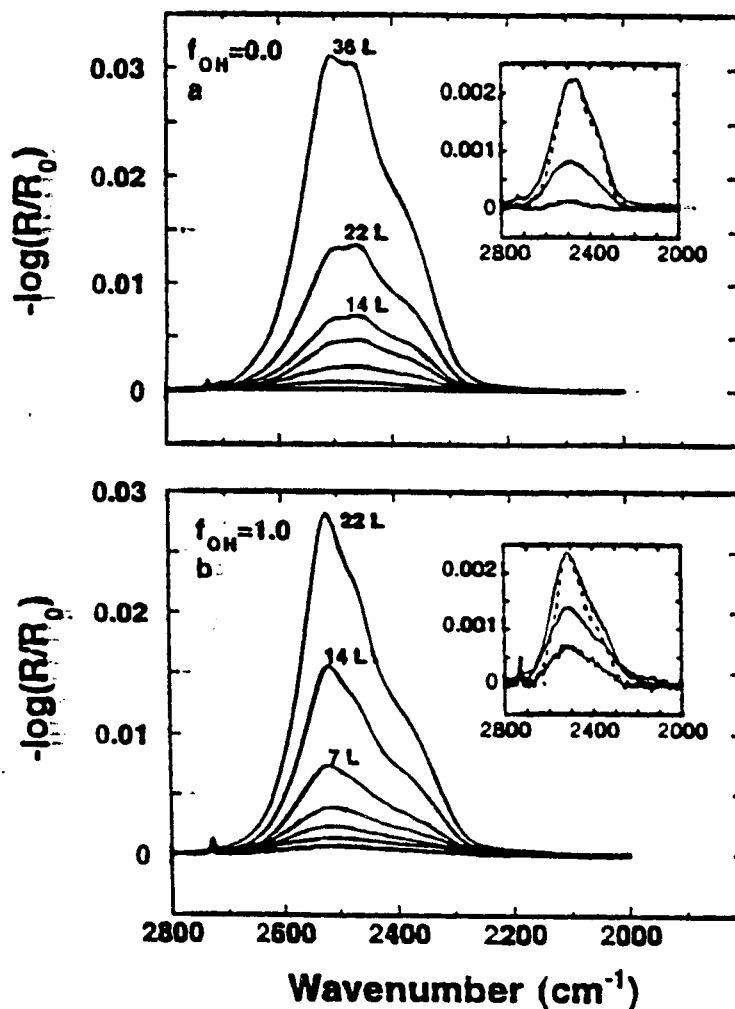


Fig. 13 IRAS, internal reflection adsorption spectroscopy, spectra of  $\text{D}_2\text{O}$  for different doses on (a) a methyl surface and (b) a hydroxyl surface. The doses were in (a) 0.7, 2, 6, 11, 14, 22, and 36 langmuirs and in (b) 0.4, 0.7 (two times), 2, 7, 14, and 21 langmuirs. The insert in each figure shows the lowest dose spectra at a larger scale. Broken lines are high-coverage spectra scaled down to illustrate the agreement with low-coverage spectra. Deposition and measurement temperatures were 120 K. Taken from Ref 22

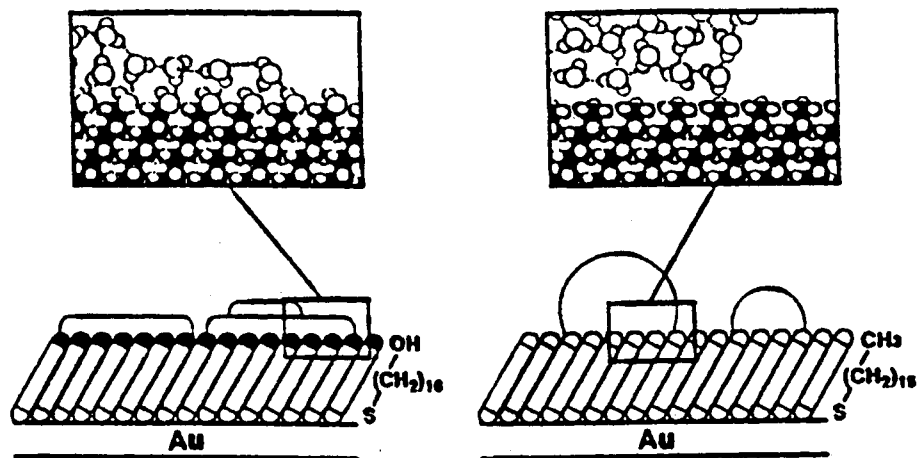


Fig. 14 Schematic drawing of -OH and -CH<sub>3</sub> terminated SAMs, self-assembled monolayers, with adsorbed D<sub>2</sub>O clusters of two- and three-dimensional shape, respectively. On the hydroxyl-terminated SAM, a second layer of D<sub>2</sub>O molecules is shown on one cluster. The enlarged sections *schematically* show hydrogen bonding of both adsorbate-adsorbate and substrate-adsorbate nature of the hydroxyl-terminated SAM. The drawing represents the situation at low temperature, where amorphous ice is formed on both surfaces. Taken from Ref. 22



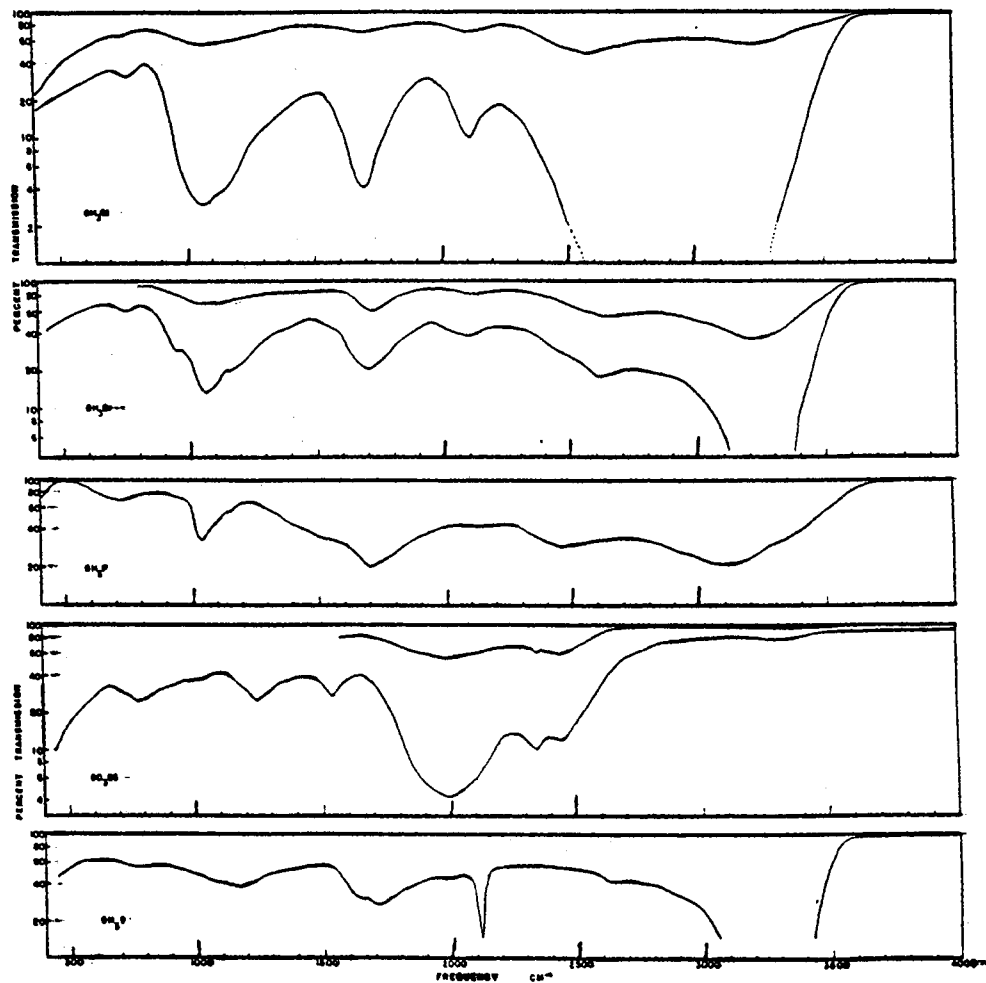


Fig. 15 Infrared spectra of oxonium slats at  $-195^\circ\text{C}$ . Taken from Ref. 24

Table 2

Vibrational frequencies in oxonium salts  
Modified from Ref. 24b

Assignment	OH <sub>2</sub> Cl	OH <sub>2</sub> Br	OD <sub>2</sub> Cl
O-H stretch (OD <sub>2</sub> H <sup>+</sup> )	...	...	3260
$\nu_2$ OF $\nu_1$	3235	3250	2445
O-D stretch (OD <sub>2</sub> H <sup>+</sup> )	...	...	2350
$\nu_2$ OF $\nu_1$	2590	2610	2000
$2\nu_2$	2109	2100	1545
$\nu_4$	1700	1705	1255
O-D bend (OD <sub>2</sub> H <sup>+</sup> )	...	...	1015
$\nu_3$	1150	1150	785
	1060	1060	
		950	
$\nu_6$	770	750	...

exceedingly broad and it is not immediately obvious which is which. Additionally, all the compounds show the  $2\nu_2$  peak near  $2100\text{ cm}^{-1}$ .

The amorphous monohydrate was later reproduced by Delzeit *et al.*<sup>25</sup> However, they also present the infrared spectra of the amorphous (see Fig. 16) and crystalline (see Fig. 17) di-, tetra-, and hexahydrates of HCl. In some related experiments, they showed that when gas-phase crystalline ice clusters were exposed to low levels of HCl, they first formed the amorphous HCl dihydrate which was then converted into the monohydrate upon increased exposure (see Fig. 18)

Graham and Roberts<sup>26a</sup> investigated the adsorption of HCl with the objective of gaining insight into how heterogeneous reactions occurred in the antarctic stratosphere. They prepared an ultrathin-film water deposit (5-20 monolayers thick) at 120 - 130 K on a W(100) single-crystal metal surface. They then exposed this film to varying amounts of HCl at 120 K which was then studied using temperature programmed desorption (warmed at  $\sim 5\text{ K/sec.}$ ) and mass spectrometry. If there was no HCl exposure to the deposit, the water sublimed at 170 K. If the deposit was exposed to low levels of HCl, the sublimation of water shifted towards 180 K with increasing amounts of HCl exposure. Hydrogen chloride was also evolved into the gas phase at 180 K with a second band appearing at 140 K with increasing amounts of HCl exposure. If the deposit was saturated with HCl, there was a single sharp sublimation of the water at 180 K and two peaks for the evolution of HCl at 140 and 180 K (see Fig. 19). These two peaks were designated  $\alpha$ -HCl and  $\beta$ -HCl, respectively. Studying the saturated deposit at varying

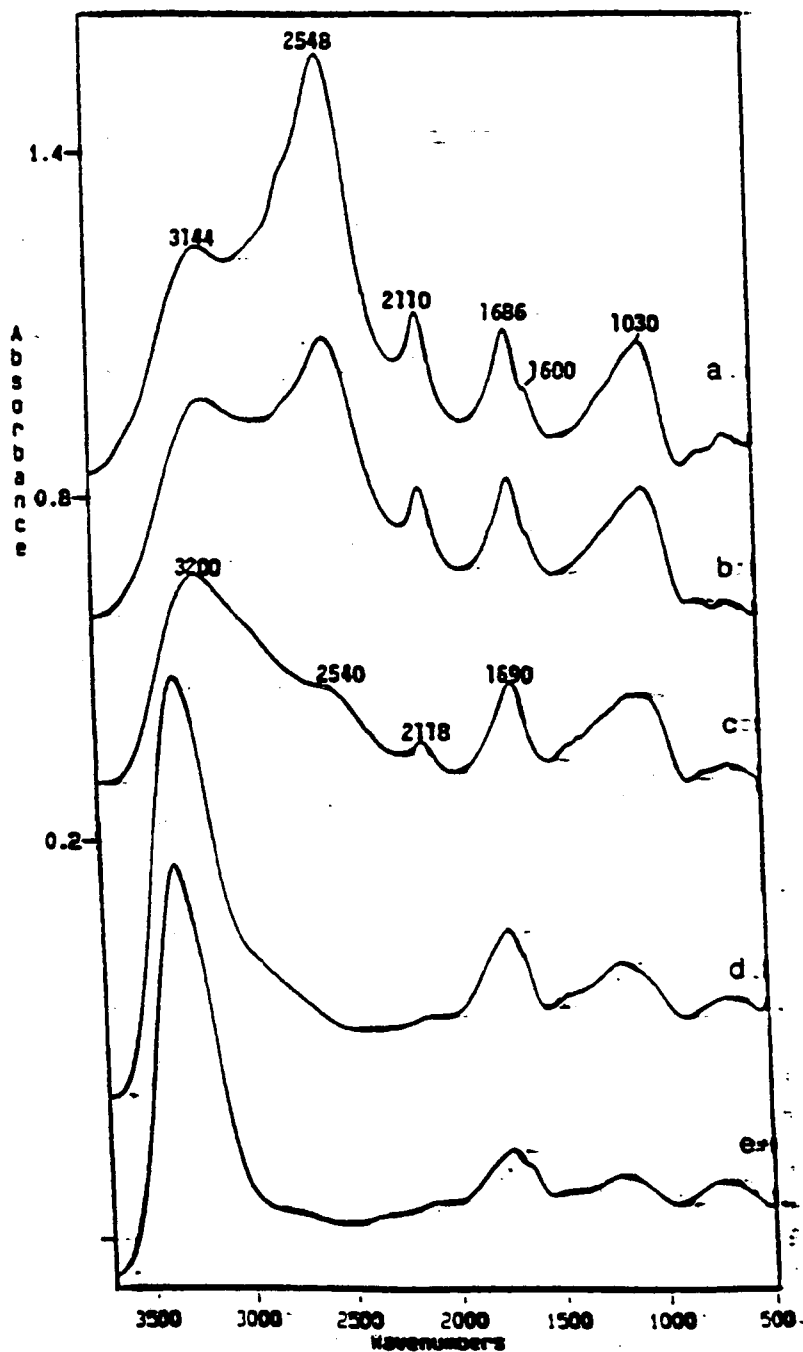


Fig. 16 Infrared spectra of cryogenically stabilized amorphous hydrates of HCl with water/acid ratios and preparation temperatures for the different samples as follows: (a) <1:1 at 85 K, (b) ~1:1 at 15 K, (c) ~2:1 at 85 K, (d) 4:1 at 80 K, and (e) 6:1 at 80 K. The spectra have been offset on the vertical axis for clarity of presentation. Taken from Ref. 25

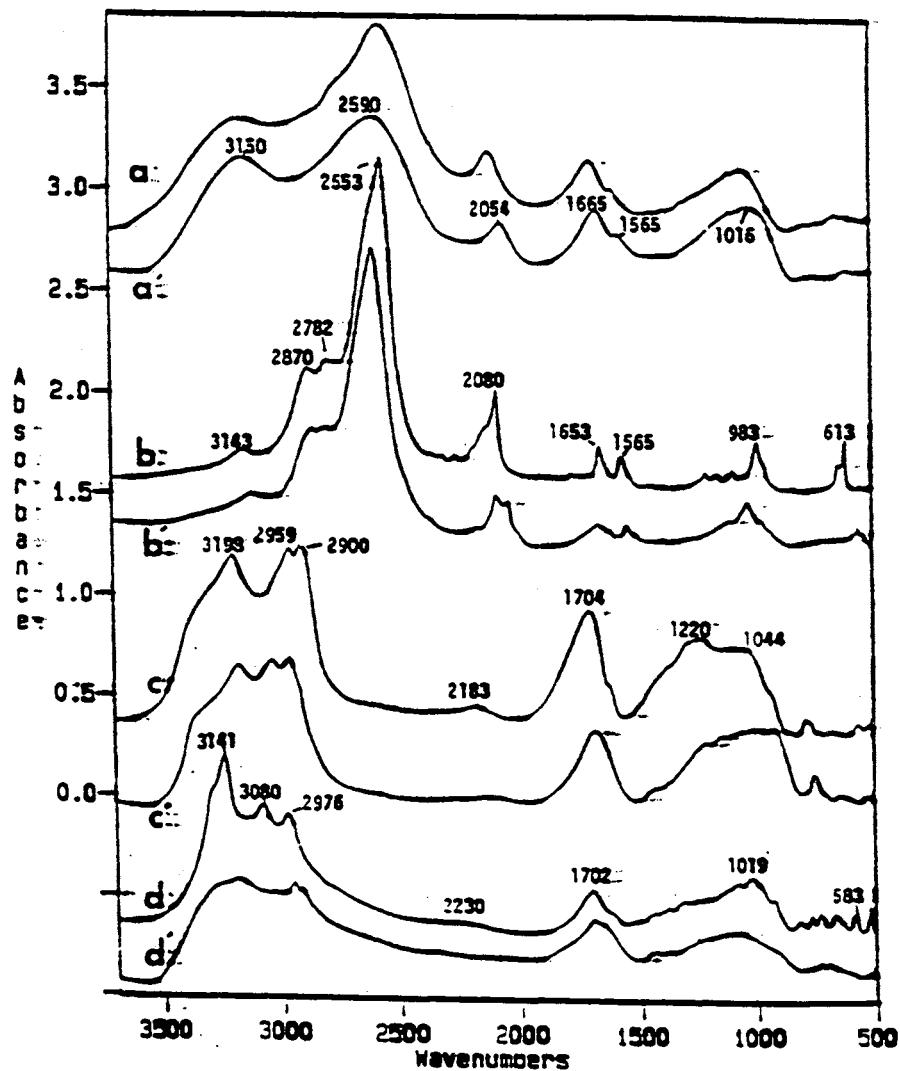


Fig. 17 Infrared spectra of the amorphous (a and a') and crystalline (b - d and b' - d') hydrates of HCl (unprimed labels) and HBr (primed labels), with the crystalline forms prepared by warming the original (a) ~1:1 amorphous hydrate deposits in a closed cell to (b) 155 K, (c) 195 K, and (d) 215 K. The spectra, which were each scanned for the samples recooled to 85 K, are on a common adsorbance scale except for (b) and (b'), which have been compressed to two-thirds scale. Taken from Ref. 25

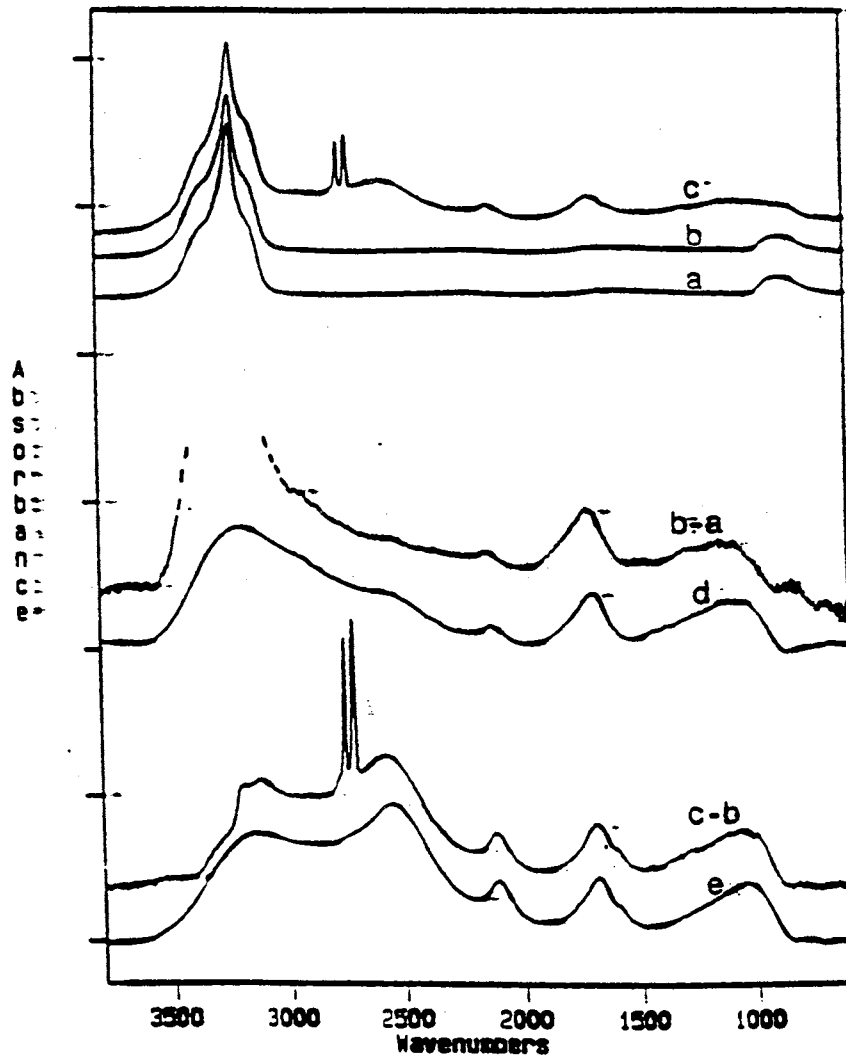


Fig. 18 Infrared spectra of gas-phase nanocrystals on ice exposed to varying levels of HCl (g) and the corresponding (labeled) difference spectra: (a) pure ice nanocrystals, (b) nanocrystals after exposure to 30 ppm HCl, and (c) nanocrystals after exposure to 120 ppm HCl. Curves d and e are the amorphous dihydrate and monohydrate, respectively, and are included for comparative purposes. Taken from Ref. 25

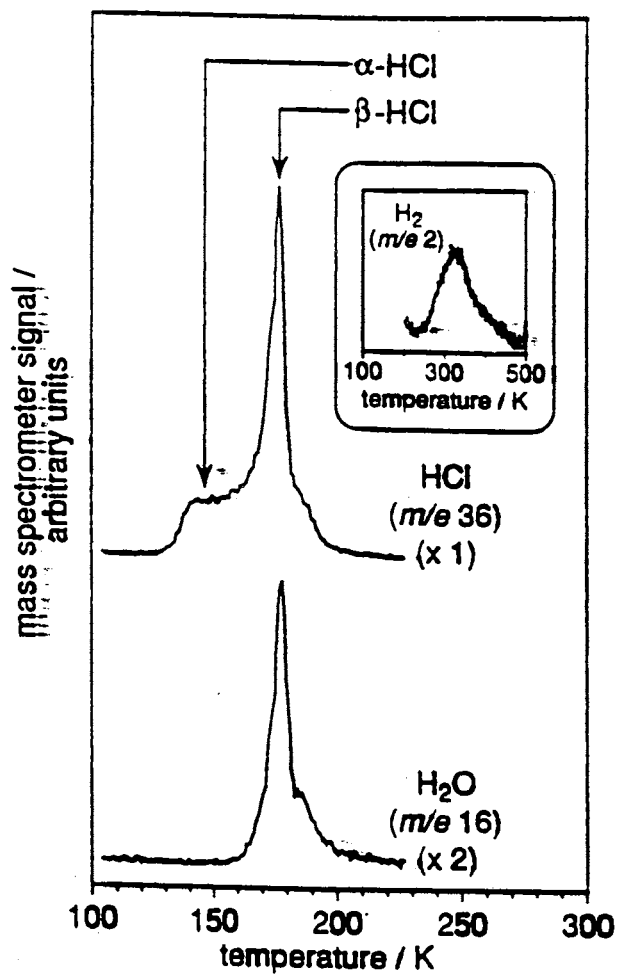


Fig. 19 Temperature-programmed desorption of HCl with a 5 monolayer thick water film on W (100). Taken from Ref. 26a

thicknesses showed that the 180 K peak of the HCl varied linearly with the film thickness, while the 140K peak was virtually independent of film thickness (see Fig. 20). These results imply that the  $\beta$ -HCl originates from the bulk. Also, a stoichiometric ratio of six water molecules to one  $\beta$ -HCl molecule was found, thus indicating the formation of the hexahydrate. This seems reasonable since, in an investigation by Horn *et al.*,<sup>26b</sup> they found that an ice surface did react with HCl when exposed at 100 K. Finally, the  $\alpha$ -HCl, being almost independent of film thickness, was derived from the adsorption of HCl onto the HCl modified ice surface.

Graham and Roberts<sup>27</sup> continued their investigation into the adsorption of HCl onto thin ice films by looking at the difference between the adsorption of HCl on amorphous and crystalline ice. They prepared amorphous deposits at 95K and crystalline deposits by annealing an amorphous deposit at 160 K for 2 minutes. HCl ( $2 \times 10^{-4}$  Pa·s, the product of the pressure times the duration of the exposure) was then adsorbed onto a 6 monolayer thick thin film. The temperature programmed desorption of the HCl exposed amorphous film was the same as mentioned above. The desorption of the HCl exposed crystalline film, however, was missing the  $\alpha$ -HCl (see Fig. 21b). Also, the desorption of H<sub>2</sub>O preceded the desorption of the  $\beta$ -HCl. These two bands are coincident in the amorphous ice temperature programmed desorption (see Fig. 21a). Also, the crystalline ice absorbed 75% of the  $\beta$ -HCl that the amorphous ice absorbed, thus implying the incomplete conversion of the crystalline film to HCl·6H<sub>2</sub>O. If the crystalline ice was exposed to  $6 \times 10^{-4}$  Pa·s of HCl, the crystalline ice would completely convert to the hexahydrate, but the desorption yield of the  $\alpha$ -HCl from the crystalline ice



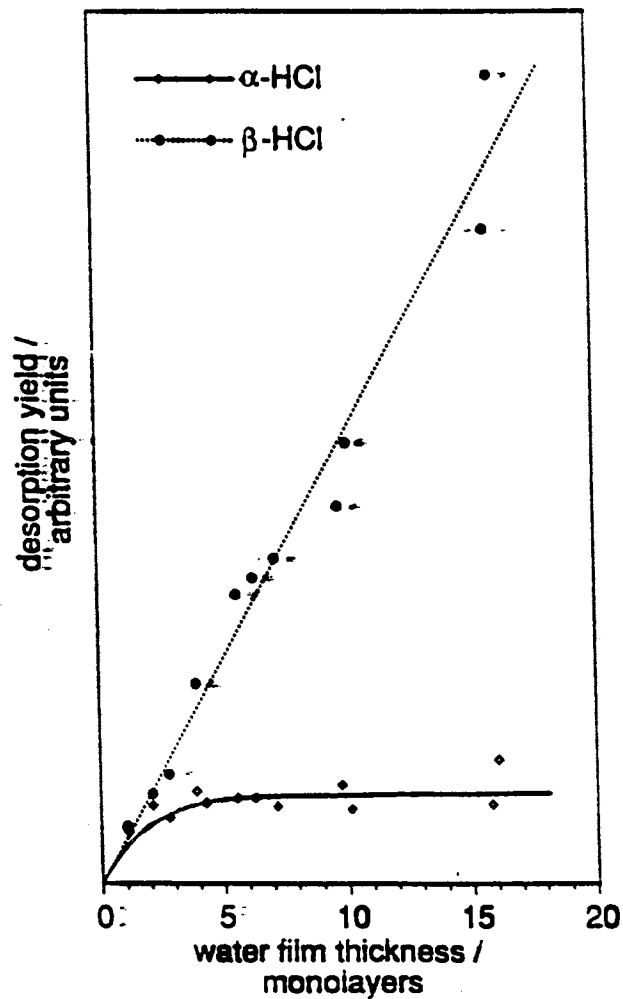


Fig. 20 Maximum yields of  $\alpha$ -HCl (diamonds) and  $\beta$ -HCl (circles) plotted versus water film thickness. Yields were determined from the time-integrated temperature-programmed desorption spectra. Lines are intended to guide the eye and do not represent a fit to the data. Taken from Ref. 26a

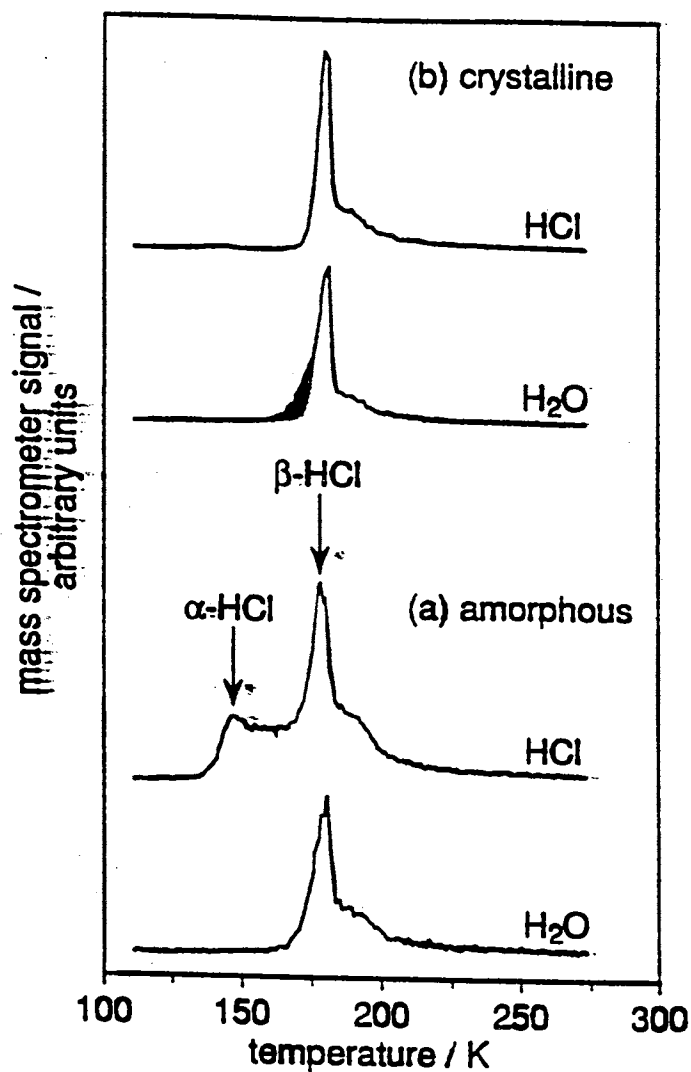


Fig. 21 Desorption spectra of HCl and H<sub>2</sub>O resulting from the interaction of HCl with 6 monolayer thick (a) amorphous and (b) crystalline ice films on W (100). The shaded region of the crystalline H<sub>2</sub>O spectrum shows where H<sub>2</sub>O sublimation precedes HCl evolution. Taken from Ref. 27

was always less than that from the amorphous ice (see Fig. 22). This demonstrated that HCl was more rapidly absorbed by an amorphous film than by a crystalline film.

However, if the  $2 \times 10^{-4}$  Pa·s HCl exposed crystalline film (no  $\alpha$ -HCl) was briefly warmed to 150K, recooled, and then reexposed to  $2 \times 10^{-4}$  Pa·s of HCl, the  $\alpha$ - and  $\beta$ -HCl were both fully developed.

Next, they exposed 30 monolayer thick amorphous and crystalline films to varying amounts of HCl (see Fig. 23). The HCl exposure was varied in two ways: the HCl pressure at the ice surface was held constant and the exposure time was varied, or the exposure time was held constant and the HCl pressure was varied. The plot of the exposure vs. HCl uptake shows that the HCl uptake is more rapid for amorphous ice, and that the uptake is determined by the total number of HCl-surface collisions, not by exposure time. This established that the rate-limiting step for  $\beta$ -HCl (hexahydrate) formation is HCl adsorption. Were the limiting step transport into the bulk, the uptake would scale with exposure time. The initial HCl adsorption probability on crystalline ice is 60% of that on amorphous ice. Moreover, the adsorption probability on the crystalline ice decreased exceedingly rapidly with increasing uptake. In fact, for a 30 monolayer thick crystalline film, it drops so precipitously that only ~30% of the film could be transformed into  $\text{HCl} \cdot 6\text{H}_2\text{O}$ . Thus only 9 layers, 4.5 bilayers (1 surface bilayer and 3.5 subsurface bilayers), were converted to the hexahydrate. The adsorption probability on the amorphous ice decreased with increasing uptake as well, but the effect was not as dramatic as it was on crystalline ice. A 30 monolayer thick amorphous film could be quantitatively converted to  $\text{HCl} \cdot 6\text{H}_2\text{O}$ . The reason for the different adsorption

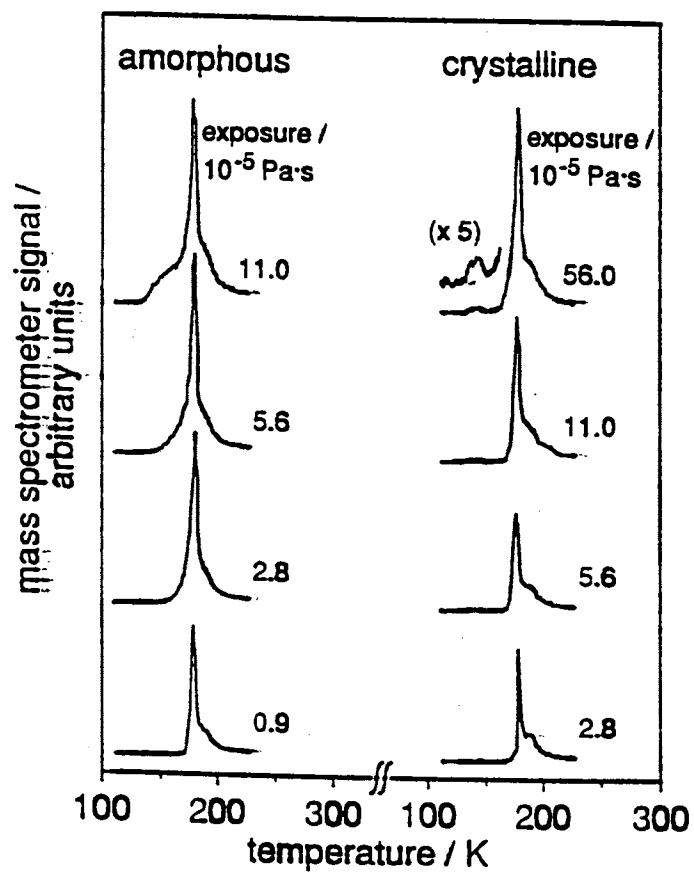


Fig. 22 Temperature programmed desorption of HCl from 8 monolayer amorphous and crystalline films as a function of HCl exposure. Taken from Ref. 27

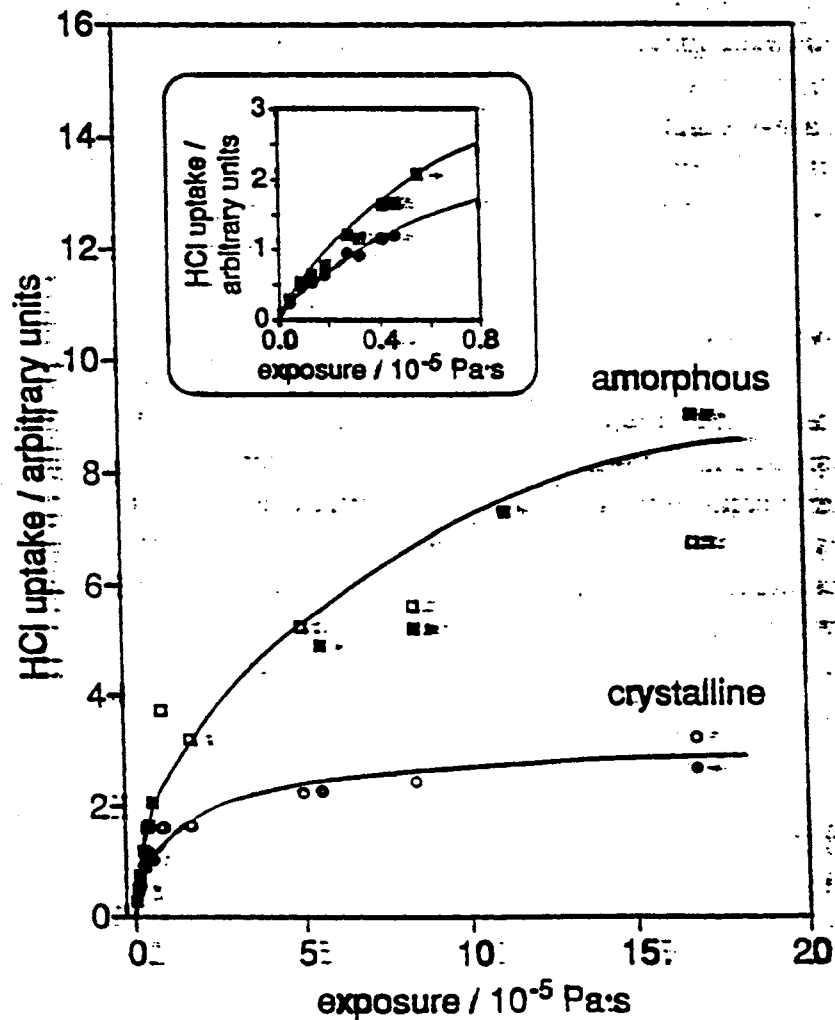


Fig. 23 The HCl yield plotted versus HCl exposure for 30 monolayer amorphous and crystalline ice films. Exposures were varied by holding the HCl pressure constant and changing the exposure time (open squares and circle), and by holding the exposure time constant and changing the HCl pressure (solid squares and circles). Taken from Ref. 27

probabilities on amorphous and crystalline ice was unclear. The initial step in  $\beta$ -HCl formation is the adsorption at sites that are active for nucleation of the hexahydrate. The nature of these sites could not be determined, but are presumably associated with defects: grain boundaries, dislocations, d-H, etc. Since an amorphous film has more defects than a crystalline film, there are more sites available for HCl adsorption.

The adsorption of hydrogen halides on alkali halide surfaces has also been studied. Smart and Sheppard<sup>28</sup> examined the adsorption of HCl, DCl, and HBr onto alkali halide surfaces at 190K (see Fig. 24). They found a red shift in the frequencies of the hydrogen halides ranging from 285-775  $\text{cm}^{-1}$ . The frequencies of the infrared absorption bands for HCl on LiCl, NaCl, and CsCl were at 2600, 2450, and 2110  $\text{cm}^{-1}$ , respectively, and DCl on NaCl and CsCl at 1870 and 1650  $\text{cm}^{-1}$ , respectively. Also, the absorption bands for HCl on NaBr and NaI were found at 2530 and *ca.* 2590  $\text{cm}^{-1}$ , respectively, and for HBr at 2210 and *ca.* 2300  $\text{cm}^{-1}$ , respectively (see Table 3). If a hydrogen halide was deposited on an alkali halide of lower atomic number, there was exchange of the halides between the adsorbate and the surface (i.e.,  $\text{HBr} + \text{NaCl} \rightarrow \text{HCl} + \text{NaBr}$ ). The resulting frequency of the adsorbed hydrogen halide after exchange with the surface was approximately that of the exchange products (see Table 3). Additionally, in a few of the cases, a small amount of water was present (covering  $\sim 5\%$  of the surface). In order to investigate this effect, water was adsorbed on NaCl, NaBr, and NaI surfaces before the adsorption of HCl or HBr. As might have been expected, these spectra showed the presence of hydronium ions on the surface after adsorption of the hydrogen

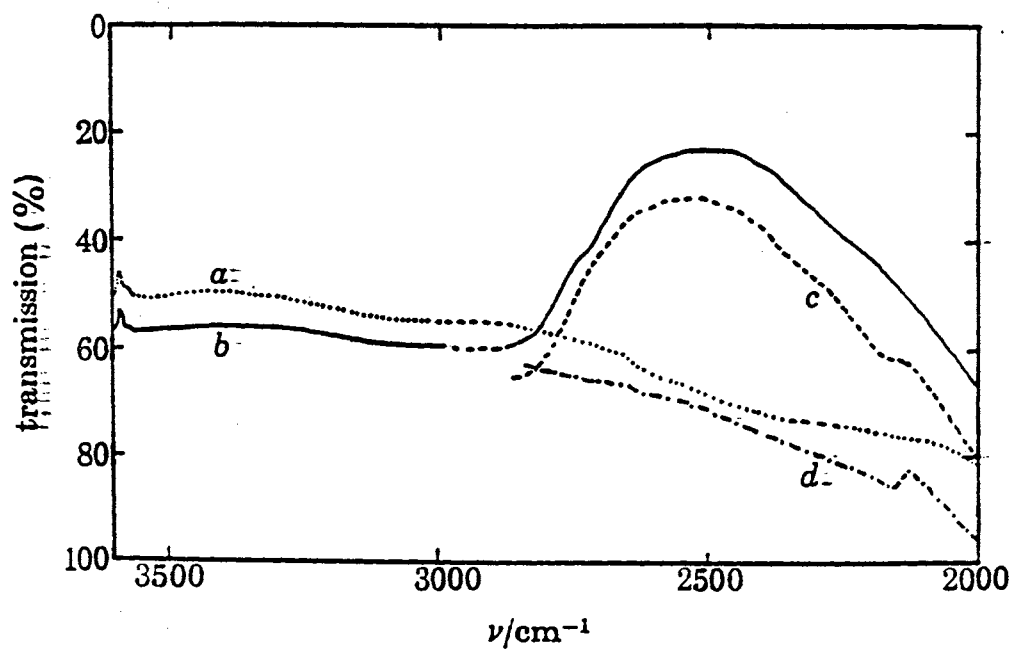


Fig. 24 The infrared spectrum resulting from the adsorption of HCl on high area NaCl. (a) Spectrum of NaCl film at 190 K, (b) spectrum after admission of a dose of 10 Torr of HCl at 190 K, (c) same spectrum after 24 hours, and (d) spectrum after evacuation for 2 1/2 hours at 190 K. Taken from Ref. 28

Table 3

Frequencies of HCl, DCl, and HBr adsorption bands on alkali halide surfaces  
Modified from Ref.

	HCl	DCl
LiCl	2600†	—
NaCl	2450	1870
CsCl	2110	1650

	HCl	HBr
NaCl	2450	2520
NaBr	2530	2210
NaI	ca. 2590	ca. 2300

† Surface also shows bands from adsorbed water.



halide (see Fig. 25). Also, the broad bands which arose from adsorption of the hydrogen halides to the surface were still present.

Blass *et. al.*<sup>29</sup> studied the adsorption of HCl and HBr on a LiF surface. However, they maintained a temperature of 55K and did not observe any exchange between the adsorbate and the surface. The adsorption of HCl on a LiF surface (see Fig. 26a) showed three different spectral features as a function of HCl exposure. The first feature to appear is a weak adsorption at  $2495\text{ cm}^{-1}$  for the first molecules adsorbed onto the surface, denoted as peak I in Fig. 26. This peak then grew with a broad adsorption centered at  $2515\text{ cm}^{-1}$  (FWHH =  $295\text{ cm}^{-1}$ ), and is slightly asymmetric with a low-frequency tail. This first feature was attributed to the first layer of HCl adsorbed directly onto the LiF surface. Next, a second peak, denoted as peak II, appeared at  $2763\text{ cm}^{-1}$  (FWHH =  $80\text{ cm}^{-1}$ ). Peak II appeared about the time that peak I reached about 40-50% of its final intensity. It was attributed to adsorption in a second layer. Finally, the third feature is a doublet, which is superimposed over peak II, at  $2752$  and  $2709\text{ cm}^{-1}$  (FWHH =  $14$  and  $11\text{ cm}^{-1}$ , respectively). These peaks were assigned to the subsequent layers of HCl and are characteristic of the orthorhombic phase of solid HCl. For the HBr adsorbed onto a LiF surface (see Fig. 26b), the first layer produced a peak frequency of  $2265\text{ cm}^{-1}$  with the first molecules being redshifted by  $40\text{-}50\text{ cm}^{-1}$ . The second layer adsorbed with a peak frequency of  $2461\text{ cm}^{-1}$  and then the subsequent layers produced the doublet at  $2439$  and  $2405\text{ cm}^{-1}$ .

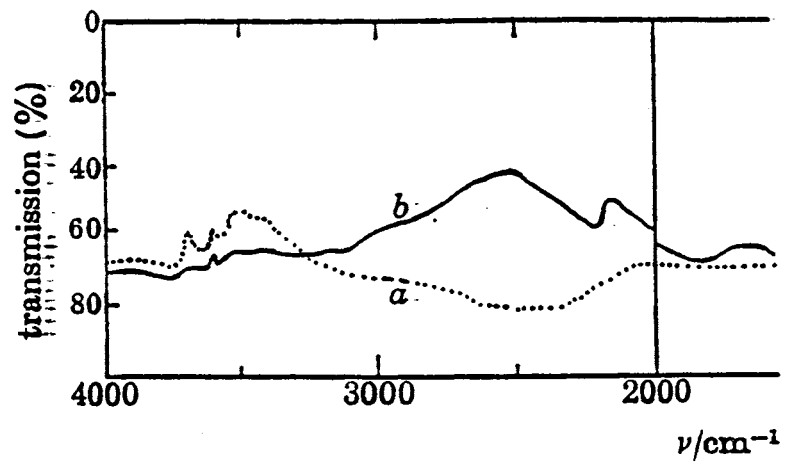


Fig. 25 Infrared spectra from the adsorption of HCl on a sodium chloride surface with preadsorbed water. (a) Spectrum of NaCl films with preadsorbed water at 190 K and (b) spectrum after admission of a dose of 10 Torr HCl at 190 K. Taken from Ref. 28

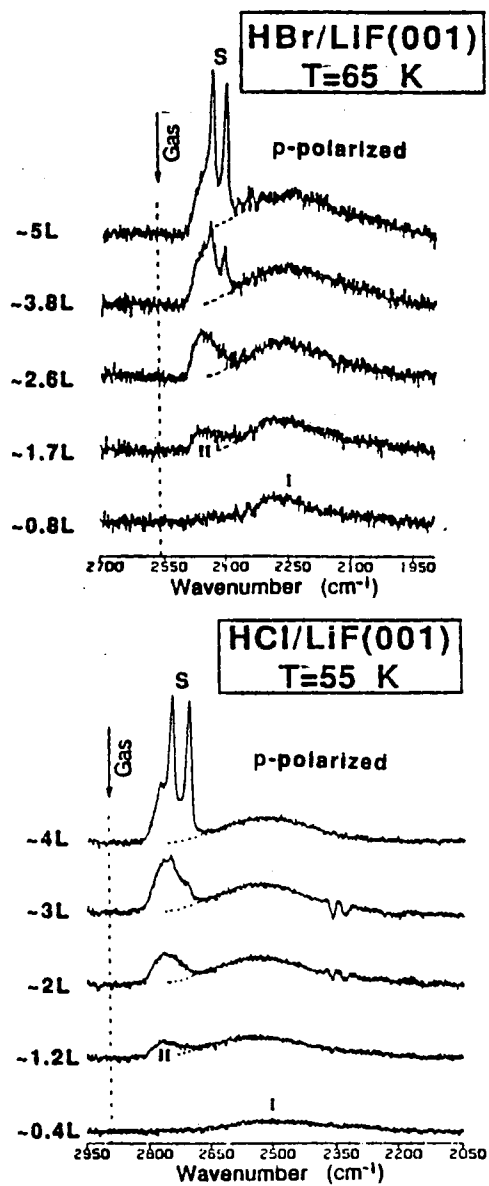


Fig. 26 Infrared transmission spectra of HCl and HBr adsorbed on LiF (001) for different acid exposures. Taken from Ref. 29

## Matrix Isolation

Matrix isolation is the simplest way to study a complex without a lot of interference from other species or interactions. Several people<sup>30-33</sup> have investigated the matrix isolation of HCl and H<sub>2</sub>O with slightly varying results, but for the most part, the differences were explainable and understandable.

Ault and Pimentel<sup>30</sup> first studied the 1:1 complex of HCl and H<sub>2</sub>O (and the deuterated counterparts) in a nitrogen matrix in order to investigate the nature of the hydrogen bond formed and to determine whether the complex could be said to involve the hydronium ion. They conducted both single- and two-jet experiments and found the formation of two new bands (in addition to the parent bands). These new bands at 2638 and 2540 cm<sup>-1</sup> had the same relative intensities in both the single and two-jet cases for HCl deposited with H<sub>2</sub>O (see Fig. 27a). The fully deuterated counterpart produced bands at 1916 and 1849 cm<sup>-1</sup> (see Fig. 27b). For the mixed isotope cases, these bands remained at approximately the same band position for the acid used. The D<sub>2</sub>O:HCl mixed isotope deposit formed bands at 2645 and 2533 cm<sup>-1</sup>, while the H<sub>2</sub>O:DCl deposit formed bands at 1915 and 1850 cm<sup>-1</sup>. See Table 4 for the frequency of all the bands.

Ault and Pimentel<sup>30</sup> deduced a structure for this new complex. The possible structures ranged from a molecular hydrogen bond to an ionized and rearranged structure (see Fig. 28, structures I through IV, respectively). In a mixed isotope experiment using two-jet deposition involving HCl and D<sub>2</sub>O, no bands were observed between 2100 and 1800 cm<sup>-1</sup>, thus indicating the complete freedom from exchange. This immediately

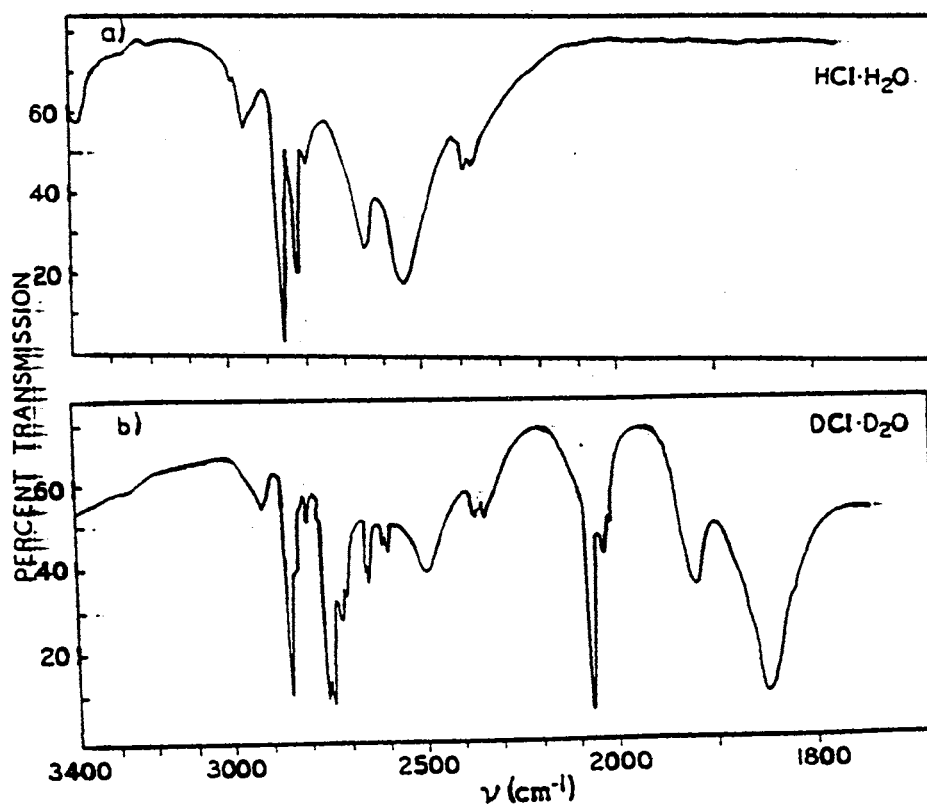


Fig. 27 The infrared spectrum of the products of (a) H<sub>2</sub>O:HCl:N<sub>2</sub> and (b) D<sub>2</sub>O:DCl:N<sub>2</sub> mixed at a ratio of 1:1:350. Taken from Ref. 30

Table 4

Absorption frequencies and optical densities of water and hydrochloric acid mixtures  
Modified from Ref. 30

H <sub>2</sub> O:HCl $\nu$ , cm <sup>-1</sup>	D <sub>2</sub> O:DCl $\nu$ , cm <sup>-1</sup>	D <sub>2</sub> O:HCl $\nu$ , cm <sup>-1</sup>	H <sub>2</sub> O:DCl $\nu$ , cm <sup>-1</sup>
2638 (0.57)		2645 (0.12)	
2540 (0.85)		2533 (0.29)	
	1916 (0.34)		1915 (0.38)
	1849 (0.38)		1850 (0.39)
520 (0.14)			
460 (0.31)			
	393 (0.06)		
	330 (0.18)		

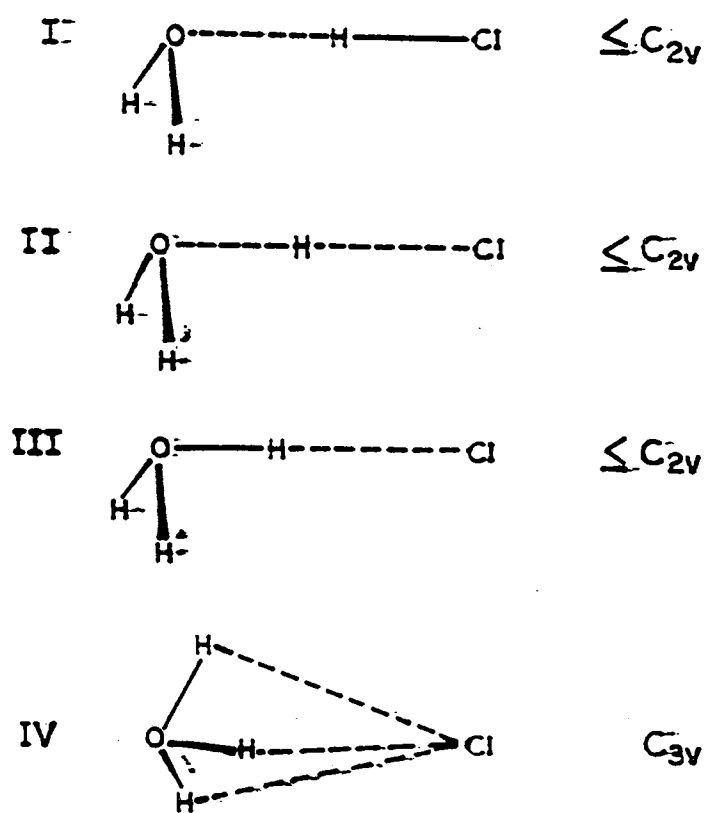


Fig. 28 Four possible prototype structures for the isolated  $H_2O:HCl$  complex. Taken from Ref. 30

ruled out structure **IV**, and disfavored structure **III** due to the low barrier to reorientation that would be expected. Also, no other bands were observed (besides the ones already mentioned), indicating the lack of formation of the hydronium ion. Structure **II** can only be reconciled if it is postulated that there is a significant barrier to interchange among the hydrogen atoms in the complex. Thus, the complex formed between the HCl and the H<sub>2</sub>O (and their deuterated counterparts) favors structure **I**, a molecular complex.

The matrix isolation of HCl and H<sub>2</sub>O has also been studied in argon matrices. Ayers and Pullin<sup>31</sup> found the HCl stretch of the water-HCl "dimer" at 2663.5 cm<sup>-1</sup> (see Fig. 29) and for DCl at 1929.5 cm<sup>-1</sup>. This was considerably higher than the main complex bands at 2540 and 1849 cm<sup>-1</sup> found by Ault and Pimentel<sup>30</sup> in a nitrogen matrix, and even higher than the secondary bands found at 2638 and 1915 cm<sup>-1</sup> for H<sub>2</sub>O and D<sub>2</sub>O, respectively.

Schrivier *et al.*<sup>32</sup> investigated the reason for the discrepancy in the frequency between the two matrixes and the reason the nitrogen matrix produces two bands associated with the HCl stretch, while only a single band was found in an argon matrix. After studying the effects of annealing and varying the dilution of the HCl and H<sub>2</sub>O and the relative concentrations of the HCl and H<sub>2</sub>O, they concluded that the low frequency band in the nitrogen matrix at 2545 cm<sup>-1</sup> should be assigned to the 1:1 complex between HCl and H<sub>2</sub>O. They also concluded that the higher frequency band at 2647 cm<sup>-1</sup> should be assigned to the 2:1 HCl:H<sub>2</sub>O complex. They also observed the 2:1 complex in the argon matrix which they assigned to a band at 2754 cm<sup>-1</sup>. They also observed the HBr(DBr):H<sub>2</sub>O complexes.



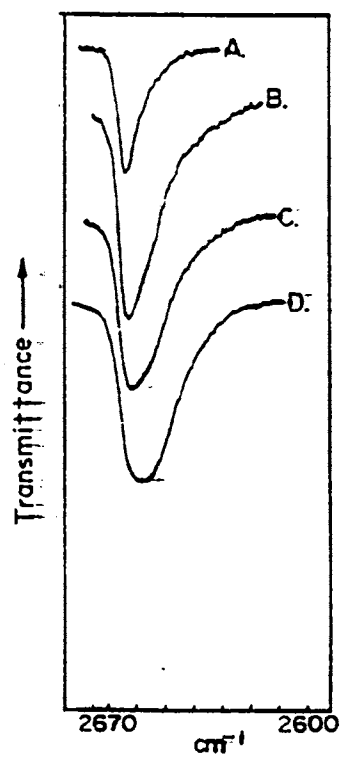


Fig. 29 Spectra of H<sub>2</sub>O/Ar matrices doped with HCl. Mix ratios were H<sub>2</sub>O:HCl:Ar of (a) 1:1:371, (b) 1:1:180, (c) 1:1:92, and (d) 1:1:50. Taken from Ref. 31

They observed the 1:1 HBr:H<sub>2</sub>O complex at 2395 cm<sup>-1</sup> in argon and 2282 cm<sup>-1</sup> (1658 cm<sup>-1</sup> for DBr) in nitrogen, while the 2:1 complex was observed at 2438 cm<sup>-1</sup> in argon and as a doublet at 2375 and 2366 cm<sup>-1</sup> (1713 and 1702 cm<sup>-1</sup> for DBr) in nitrogen. See Table 5 for complete assignments.

Schrivver *et. al.*<sup>32</sup> agreed with Ault *et al.*<sup>30</sup> on the structure of the 1:1 HCl:H<sub>2</sub>O complex. They also proposed three different possibilities for the structure of the 2:1 complex (see Fig. 30), which ranged from a linear, to bifid, to cyclic. They used the frequency of the HCl stretch and the frequencies of the water molecules to deduce the structure of the 2:1 complex. From this, the linear complex was eliminated because the water perturbation would be expected to stay in the same range of magnitude as in the 1:1 complex, the frequency of the end HCl would be in the HCl polymer range 2800 - 2700 cm<sup>-1</sup>, and the frequency of the central HCl should have appeared at a lower frequency than the 1:1 complex. The cyclic structure was eliminated because in this geometry the water molecule is acting as both an electron acceptor and donor, a configuration in which the vibration of the water molecule is strongly perturbed; this situation does not correspond to the observed spectrum where the water was only weakly perturbed. This left only the bifid complex, in which, the water perturbation was only slightly stronger than in the 1:1 complex and the HCl perturbation weaker.

Finally, to investigate the difference in the frequencies obtained from the argon and the nitrogen matrices, Schrivver *et. al.*<sup>32</sup> added a few percent of nitrogen to a HCl/H<sub>2</sub>O/argon matrix. They observed the formation of a new band at 2640 cm<sup>-1</sup> in addition to the usual band at 2663 cm<sup>-1</sup> for the 1:1 complex. From this, they concluded

Table 5

HX absorption frequencies of H<sub>2</sub>O/HX mixtures in nitrogen and argon matrices  
Modified from Ref. 32

	N <sub>2</sub>	Ar	Attribution
HCl/H <sub>2</sub> O	C <sub>2</sub> 2647	2754	1-2 complex
	C <sub>1</sub> 2545	2663	1-1 complex
HBr/H <sub>2</sub> O	C <sub>2</sub> { 2375 2366	2438	1-2 complex
	C <sub>1</sub> 2282	2395	1-1 complex
DBr/H <sub>2</sub> O	C <sub>2</sub> { 1713 1702		1-2 complex
	C <sub>1</sub> 1657		1-1 complex

Table 6

HX (DX) frequencies ( $\text{cm}^{-1}$ ) of  $(\text{HX})_m(\text{H}_2\text{O})_n$  aggregates and their deuterated counterparts  
 Modified from Ref. 33

Aggregate		$(\text{HCl})_m(\text{H}_2\text{O})_n$	$(\text{DCl})_m(\text{D}_2\text{O})_n$	$(\text{HBr})_m(\text{H}_2\text{O})_n$	$(\text{DBr})_m(\text{D}_2\text{O})_n$
$m$	$n$	$\nu\text{HCl}$	$\nu\text{DCI}$	$\nu\text{HBr}$	$\nu\text{DBR}$
2	1	2753	1993	2436	1752
1	1	2659	1929	2392	1720
1	3	} 2500	1842	} 2300	1674
2	1		1820		1662
1	2	(2390)*	1741	2245	1620

\*Deduced from the  $\nu\text{DCI}$  absorption.

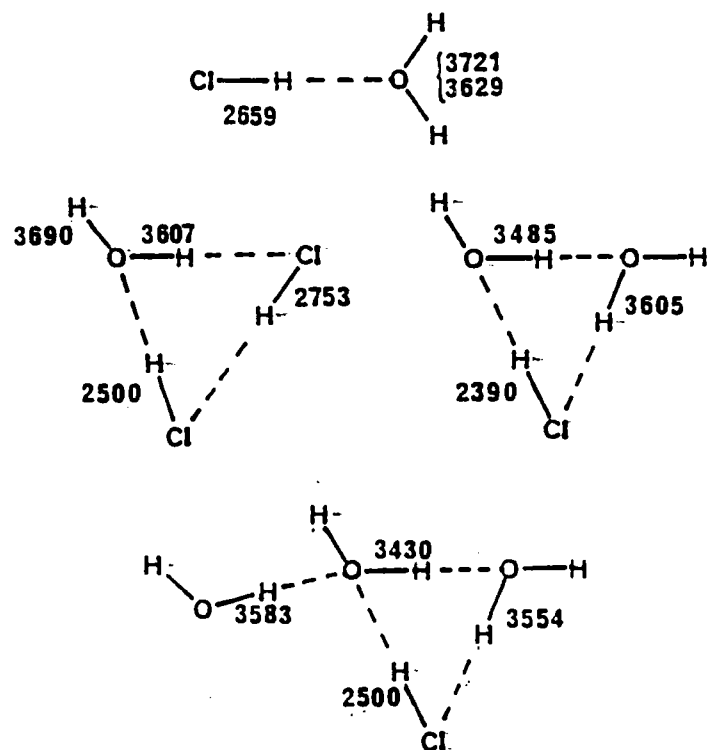


Fig. 31 Structure and frequencies of several  $(\text{HCl})_m(\text{H}_2\text{O})_n$  complexes. Taken from Ref. 33

They also assigned structures to the 1:2 and the 1:3 HCl:H<sub>2</sub>O complexes and these are also given in Fig. 31.

### Theoretical

The interaction of HCl with H<sub>2</sub>O has also been studied theoretically. Kroes and Clary<sup>34</sup> conducted classical trajectory calculations modeling the physical adsorption of HCl to a (0001) ice surface. Under the conditions of their simulation, HCl was not allowed to dissociate. They thought this to be a reasonable assumption because according to the HCl-ice phase diagram (see ref. 16 in Kroes and Clary, Ref. 36) gaseous HCl is in equilibrium with HCl in a solid solution of ice rather than with one of the HCl hydrates. They found that the HCl adsorbed onto the ice surface with the H-atom of the HCl pointing obliquely down to the oxygen of a dangling-oxygen molecule, while the Cl-atom interacted with the protons of two neighboring dangling-hydrogen molecules (see Fig. 32).

Packer and Clary<sup>35</sup> investigated the interaction of HCl with 1-3 water molecules in *ab initio* MP2 equilibrium geometry calculations. Their model allowed for the dissociation of the HCl molecule, but no dissociation was found. They did, however, observe an increase in the bond length, a large red-shift in the stretching frequency, and an increase in the positive charge on the H-atom of the HCl as the cluster size increased. However, they did not observe any ionization of the HCl, even for the 1:3 complex. They concluded, as Amirand and Maillard<sup>33</sup> had, that a cluster of at least four water molecules was required in order to dissociate HCl.

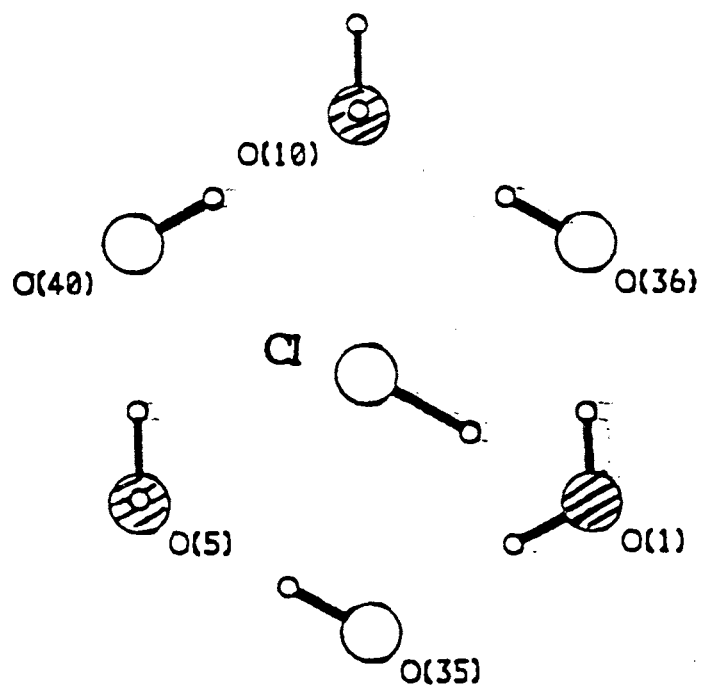


Fig. 32 Potential minimum geometry of HCl interaction with an ideal (0001) ice surface. The molecules on the top layer are shown with the oxygens shaded in. The HCl molecule points its H-atom down to the oxygen of molecule 1 (d-O), while the chlorine interacts strongly with the upward pointing H-atoms of molecules 5 and 10 (d-H). Taken from Ref. 34

Packer and Clary<sup>35</sup> also presented the structures which they had calculated for the HCl:(H<sub>2</sub>O)<sub>n</sub> aggregates (see Fig. 33). They agree with the previously given structures<sup>30-34</sup> for the 1:1 and 1:2 complexes. However, they disagreed with the structure for the 1:3 complex proposed by Amirand and Maillard.<sup>33</sup> Packer and Clary calculated a ring structure for the 1:3 complex in which the hydrogen of the HCl is hydrogen bonded to one of the water molecules and there is a weak interaction between the hydrogen of another of the water molecules and the chlorine of the HCl (see Fig. 33). Although there is an interaction between this hydrogen and the chlorine, it is too weak to be considered a hydrogen bond. For this reason, although the structure proposed by Packer and Clary was different from that proposed by Amirand and Maillard, the data on which these structures were based was consistent. The HCl acts as a proton donor, two of the water molecules were both a proton donor and acceptor, and then the third water molecule was only a proton acceptor with the understanding that the weak interaction between its hydrogen and the chlorine is not a hydrogen bond, but is strong enough to stabilize the ring structure of the 1:3 complex.

The solvation of hydrogen halides on the surface of ice was also studied by Robertson and Clary.<sup>36</sup> They investigated the solvation of HCl, HBr, and HF on the surface of a 6 bilayer slab in a molecular dynamics simulation. They concluded that the solvation of HCl and HBr at atmospheric conditions (~190 K) is energetically feasible. They did not, however, look at the kinetics of the solvation, nor did they comment on the effects of temperature on this solvation process.



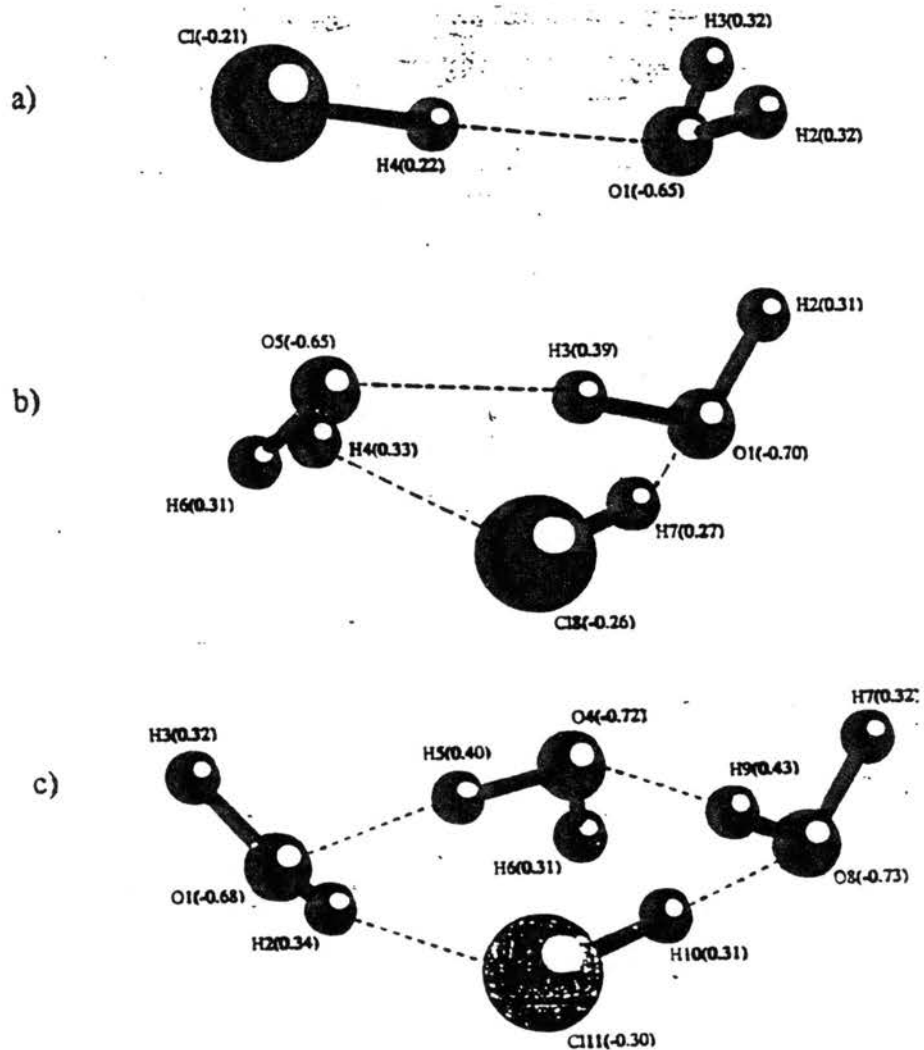


Fig. 33 Structure and atomic charges for the (a)  $\text{H}_2\text{O}-\text{HCl}$ , (b)  $(\text{H}_2\text{O})_2\text{HCl}$ , and (c)  $(\text{H}_2\text{O})_3\text{HCl}$  complexes. Taken from Ref. 35

## HCN

Spectroscopic data for the complexes of HCN and H<sub>2</sub>O are quite limited. The few papers which do include infrared data on HCN complexes are mostly limited to the H-C stretch and the bending motion of the HCN molecule. The C≡N stretch has been mostly ignored due to the small spectral shifts which it experiences upon complexation and the weak intensity of the C≡N band in the dimer complex.

The H<sub>2</sub>O:HCN dimer has a pseudoplanar C<sub>2v</sub> structure in which the HCN is hydrogen-bonded through its hydrogen to the oxygen of the H<sub>2</sub>O molecule (see Fig. 34).<sup>37</sup> The H<sub>2</sub>O and HCN experience in-plane and out-of-plane bending vibrations of up to 20°.<sup>37</sup>

### Matrix Isolation

One of the few studies that included the use of IR investigated the C-H stretch of HCN in Ar and CCl<sub>4</sub> matrices.<sup>38</sup> They observed that the frequency of the C-H stretch changes according to whether it was at the head, end, or middle of a chain of HCN molecules (see Fig. 35). The HCN molecule at the head of the HCN chain, labeled  $\nu_p$ , has a C-H stretching frequency of  $\sim 3270\text{ cm}^{-1}$ . The molecule at the end of the chain, labeled  $\nu_{sb}$ , has a stretching frequency of  $\sim 3200\text{ cm}^{-1}$ . While the molecule in the middle of the HCN chain, labeled  $\nu_{db}$ , has the lowest vibrational frequency of  $\sim 3150\text{ cm}^{-1}$ . Thus, the C-H stretching frequency decreases as the HCN molecule goes from being an electron donor, to an electron acceptor, to both an electron donor and acceptor.

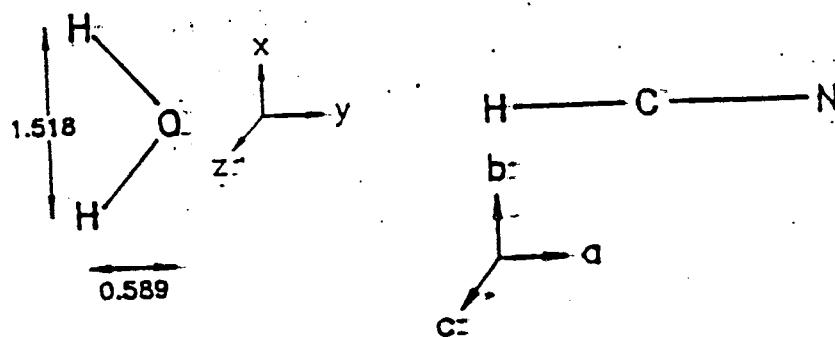


Fig. 34 Inertial axis system of free  $\text{H}_2\text{O}$  and of the  $\text{H}_2\text{O}-\text{HCN}$  dimer drawn to scale. Taken from Ref. 37

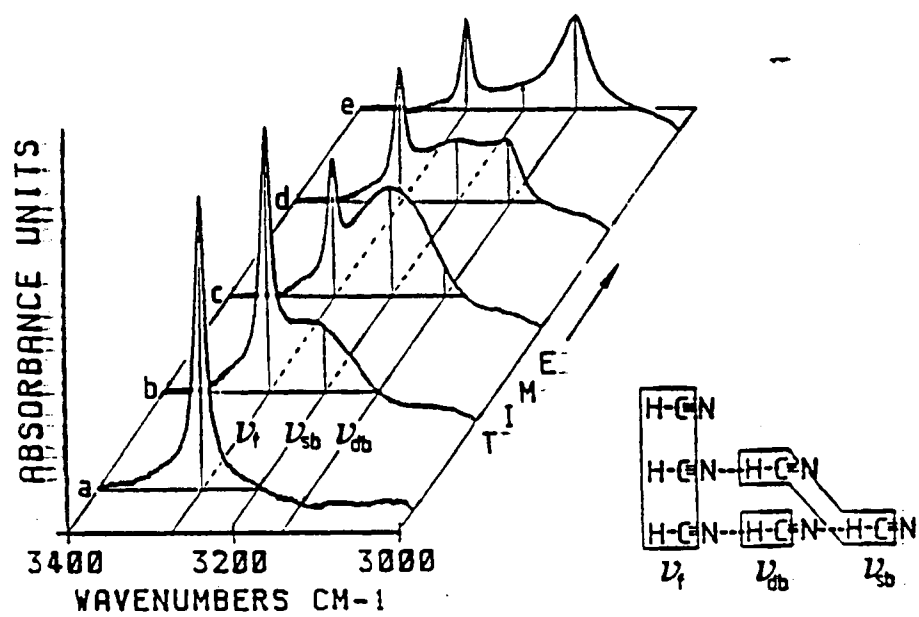


Fig. 35 CH-stretching region of various HCN species imbedded in solid  $\text{CCl}_4$ , as a function of time: (a)  $t = 0$ , (b)  $t = 15$  min, (c)  $t = 30$  min, (d)  $t = 45$  min, and (e)  $t = 60$  min. Taken from Ref. 38

In another study, the harmonic frequency of the C≡N mode was investigated.<sup>39</sup> Contrary to the C-H stretch which decreases in frequency when the HCN molecule goes from being an electron donor, to acceptor, to both, the harmonic frequency of the C≡N decreases as the HCN molecule goes from being an electron donor, to both an acceptor and donor, to being an electron acceptor with the frequency of the C≡N stretch for these three molecules being 2134.0, 2132.1, and presumably 2128.5 cm<sup>-1</sup> (under the monomer band), respectively (see Table 7). The experimentally determined harmonic frequencies for the first two of these molecules (the two which are actually hydrogen-bonded through the N) are 2134.0 and 2132.1 cm<sup>-1</sup>, respectively, values fairly close to the calculated frequencies and ~12 cm<sup>-1</sup> above the calculated frequency of the third molecule (which is not hydrogen-bonded through its N). However, the same calculation for DCN shows a different trend. The DCN, which is acting as both the electron donor and acceptor, has the lowest calculated frequency of the three molecules.

In a comparison of the frequency of C≡N groups which were hydrogen-bonded to those which were nonhydrogen-bonded for two molecules in an HCN:HX dimer, except for the arrangement in which they are bonded, HCN-HX or HX-HCN, the frequency of the bonded C≡N group is higher in frequency than the non-bonded C≡N group (see Table 8 and 9).<sup>39,40</sup> The difference in their frequencies range from ~10 cm<sup>-1</sup> for the HCN---HCN dimer in the gas phase to 16 - 20 cm<sup>-1</sup> in a variety of matrices. The difference in frequency for the HCN---HF and HF---HCN dimers is presumably 30 cm<sup>-1</sup> but may be less due to the fact that the frequency of the non-bonded C≡N group was not

Table 7

Summary of normal coordinate calculations.  
Modified from Ref. 39

Harmonic frequency (cm <sup>-1</sup> )	Calculated frequency (cm <sup>-1</sup> )	Shift D-M,T-M (cm <sup>-1</sup> )	Infrared intensity (Calc.)	Mode description (PED %)
				HCN
3441.2	3441.2	--	100	CH(95) - CN(5)
2128.7	2128.7	--	0.1	CN(94) + CH(6)
				DCN
2703.3	2703.3	--	51	CD(68) - CN(32)
1952.1	1952.1	--	5	CN(67) + CD(33)
				HCN[1]-HCN[2]
--	3452.0	+ 10.9	98	CH1(94)
3376.2	3376.0	- 65.1	102	CH2(93)
2136.5	2136.7	+ 8.0	0.3	CN1(89)
2126.6	2122.6	- 6.1	0.2	CN2(88)
--	116.3	--	--	HB(98)
				DCN[1]-DCN[2]
--	2724.5	+ 21.2	48	CD1(66) + CN1(33)
--	2673.8	- 29.5	53	CD2(63) - CN2(36)
--	1950.9	- 1.3	8	CN1(63) + CD1(33)
1927.2	1929.4	- 22.7	4	CN2(61) + CD2(35)
--	114.3	--	--	HB(98)
				HCN[1]-HCN[2]-HCN[3]
--	3452.0	+ 10.9	99	CH1(94)
--	3376.0	- 65.1	98	CH2(92)
3289.2	3289.7	- 151.4	103	CH2(91)
2134.0	2138.1	+ 9.4	0.6	CN1(64) + CN2(27)
2132.1	2131.7	+ 3.0	0.2	CN2(58) - CN1(29)
--	2121.5	- 7.2	0.1	CN3(86)
--	142.6	--	--	HB1 - HB2
--	82.2	--	--	HB1 + HB2
				DCN[1]-DCN[2]-DCN[3]
--	2724.5	+ 21.1	50	CD1(66) - CN1(33)
--	2673.6	- 29.7	46	CD3(63) - CN3(36)
--	2635.2	- 68.1	54	CD2(58) - CN2(41)
--	1950.6	- 1.5	8	CN1(64) + CD1(34)
--	1930.4	- 21.7	10	CN3(59) + CD3(33)
1917.4	1915.6	- 36.5	3	CN2(53) + CD2(38)
--	140.2	--	--	HB1 - HB2
--	80.7	--	--	HB1 + HB2

Table 8

Comparison of HCN dimer-monomer shifts with those in related systems.  
Modified from Ref. 39

System		HCN[1]—HCN[2]			
		$\nu_1$ region		$\nu_2$ region	
		CN1	CN2	CH1	CH2
HCN—HCN (this work)	Gas <sup>a</sup>	+ 7.8	- 2.1	(10.8)	- 65
HCN—HCN (Ref. 21)	Ne	+ 21.6	+ 5.7	+ 11.7	- 68.5
	Ar	+ 21.4	+ 3.6	- 1.3	- 101.7
	Kr	+ 23.6	+ 3.3	- 5.2	- 97.7
	N <sub>2</sub>	+ 13.1	- 4.9	- 5.3	- 82.7
HF—HCN	Ar		...		- 32.2
HCN—HF (Ref. 42)	Ar	+ 29.7		...	
Me <sub>2</sub> O—HCN (Ref. 43)	Gas		- 11		- 127
H <sub>3</sub> N—HCN (Ref. 26)	Gas		- 11		- 161

<sup>a</sup> Values in parentheses are shifts calculated

Table 9

Monomer and open chain dimer bands of HCN and DCN in a range of matrices.  
Modified from Ref. 40

mode	gas	Ne	Ar	Kr	Xe	N <sub>2</sub>	CO
HCN							
monomer $\nu_3$	3311.5	3294.7	3303.9	3291.2		3287.5	3258.6
$\nu_1$	2096.9	2091.4	2088.8	2085.6		2096.7	- <sup>c</sup>
$\nu_2$	713.5	718.2	721.5	719.6	718.0	{744.6} {736.8}	{760.8} {738.4}
dimer $\nu_3$ (1)		3306.4	3302.6	3286.0		3282.2	3244.1
$\nu_3$ (2)		3226.2	3202.1	3194.5		3204.8	3200.4
$\nu_1$ (1)		2113	2113.2	2109.2		2109.8	- <sup>c</sup>
$\nu_1$ (2)		2097.1	2092.4	2088.9		2091.8	- <sup>c</sup>
$\nu_2$ (1)		735.2	733.7	731.6	730.9	{757.5} {749.5}	{778} {756}
$\nu_2$ (2)		788.8	{798.0} {797.2}	796.8	794.1	{798.4} {794.2}	{803.4} {793.4}
DCN							
monomer $\nu_3$	2630.3	2620.2	2625.5	2617.4		2616.3	2601.8
$\nu_1$	1925.2	1917.2	1924.5	1919.5		1920.7	1912.8
$\nu_2$	570.3	573.2	575.6	574.9	573.9	{593} {588}	{603} {590}
dimer $\nu_3$ (1)		2626.4	2630.6	2620.5		2617.4	2602
$\nu_3$ (2)		2584.0	2573.2	2567.0		2574.4	2572.5
$\nu_1$ (1)		1921.7	1935.2	1929.2		1928.3	1917.4
$\nu_1$ (2)		1905.4	1900.2	1894.9		1899.2	1898.9
$\nu_2$ (1)		582.1	584.6	584.0	582.1	{609.9} {597}	{615} {602}
$\nu_2$ (2)		620.9	627.9	626.8	624.2	{627.5} {625.8}	{631.8} {620.1}





identified and is presumably approximately equal to the monomer value.<sup>41</sup>

In a related paper, in which the (HCN)<sub>2</sub> dimer was formed by the photodecomposition of s-tetrazine in an Ar matrix, Pacansky<sup>42</sup> reported that the C≡N stretch of the two molecules are found at 2112 and 2093 cm<sup>-1</sup>. However, due to conflicting statements within the paper, it is not clear which frequency is assigned to which half of the dimer. However, the fact remains that for a matrix which contains only HCN dimer, the splitting between the two C≡N stretching frequencies is 19 cm<sup>-1</sup>.

### **Thin Film**

Due to the close similarities of the H<sub>2</sub>O:HCl dimer to the adsorption of HCl on alkali halide surfaces,<sup>28,29</sup> the adsorption of HCN onto the surface of alkali halides should give a good indication of the type of interactions which will be present upon its adsorption to an ice surface. Kozirovski and Folman<sup>43</sup> studied the adsorption of HCN onto several alkali halide surfaces. The spectrum of HCN adsorbed onto a NaCl film shows the  $\nu_1$ ,  $\nu_2$ , and  $\nu_3$  vibrations of HCN (see Fig. 36). The  $\nu_3$  vibration, the C-H stretch, is seen with a maximum at 3145 cm<sup>-1</sup> and a shoulder at 3040 cm<sup>-1</sup>. It is a strong band with a FWHH (full width at half height) of about 200 cm<sup>-1</sup>. The  $\nu_1$  vibration, C≡N stretch, has the same peak intensity as the  $\nu_3$  vibration but has a FWHH of only 20 cm<sup>-1</sup>. Its band center is at 2095 cm<sup>-1</sup> which can be resolved into a doublet with a spacing of 10 cm<sup>-1</sup> under better resolution. The  $\nu_2$  vibration, H-C≡N bend, consists of three different bands located between 700 and 800 cm<sup>-1</sup>. The splitting in the three fundamental

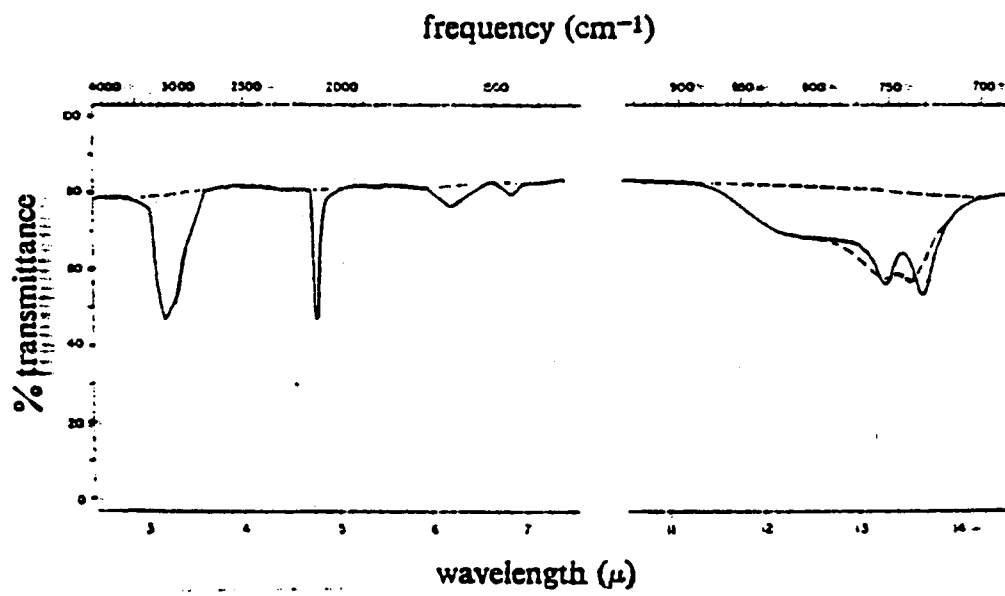


Fig. 36 Spectrum of HCN adsorbed on NaCl films. Taken from Ref. 43

vibrations is explained by the adsorption of HCN with two different orientations on the surface. These two orientations are: a) the HCN standing up perpendicular to the surface with the hydrogen of the HCN pointing towards a  $\text{Cl}^-$  of the surface with the permanent dipole of the HCN, 2.94 D, interacting with the  $\text{Cl}^-$ , and b) the HCN can alternatively be lying on the surface with the hydrogen of the HCN above the  $\text{Cl}^-$  ion and the other end pointing towards a  $\text{Na}^+$ .

The adsorption of HCN onto a film of NaI produces a  $\nu_3$  vibration centered at  $3095\text{ cm}^{-1}$  with a FWHH of only  $100\text{ cm}^{-1}$ . The  $\nu_1$  vibration is at  $2105\text{ cm}^{-1}$  and again is very sharp with no indication of splitting. The  $\nu_2$  mode produces a single broad flat band. The smaller half-width of the C-H stretch and the lack of splitting in the  $\text{C}\equiv\text{N}$  stretch or in the bending motion tends to indicate that the HCN is oriented in a single direction, namely perpendicular to the surface.

The adsorption of HCN onto a CsCl film produces two  $\nu_3$  adsorptions, one at  $3165\text{ cm}^{-1}$  and a stronger one at  $3012\text{ cm}^{-1}$ . The  $\nu_1$  band is again very sharp and centered at  $2085\text{ cm}^{-1}$  with a shoulder at  $2100\text{ cm}^{-1}$ . The  $\nu_2$  absorption at  $820\text{ cm}^{-1}$  does not show any structure. The splitting in the  $\nu_1$  and  $\nu_3$  bands is due to the fact that CsCl, prepared under the conditions of the experiment, produces a mixture of body-centered and cubic lattice structures.

The adsorption of HCN onto Ca-montmorillonite behaves very similarly to the adsorption of HCN onto the alkali halide surfaces.<sup>44</sup> The adsorbed HCN produces a large red shift in the  $\nu_3$  mode and a large increase in the intensity of the  $\nu_1$  mode. The  $\nu_3$

mode is shifted to  $3216\text{ cm}^{-1}$  and appears as a single band. The  $\nu_1$  mode has two bands. The first which is found at  $2100\text{ cm}^{-1}$  is assigned to the adsorption of HCN into the interlayer spaces, while the second at  $2120\text{ cm}^{-1}$  is assigned to the HCN adsorbed to the  $\text{Ca}^{2+}$  ions.

## **H<sub>2</sub>S**

Only a single investigation of the  $\text{H}_2\text{O}:\text{H}_2\text{S}$  complex could be found.<sup>45</sup> It is a theoretical investigation of the  $\text{H}_2\text{O}:\text{H}_2\text{S}$  dimer using the 6-31G\*\* basis at the SCF level. It was found for the mixed dimers, that  $\text{H}_2\text{S}$  acting as the proton donor,  $\text{H}_2\text{O}-\text{HSH}$ , is the most stable structure. Also, the calculated frequencies are only slightly shifted from the monomer values. In a study looking at  $\text{H}_2\text{S}$  adsorbed to an activated alumina surface, the  $\text{H}_2\text{S}$  produces an S-H stretching band centered at  $\sim 2560\text{ cm}^{-1}$  (see Fig. 37) and a bending mode at  $1331\text{ cm}^{-1}$ .<sup>46</sup>

## **SO<sub>3</sub>**

The  $\text{H}_2\text{O}-\text{SO}_3$  complex has been studied by microwave, infrared, and theoretical investigations. The structure of the complex is one in which the oxygen of the water interacts with the sulfur of the  $\text{SO}_3$  molecule. The angle between the S---O bonds is  $103^\circ$ , nearly the tetrahedral angle. The oxygens of the  $\text{SO}_3$  are pushed back, out of the plane of the  $\text{SO}_3$  molecule, by  $2.6^\circ$  (see Fig. 38).<sup>47</sup>

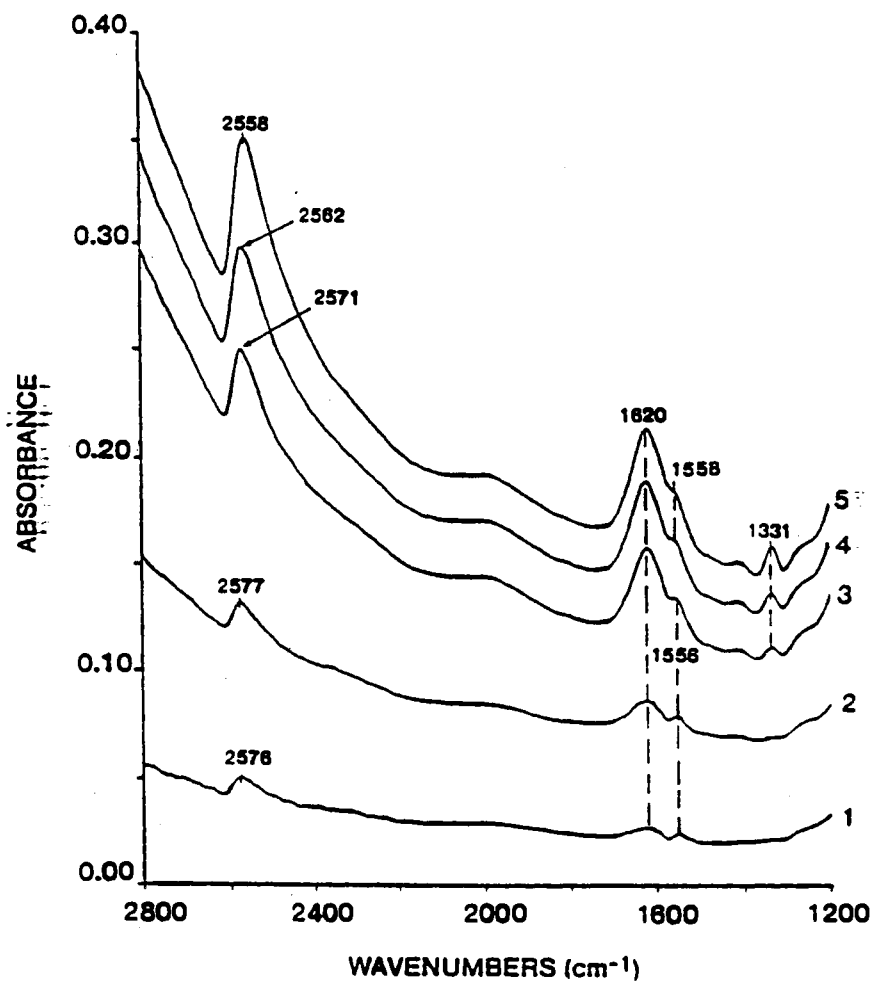


Fig. 37 FTIR spectra (SH-stretch region) of the adsorption of H<sub>2</sub>S on alumina which has been activated at 400°C. The curves show the resultant spectra after exposure to (1) 0.03, (2) 0.06, (3) 0.09, (4) 0.20, and (5) 0.50 mmol of H<sub>2</sub>S. Taken from Ref. 46

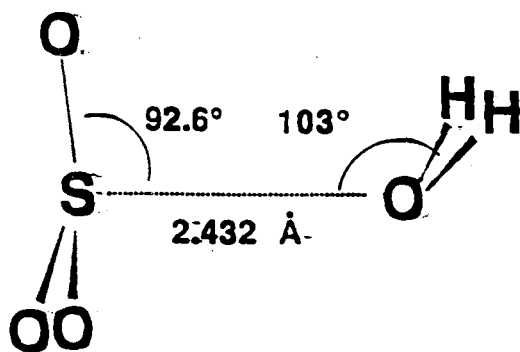


Fig. 38 Structure of H<sub>2</sub>O-SO<sub>3</sub>, drawn in the staggered configuration. The intermolecular torsional angle is not determined. Taken from Ref. 47

## Matrix Isolation

The matrix isolation of H<sub>2</sub>O and SO<sub>3</sub> has been studied by several groups.<sup>48-50</sup> They have identified several bands due to the H<sub>2</sub>O:SO<sub>3</sub> complex. The most relevant of these bands is that of the  $\nu_3$  (antisymmetric stretch) mode, with a vibrational frequency found in the 1390 - 1400 cm<sup>-1</sup> frequency range. There are also bands found in the 2400 - 2500 cm<sup>-1</sup> and in the 1000 - 1100 cm<sup>-1</sup> range due to polymeric SO<sub>3</sub>.<sup>49</sup>

## Theoretical

*Ab initio* molecular orbital theory has been used to study the association reaction of SO<sub>3</sub> with H<sub>2</sub>O to form H<sub>2</sub>SO<sub>4</sub>.<sup>51-53</sup> These studies give the relative energies and barriers to these reactions, and a general insight into the reaction of SO<sub>3</sub> on the surface of ice.

Chen and Plummer<sup>51</sup> performed the first *ab initio* molecular orbital calculation on the SO<sub>3</sub>:H<sub>2</sub>O complex and its reaction to form H<sub>2</sub>SO<sub>4</sub>. Their calculations were at the restricted Hartree-Fock (RHF) level using a 3-21G(\*) basis to obtain the minimum energy structures followed by a single Moller-Plesset (MP2) calculation with the core orbitals frozen. They obtained an SO<sub>3</sub>:H<sub>2</sub>O complex which is stabilized by -21.4 kcal/mol over the isolated reactants (see Fig. 39, dot-dashed line). The transition state (TS) from the SO<sub>3</sub>:H<sub>2</sub>O complex to H<sub>2</sub>SO<sub>4</sub> has an energy of 1.8 kcal/mole, for a barrier of 23.2 kcal/mol. Finally, the H<sub>2</sub>SO<sub>4</sub> is -29.7 kcal/mol more stable than the separated reactants, a value in good agreement with the experimental value of -28.3 kcal/mol.

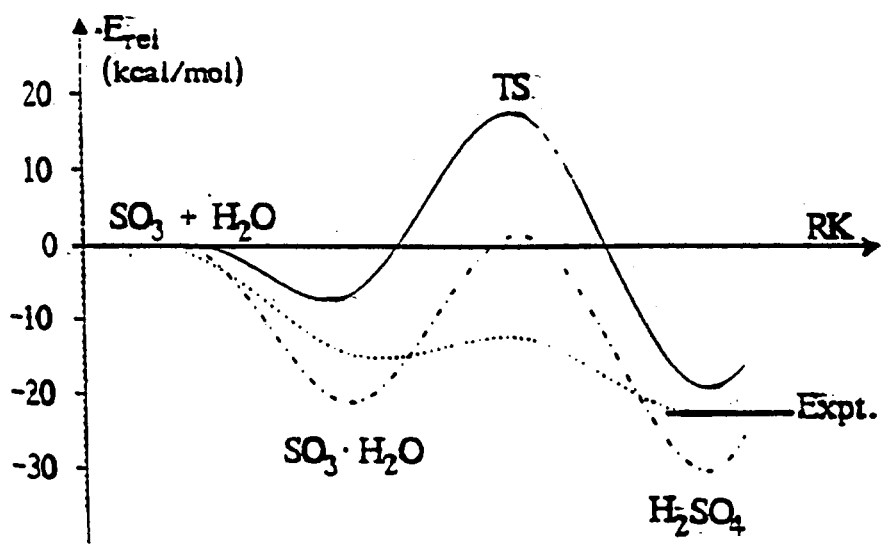


Fig. 39 Comparison of the various computational studies. Also note the experimental reaction data. dotted line: CNDO/2 calculation; dot-dashed line: RMP2(fc)/3-31g\* //RHF/3-21G\*; and solid line: RMP4SDQ(fc)/6-311+G(2df,p)/(RMP2(fu)/6-31G\* + ZPE(RMP2(fu)/6-31g\*). See text for details. Taken from Ref. 51



A later *ab initio* investigation by Hofmann and Schleyer,<sup>52</sup> using a 6-31G\* and 6-31G+\* basis sets at the correlated MP2 level, gave slightly different results. They found that the complex is stabilized by -7.9 kcal/mol over the isolated reactants (see Fig. 39, solid line) compared to Plummer's value of -21.4 kcal/mol. The barrier is found to be 27.0 kcal/mol, a fairly close comparison to Plummer's value of 23.2 kcal/mol, especially when you consider that in either case the barrier is relatively large. This large barrier will inhibit the formation of H<sub>2</sub>SO<sub>4</sub>, a fact which is contrary to experimental evidence.<sup>53</sup>

An explanation for the apparent high reactivity of the H<sub>2</sub>O:SO<sub>3</sub> complex, considering the high activation barrier to the formation of H<sub>2</sub>SO<sub>4</sub>, must be presented. The explanation comes from the addition of a second water molecule to the complex. This alternative reaction was studied by Morokuma and Muguruma<sup>54</sup> at the MP2 and MP4 level with a 6-311+G(d,p) basis set. They found that the energy of the transition state from the SO<sub>3</sub>(H<sub>2</sub>O)<sub>2</sub> complex to H<sub>2</sub>SO<sub>4</sub> is greatly reduced due to the presence of a second water molecule. As can be seen in Fig. 40, the barrier, depending on the path of the reaction, can be as small as 0.7 kcal/mol. This means that the reaction of H<sub>2</sub>O and SO<sub>3</sub> to form H<sub>2</sub>SO<sub>4</sub> can proceed with a much lower barrier (faster rate) than was previously believed, provided that an additional water molecule is available. The structure of these complexes may be seen in Fig. 41.

## SO<sub>2</sub>

The structure of the H<sub>2</sub>O:SO<sub>2</sub> complex is very similar to that of the H<sub>2</sub>O:SO<sub>3</sub> complex. The oxygen of the water interacts with the sulfur of the SO<sub>2</sub> with the

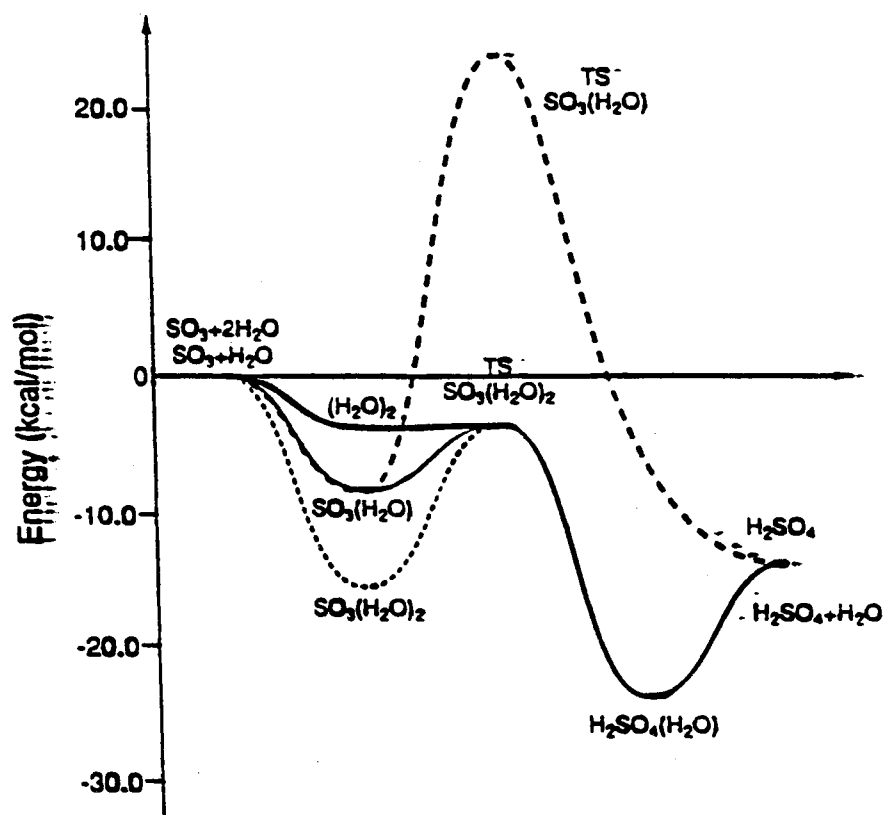


Fig. 40 Potential energy profiles at the MP4SDQ/6-311+G(d,p) level, including the zero-point correction obtained at the scaled HF/6-311+G(d,p) level. Taken from Ref. 54

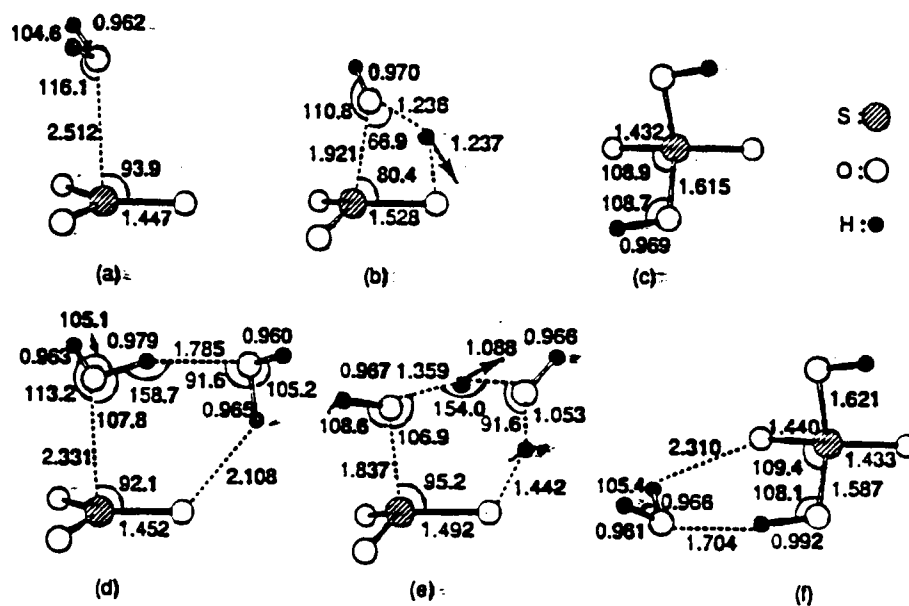


Fig. 41 Optimized geometries, in angstroms and degrees, at the MP2/6-311+G(d,p) level for (a) the complex  $(\text{H}_2\text{O})(\text{SO}_3)$ , (b) the transition state TS1 for  $\text{H}_2\text{O} + \text{SO}_3 \rightarrow \text{H}_2\text{SO}_4$ , (c) the product  $\text{H}_2\text{SO}_4$ , (d) the complex  $(\text{H}_2\text{O})_2(\text{SO}_3)$ , (e) the transition state TS2 for  $2\text{H}_2\text{O} + \text{SO}_3 \rightarrow \text{H}_2\text{O} + \text{H}_2\text{SO}_4$ , and (f) the product complex of  $(\text{H}_2\text{O})(\text{H}_2\text{SO}_4)$ . The arrows at the TSs are the reaction coordinate vectors calculated at the HF/6-311+G(d,p) level. Taken from Ref. 54

hydrogens of the water over the oxygens of the  $\text{SO}_2$  molecule (see Fig. 42).<sup>55</sup> The infrared spectra of this complex<sup>48,50,56</sup> has also been obtained and gives IR absorptions for the antisymmetric stretch of the  $\text{SO}_2$  in the  $1345 - 1355 \text{ cm}^{-1}$  range. The  $\text{SO}_2$ , however, is not reactive as the  $\text{SO}_3$  molecule is.

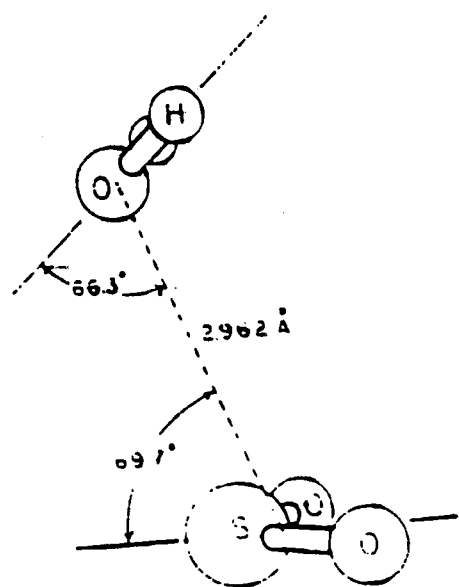


Fig. 42 Molecular structure of H<sub>2</sub>O-SO<sub>2</sub>. Taken from Ref. 55

## **CHAPTER II**

### **EXPERIMENTAL**

#### **Introduction**

We used infrared spectroscopy to investigate the behavior of the ice surface to the adsorption of strong hydrogen-bonding adsorbates. It was conducted using both vapor deposition and cluster techniques to prepare ice surfaces at cryogenic temperatures. Difference spectra were used to see the comparatively weak changes which occur in the OH-stretching region of the infrared spectra.

#### **Equipment**

##### **Introduction**

These experiments initially used thin-film amorphous ice deposited onto a CsI cold window. The adsorbate was deposited over this thin film and allowed to diffuse with increasing temperature. Unfortunately, this setup, although it had its advantages, did not prove to be as advantageous as was originally hoped. Thus, this system was changed from a cold window to a mini cluster cell. The mini cluster cell system was later redesigned to use two vacuum systems; the first of which was used to provide thermal isolation for the cryogenic system, and the second was used for deposition of the ice and the adsorbate. Two different mini cluster cells of slightly different design were used and will be described below.

## **Vacuum System**

The vacuum for this system was provided by a Duo Seal Vacuum Pump model 1402 which was used as the ruffing pump for an oil diffusion pump. This provided the vacuum for the "vacuum line" and the cryogenic cell. A pressure of  $\sim 10^{-5}$  torr could be obtained in this vacuum system as measured by an ionization gauge. The daily check that the system had not developed a leak and was at the minimum pressure was obtained by a Hastings Vacuum Gauge Model VT-5AB. After the system was redesigned to have a separate vacuum system for thermal isolation of the cryogenic cell, the minimum pressure of the second vacuum system was measured with a Hastings Vacuum Gauge model LV-1. The pressure of the system during a deposit was measured by using a Validine gauge model AP10-32 or AP10-42, which measures pressures from 0.01 to 150.00 and 0.1 to 1000.0 torr, respectively.

## **Cryogenic System**

The cryogenic system was an Air Products Cryogenic Refrigerator Model CS202. This refrigerator allowed for a minimum temperature of  $\sim 11$  K for a cold window and  $\sim 22$  K for a mini cluster cell. The end of the cryogenic cold finger had a 45 ohm resistance heater attached which allowed for temperature control. A gold-constantan thermocouple was attached to the end of the cryogenic cold finger. There were also lead-throughs for a diode to measure the temperature of the cryogenic cell, and for a thermocouple and heater for the inlet jet of one of the clusters cells to allow for heating of that inlet jet (described below).

The vacuum shroud which covered the cold finger was actually made of two parts, with the bottom half metal, and the top half glass. They were connected together by a double o-ring seal which allowed the top to be rotated. This was necessary in order to go from making the vapor deposit (where the inlet jets were facing towards the face of the CsI window) to collecting the infrared spectrum (where the IR transparent windows of the shroud top needed to be facing the CsI window).

### **Cryogenic Cells**

The first "cell" used was simply a CsI plate attached to the end of the cryogenic cold finger. In this setup, a jet of H<sub>2</sub>O vapor was directed towards the CsI plate where the H<sub>2</sub>O vapor formed a thin film amorphous deposit at ~11 K. Then, a thin layer of the adsorbate could be adsorbed onto the deposit.

Later this window was replaced by a mini cluster cell. The original mini cluster cell used was approximately 1 inch in length and 0.5 inches in width (see Fig. 43). It screwed into the top of the cryogenic coldfinger and was designed to be enveloped by a radiation shield, and a vacuum maintained by the vacuum shroud. The inlet jet into the cell was thermally isolated from the rest of the cluster cell through a piece of non-thermally conducting plastic. This kept the inlet jet at a temperature of no less than 120 K, even when the cluster cell itself was at its minimum temperature (22 K). Further, the inlet jet was directed towards the windows of the cluster cell so that any adsorbate let into the cell was directed towards the cluster deposit. This allowed for the deposition of



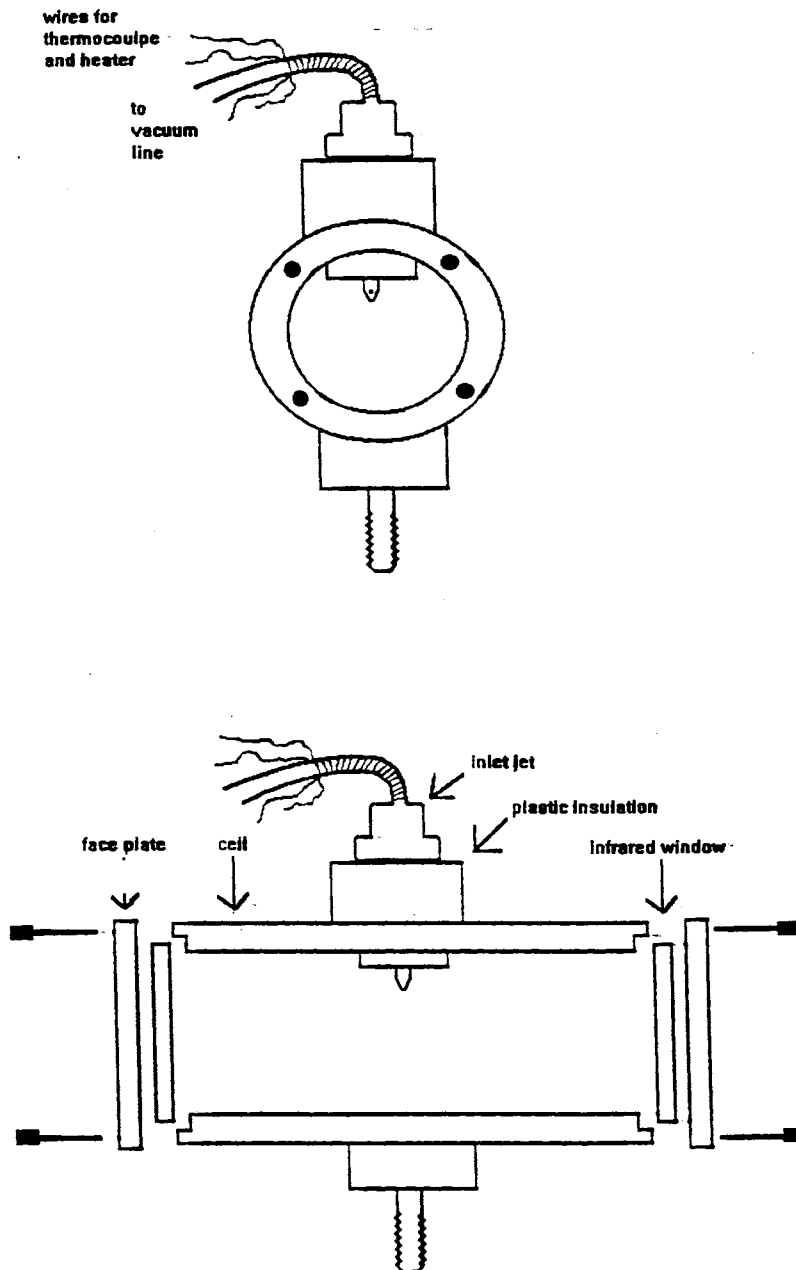


Fig. 43 Drawing showing the major features of the mini cluster cell.

the HCl, DCl, HBr, and DBr onto clusters at ~20 K, well below the temperature at which the acids have any appreciable vapor pressure or mobility on the cluster surface.

The second mini cluster cell was similar in design to the first with the exception of the inlet jet. The inlet into the cell was nondirectional and simply pointed into the center of the cell. It also was connected directly to the cell without anything to provide thermal isolation of the inlet jet. The advantage of the second cell was that any adsorbate which did make it to the cluster deposit was indeed a true adsorbate, as compared to the first mini cluster cell where the "adsorbate" was actually being deposited on top of the cluster deposit. Also, due to the design of the cluster cell, this cell had no leak problems which the first mini cluster cell had, presumably due to the inability to completely seal the plastic-to-metal connections of the first mini cluster cell, see Fig. 43.

### **FT-IR Instrument and Computer**

The FT-IR absorbance spectra were collected by using a Bio-Rad FTS-40 spectrometer. It was originally connected to a Digilab 3280 data system which was later upgraded to a HP 486 66Mhz DX2 computer. The spectra were collected using triangular apodization at a resolution of  $2\text{ cm}^{-1}$ . A few of the last experiments used a resolution of  $4\text{ cm}^{-1}$ . A background single-beam was collected using 500 to 1000 co-added scans and the absorbance spectra using 100 to 400 scans. The lower values were generally used in the thin-film experiments with the higher values being used in the later cluster cell experiments. The HP 486 along with the upgraded software allowed for

extensive data evaluation and manipulation and was a great help in the examination of the data.

## **Procedure**

### **Introduction**

The procedures followed during the course of these experiments were slowly changed and improved, but a general description of the methods used will be given along with the best procedures as they are currently understood.

### **Thin Films**

Thin films of amorphous ice were deposited at the minimum temperature of the system. This temperature generally averaged 11-12 K. A 0.5 to 1.0 micron thick thin film of amorphous ice, as measured by the formation of newton rings, was deposited on the CsI window and then covered with a thin deposit of acid (HCl, DCl, HBr, or DBr). After the deposit was prepared, the cell was placed into the FT-IR where the absorbance spectra were collected. The temperature of cell was generally increased in 10 K steps to 20, 30, 40 K, etc. with an absorbance spectra collected at each step. These spectra can then have a standard bare (no adsorbate) spectrum subtracted from them in order to allow the changes which have occurred to be observed.

## Clusters

With the discovery that clusters formed in the aerosol will deposit and become suspended on the windows of a cluster cell, a procedure was adopted to take advantage of this process. A 1% water vapor in Helium mixture was injected into the mini cluster cell to a pressure of 100 to 200 torr. This mixture, which clustered upon entering the cell, was allowed to stand in the cell for ~10 seconds and was then evacuated from the cell. This process was repeated over and over until a deposit of nanoclusters had become suspended on the windows of the cluster cell thick enough to be optimized for the experiments. The temperature of the cell during the deposition of the clusters was ~88 K. After the clusters had been deposited, the deposit was generally annealed for 10 to 60 minutes to at least 100 K or a temperature at least 10 K higher than that at which the adsorbate experiment was to be conducted. After the clusters had been annealed, the temperature was lowered to that at which the adsorbate was to be adsorbed.

The adsorbates were studied by two different procedures. The first of which was as the adsorbate slowly coated the clusters, to see the effects of percent surface coverage. This procedure was followed for all of the adsorbates. The second procedure that was used was after the surface was fully coated, the temperature of the sample was increased in order to see the effects of temperature upon the adsorbate coated deposit. This second procedure was used almost exclusively for the HCl, DCl, HBr, and DBr deposits. The adsorbates were also deposited at the lowest temperature at which they would adsorb, with the exception of the HCl, DCl, HBr, and DBr which were all deposited at the minimum temperature of the cluster cell.

## **Difference Spectra**

After the spectra of the adsorbate-coated clusters have been collected, the difference spectra between the coated (or partially coated) and bare (or less partially coated) deposits can be examined. The use of difference spectra allows for the elimination of the bulk intensity, and allows the changes which are occurring on the surface of the clusters to be followed. However, care must be taken when interpreting difference spectra because they are a composite of negative and positive bands imposed on top of each other due to the shifting of infrared vibrational intensity.

## CHAPTER III

### ACID COATED THIN FILMS AND CLUSTERS

#### General

The investigation of the interaction of HCl with ice surfaces started with the adsorption of HCl onto thin-film amorphous ice in order to reproduce the already established spectra of the HCl hydrates and to familiarize ourselves with the HCl-H<sub>2</sub>O system. Next, the molecular adsorption of HCl onto the surface of thin-film amorphous ice was attempted in order to see the molecular complex formed between the HCl and the H<sub>2</sub>O surface. Unfortunately, even at the lowest temperature obtainable by our system, the HCl still proved to be reactive with the ice surface, shedding doubt upon the existence of the molecular complex between the HCl and the H<sub>2</sub>O surface. This doubt was due to the fact that the molecular complex formed between the HCl and the H<sub>2</sub>O surface and one of the bands due to the ionization of the HCl on the surface are both broad bands in the 2500 cm<sup>-1</sup> region. Although the molecularly adsorbed HCl should be found in the lower 2500 cm<sup>-1</sup> region and the ionized HCl band in the upper 2500 cm<sup>-1</sup> region, no clear distinction could be found between these two bands. In an attempt to distinguish between these two bands, three alternative acids were also investigated: namely, DCl, HBr, and DBr. These systems were used in hopes that the separation between the bands due to the molecularly adsorbed and the surface ionized species would be large enough that the two bands would be observable separably, and hence distinguishable.

Next, the thin-film amorphous ice system was switched to crystalline nanoclusters suspended on the IR transparent windows of a cluster cell in an attempt to form a surface which was less reactive to the adsorbed HCl. Further, the results obtained with the crystalline nanocluster surface could be used to compare to the computational results of Clary *et al.*<sup>34-36</sup> This surface, although slightly less reactive to the adsorbed HCl, still proved to be a very reactive surface.

The final attempt to limit the reactivity of the HCl with the ice surface was to coadsorb the HCl onto the ice surface with of a second, weak adsorbate. Due to the experimental setup, the weak adsorbate entered the cell prior to the HCl and coated the ice surface. Then, when the HCl did finally enter the cell, it was actually adsorbed onto a cluster surface which had been precoated with a weak adsorbate. The HCl then diffused through or displaced the weak adsorbate on the ice surface. Thus, the HCl reached the ice surface with a much lower energy, which in turn lessened its reactivity with that surface.



The amorphous HCl mono-, di-, tetra-, and hexahydrates have already been presented in Fig. 16. They are prepared by depositing the appropriately mixed samples at a relatively low temperature. One more bit of information is needed. At what temperatures are these hydrates formed, starting from the amorphous monohydrate or a water surface which has been exposed to an excess of acid and left to react? Figure 17 shows this information for a 1:1 H<sub>2</sub>O:HCl(HBr) mixture which was deposited and then

warmed. When the sample is warmed to 155, 195, and 215 K, the crystalline mono-, di-, and tetrahydrates are formed, respectively, with the excess HCl being expelled into the gas phase as each higher hydrate in the sequence is formed. A very similar series can be produced if a thin-film amorphous deposit of water is exposed to HCl, with the exception that the amorphous monohydrate will be slowly formed until the complete conversion is accomplished by 120 K.

As has already been stated, there is a very distinct and easily noticeable change in the IR spectrum upon formation of the hydronium ion, the formation of the bands at approximately 2100, 1700, and 1100  $\text{cm}^{-1}$ . These three bands which are used to determine if there is any ionization of the acid on the ice surface.

One final comment, as is shown in Fig. 18, when an ice surface is exposed to an acid, it is the lower hydrates which are formed first, with the higher hydrates only forming after greater exposure.

## **Thin Film**

### **Introduction**

The initial attempt to identify the molecular complex of HCl with an ice surface was performed on thin-film amorphous ice. This ice surface was chosen due to the high surface area along with the long lived stability of the ice at any given condition.

The acids which were studied on the amorphous ice surface are HCl, DCl, HBr, and DBr. These acids were chosen not only due to their importance in upper atmospheric chemistry, but also due their volatility which allowed them to reach and then diffuse on



the ice surface. HCl was the molecule of major interest with DCl and HBr being used as parallel systems for comparison. The DBr was included for completeness.

## HCl

The deposition of HCl onto a thin-film amorphous ice deposit produced several changes in the IR spectrum. These changes reflected the formation of the molecular complex between the HCl and the ice surface, a thin film of acid deposited on top of the amorphous ice, the formation of the hydronium ion bands, and complicated changes within the OH-stretching region of the ice spectrum. Each of these issues will be addressed in order.

The changes which occurred in the OH-stretching region of the IR spectrum are at this point too complicated to be explained. They will, however, be addressed later after a more thorough understanding of the behavior of strong hydrogen-bonding adsorbates has been developed.

In the initial experiments, when the HCl was deposited onto the amorphous ice at 15 K, this deposition was accompanied by the reaction of the acid with the ice surface to form the hydronium ion. This reaction was presumably due to the excess thermal energy which the acid possessed and then released upon deposition. This energy which these molecules released upon deposition increased the local temperature and allowed for the ionization of the acid on the ice surface. In an attempt to reduce or actually eliminate this reaction, great care was taken to reduce the rate at which the acid was deposited. In this way, the energy released to the surface upon adsorption of an acid molecule would

have a chance to disperse before the next molecule would adsorb and release its energy into the same area of the surface. After several times modifying the method of depositing the acid, a method was finally found which resulted in the deposition of the acid to nearly eliminate its reaction with the surface.

As has already been stated, the OH-stretching region will be discussed later. The only other major features are the bands centered at approximately 2750 and 2540  $\text{cm}^{-1}$  (see Fig. 44). These bands are due to the amorphous HCl layer formed on top of the amorphous ice and the molecular complex formed between the HCl and ice surface, respectively. As will be seen, the molecular complex increases in intensity as the sample is warmed. Predictably, the amorphous HCl overlayer decreases in intensity, presumably due to diffusion of the HCl into the pores of the amorphous ice and, ultimately, from vaporization and/or more general reaction. Further, one would expect only limited diffusional motion of the HCl into the micropores of the ice at 15 K, so that only adsorption at the bulk interface of the HCl overlayer and the ice deposit is expected.

Upon warming the sample from its minimum temperature of approximately 15 K to 40 K, there are no major changes which take place below 2300  $\text{cm}^{-1}$ . This signifies that there is no hydronium ion formed, since it has three prominent bands at 2100, 1700, and 1100  $\text{cm}^{-1}$ , and hence, no ionization of the acid on the ice surface. Also, as the sample is warmed to 40 K, there is an increase in the intensity of the molecular complex band. This increase with the lack of formation of any bands below 2300  $\text{cm}^{-1}$  signifies the growth of the molecular complex of HCl with the ice surface. However, there was

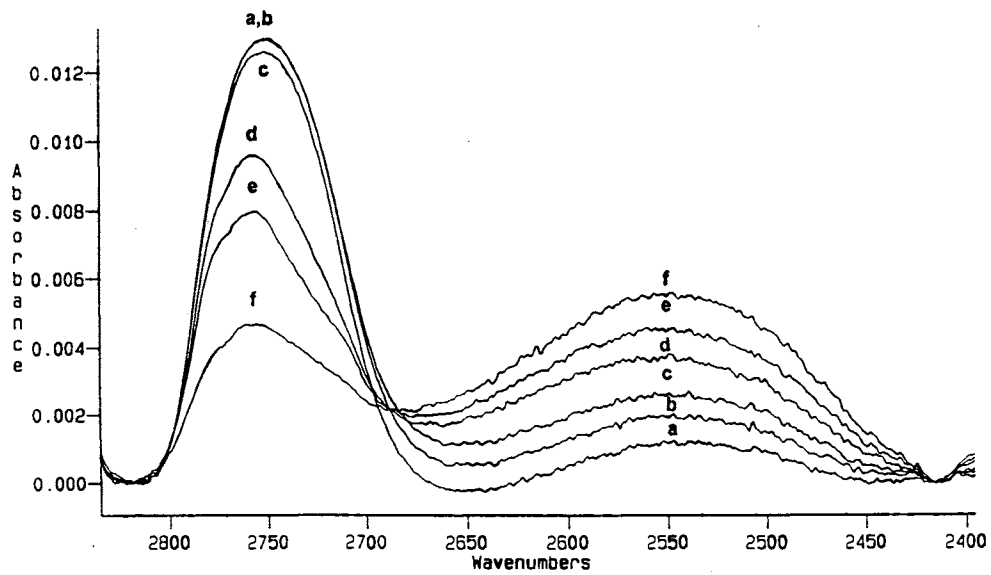


Fig. 44 Infrared spectra showing the changes which occur as an HCl coated thin film deposit is warmed from nominally a) 12 to f) 60 K. The 2750  $\text{cm}^{-1}$  band is the HCl overlayer and the 2550  $\text{cm}^{-1}$  band is due to the "molecular complex".

one reservation. The increase in the intensity in the  $2675\text{ cm}^{-1}$  region does indicate the possibility that a limited amount of ionization of the acid has taken place, so little that the hydronium ion bands below  $2300\text{ cm}^{-1}$  are not detectable spectroscopically. Thus, the conclusion that the  $2540\text{ cm}^{-1}$  band is due to the molecular complex stands firm.

As the temperature is increased to 60 K, the intensity of the "molecular complex" continues to increase, and the intensity of the HCl overlayer decreases. Also, as the temperature is increased above 40 K, bands form at 2100, 1700, and  $1100\text{ cm}^{-1}$  indicating the formation of the hydronium ion from the dissociative ionization of the HCl on the ice surface. The question then became, is the growth in the "molecular complex" band in the  $2500\text{ cm}^{-1}$  region as the temperature is increased above 40 K due to the actual formation of more molecularly complexed HCl with the ice surface, or is it due to one of the higher frequency hydronium ion bands which, to this point, has been ignored.

There are two possibilities for the increase in intensity in the  $2540\text{ cm}^{-1}$  region due to the hydronium ion. They both include the ionization of the HCl to form an amorphous hydrate on the surface. The first is the formation of the amorphous monohydrate which contains a strong adsorption peak at  $2548\text{ cm}^{-1}$ .<sup>25</sup> This possibility, however, is not seriously considered due to the breadths of these two bands. The FWHH of the  $2548\text{ cm}^{-1}$  band due to the hydronium ion is approximately  $300\text{ cm}^{-1}$ , the FWHH of the "molecular complex" band is only approximately  $150\text{ cm}^{-1}$ , too narrow to be due to the amorphous monohydrate. Also, the amorphous monohydrate has a second strong band at  $3144\text{ cm}^{-1}$ . There is no sign of this band, signifying that the amorphous monohydrate is not formed. This idea, although not readily supported by the work done

on the amorphous ice, will become more apparent after looking at the adsorption of HCl onto crystalline ice clusters.

The second possibility is the formation of the amorphous dihydrate. It contains a comparatively weak, broad band at  $2540\text{ cm}^{-1}$  which can be adding to the intensity in the  $2700 - 2400\text{ cm}^{-1}$  region. Again, due to the complicated changes which occur in the OH-stretching region upon warming the amorphous ice, support for this possibility will also have to wait until the discussion of HCl adsorbed to crystalline ice clusters. However, the formation of the amorphous dihydrate will explain the gentle increase in intensity in the  $2675\text{ cm}^{-1}$  region. Figure 44 shows the increase in the "molecular complex", the loss of the HCl overlayer, and the increase in intensity at  $2675\text{ cm}^{-1}$  upon warming the sample from nominally 10 - 60 K using 10 K increments.

Since it has now been determined that the HCl overlayer begins to react (ionize) with the ice surface at 40 K, let's look at what happens as the sample sits at a slightly higher temperature for an extended period of time. A sample was prepared and an HCl overlayer was deposited. The temperature was increased stepwise as was normally done to 40 K but was then increased to 45 K and allowed to stand. Spectra were collected occasionally and the changes in the spectra were recorded (see Fig. 45). No reaction took place as the temperature of the sample was increased to 40 K, but when the sample was increased to 45 K, a weak band formed at  $2100\text{ cm}^{-1}$  indicating the formation of the hydronium ion and the reaction (ionization) of the HCl with the surface. As the sample was held at 45 K, the "molecular complex" band continued to grow as well as the hydronium ion band at  $2100\text{ cm}^{-1}$ . Thus, the band at  $2540\text{ cm}^{-1}$  is due to the molecular

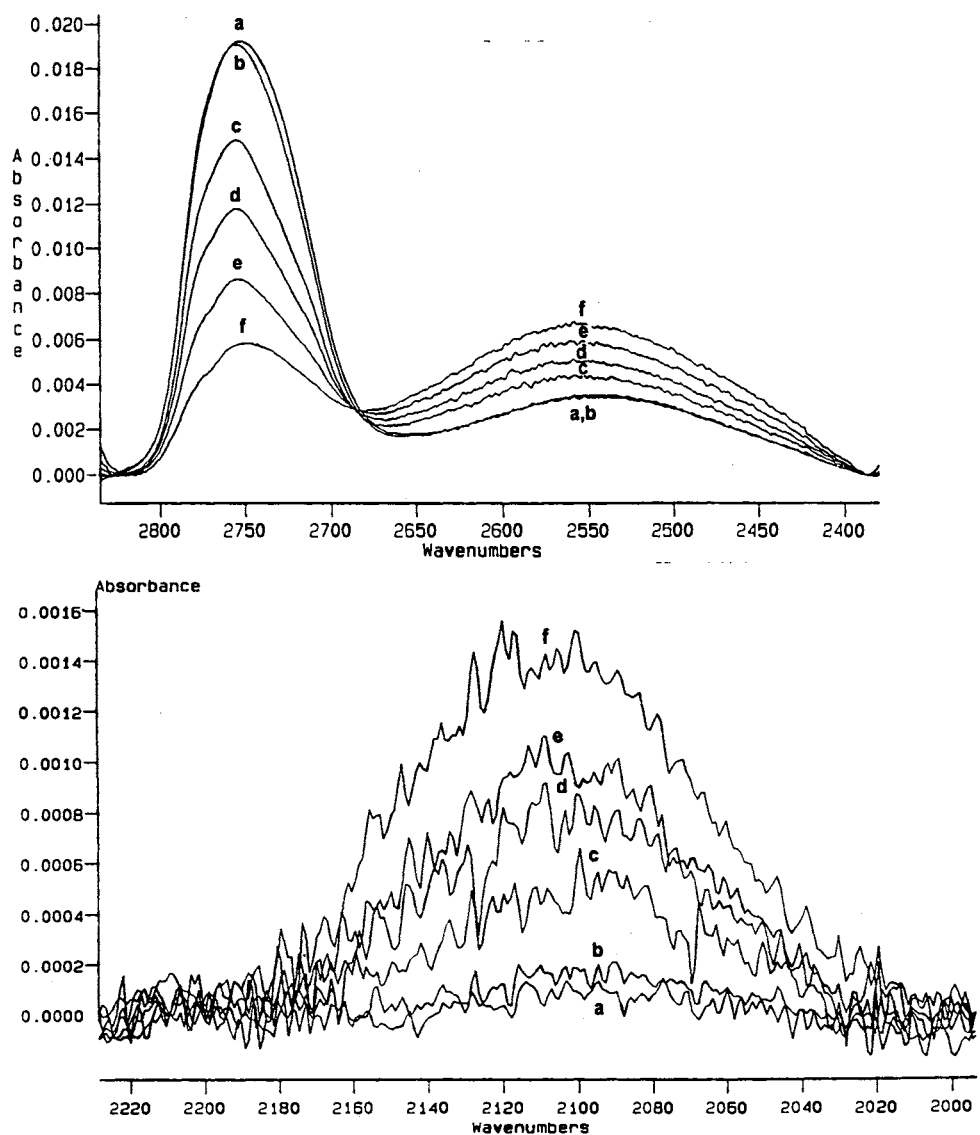


Fig. 45 Infrared spectra showing the changes which occur as an HCl coated thin film deposit is warmed from 40 to 45 K and then held at 45 K for 48 hours. As the sample is warmed from (a) 40 to (b) 45 K, very little change occurs in the spectra. However, as the sample is held at 45 K for (c) 6, (d) 12, (e) 24 and (f) 48 hours, the acid overlayer reacts with the cluster surface forming the acid hydrates of HCl.

complex of HCl with the ice surface below 40 K, and is the composite of the molecular complex band and a band due to the hydronium ion above 40 K.

## DCl

In order to verify that the  $2540\text{ cm}^{-1}$  band is at least in part due to the molecular complex above 40 K, deuterated hydrogen chloride was also investigated as an adsorbate. The band for the molecular complex of  $\text{D}_2\text{O}:\text{DCl}$  will have a peak in the  $1800\text{ cm}^{-1}$  range,<sup>30,33</sup> while the reacted (ionized) product,  $\text{OD}_3^+\text{Cl}^-$ , has its nearest bands at  $2000$  and  $1545\text{ cm}^{-1}$ .<sup>24</sup> Thus, there are no bands due to the reaction of DCl with the surface which will be coincident with the molecular complex. Therefore, if the DCl mimics the behavior of the HCl when it is deposited on the ice surface, this will be good evidence that the molecular complex does in fact exist at temperatures above 40 K. As is seen in Fig. 46, the DCl deposited on an ice surface does in fact mimic the behavior of HCl, and increases in intensity by approximately a factor of five as the temperature of the sample is increased from 15 to 60 K.

In a related experiment, 5 layers of DCl were sandwiched between 6 layers of amorphous ice in an attempt to increase the intensity of the molecular complex and reaction (ionization) product bands. This sample was then followed using the procedures of the previous experiments. As is seen in Fig. 47, at 30 K there is no band formed in the  $2000\text{ cm}^{-1}$  region due to the deuterated hydronium ion. Therefore, there is no ionization of the DCl at this temperature. After the temperature is increased to 50 K, there is an increase in the intensity of the baseline, thus signifying the formation of the

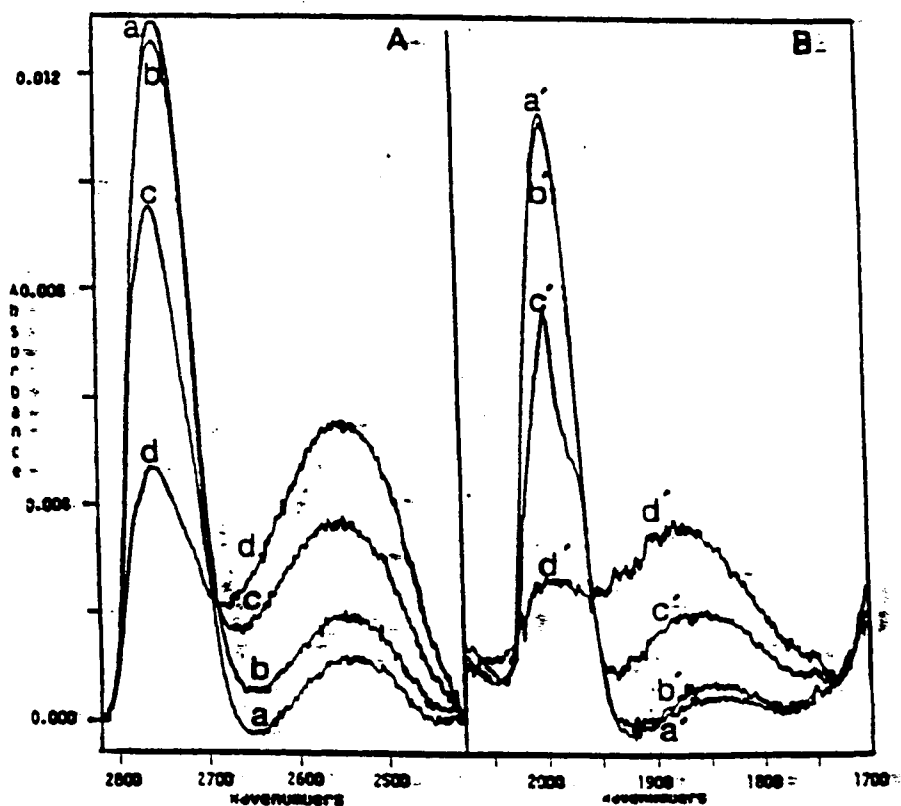


Fig. 46 (A) Infrared spectrum (a) of a  $0.05 \mu\text{m}$  layer of amorphous HCl on a  $1.5 \mu\text{m}$  film of microporous amorphous ice prepared at 15 K. Curves b - d are for a sample warmed and held for 10 min at 20, 40, and 60 K. (B) Infrared spectrum (a') of a  $0.05 \mu\text{m}$  layer of amorphous DCl on a  $1.5 \mu\text{m}$  film of microporous amorphous D<sub>2</sub>O ice prepared at 15 K. Curves b' - d' are for a sample warmed and held for 10 min at 20, 40, and 60 K.



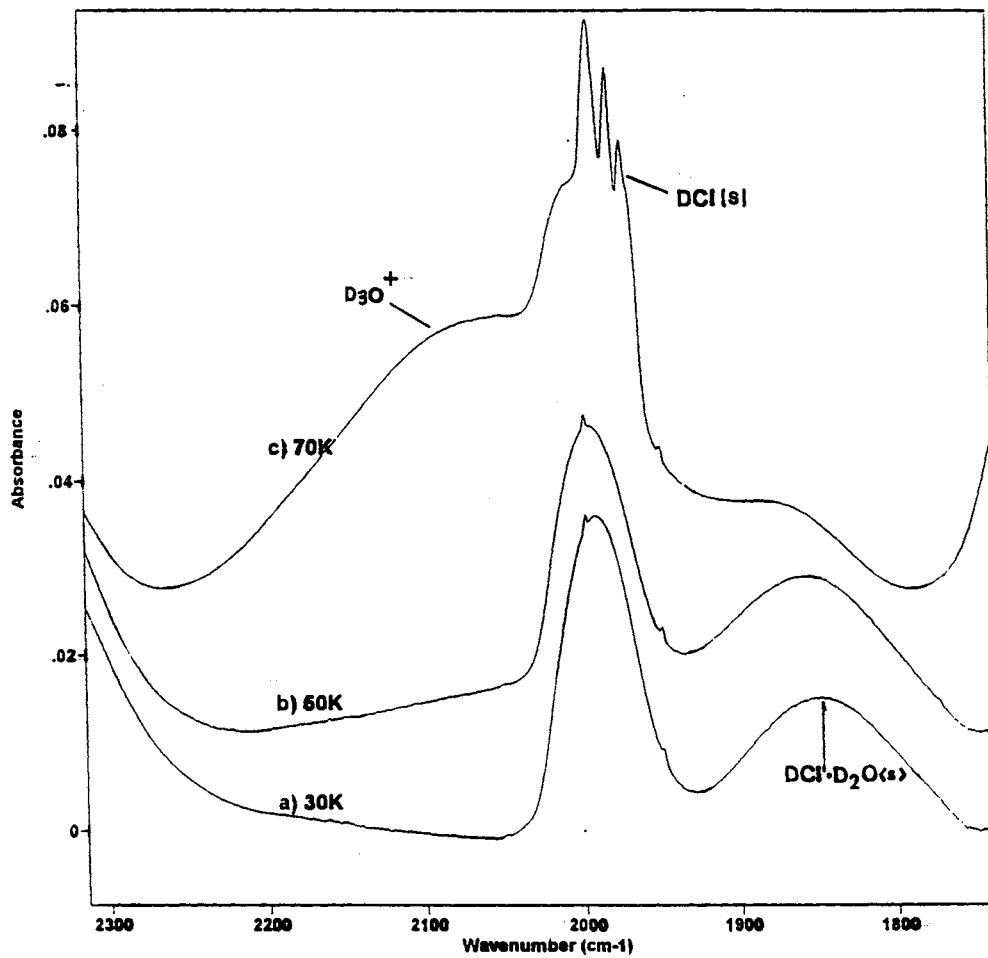


Fig. 47 Infrared spectrum of five amorphous DCl layers sandwiched between six layers of microporous amorphous ice deposited at 13 K. Curves a - c show the formation of the deuterated hydronium ion and the loss of the molecular complex at 30, 50, and 70 K.

deuterated hydronium ion. Notice from the  $1850\text{ cm}^{-1}$  band that the molecular complex of the DCl with the ice surface is still present and as intense as it was in the 30 K spectrum. When the temperature is increased to 70 K, there is a large increase in the intensity of the deuterated hydronium ion and a substantial reduction in the intensity of the molecular complex. However, the molecular complex is still present even at 70 K.

## **HBr**

As one final check on the existence of the molecular complex on an amorphous ice surface, HBr was deposited onto amorphous ice. The  $\text{H}_2\text{O}:\text{HBr}$  molecular complex, as predicted by matrix isolation, should be found around  $2280\text{ cm}^{-1}$  with the corresponding band due to the hydronium ion at  $2590\text{ cm}^{-1}$ .

Figure 48 shows the changes which occur in the HBr coated amorphous ice as the temperature is increased from 20 to 60 K. This picture is complicated greatly due to the contamination of the HBr by HCl, and by the increased reactivity of the HBr compared to the HCl. The bands at  $2750$  and  $2440\text{ cm}^{-1}$  are the amorphous HCl and HBr overlayer bands, respectively. The band which forms at  $2560\text{ cm}^{-1}$  is due to the HCl molecular complex and/or hydronium ion. The big broad band in the  $2400$  through  $2000\text{ cm}^{-1}$  region is most likely due to several different bands, two of which are the HBr molecular complex and the  $2100\text{ cm}^{-1}$  band of the hydronium ion. However, the molecular complex of the HBr with the amorphous ice surface has been identified. If the difference spectrum is taken between the 40 and 60 K samples and subtracted to eliminate the hydronium ion

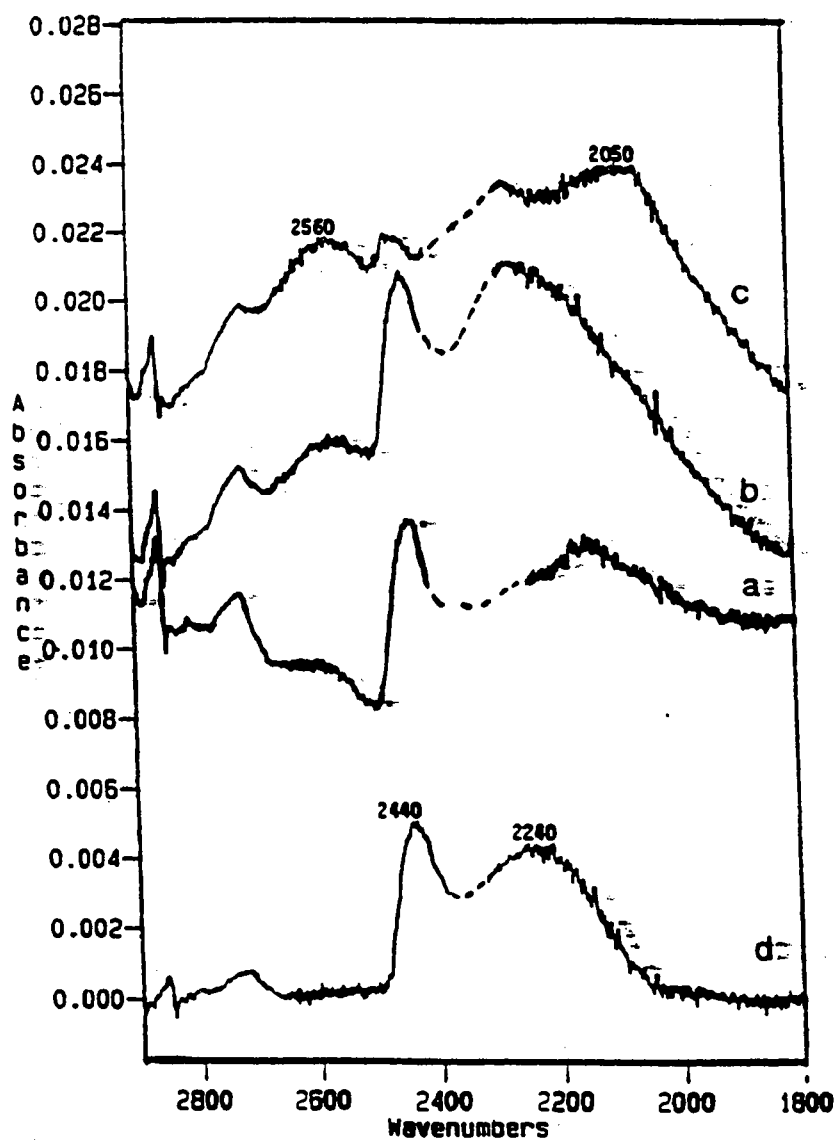


Fig. 48 Infrared spectrum of amorphous HBr on a film of microporous amorphous ice at (a) 20 K, and warmed to (b) 40 and (c) 60 K. Curve d is the difference spectrum obtained by subtraction of  $0.7 \times$  curve c from curve b.

from the 40 K spectrum, what is left are the bands at 2440 and 2240  $\text{cm}^{-1}$  due to the HBr overlayer and the molecular complex, respectively (see Fig. 48d).

## **DBr**

The observation of the DBr molecular complex, although tried, was quickly abandoned because of the complexity of the spectrum. Hydrogen and chloride contamination caused the presence of four species; DBr, HBr, HCl, and DCl. Also, the DBr molecular complex was predicted to be at 1657  $\text{cm}^{-1}$ , a region of the spectrum where several other bands are found. For these reason, the use of DBr as an adsorbate was abandoned.

## **Clusters**

### **Introduction**

In an attempt to find a surface which was less reactive to the adsorption of the acid and to observe the changes which were taking place in the OH-stretching region of the spectrum, HCl, DCl, and HBr were all adsorbed onto crystalline nanoclusters. This surface was made possible due to the discovery of a technique which allowed for the suspension of the aerosol clusters onto the windows of a cluster cell. These suspended clusters proved to be stable in time which allowed for the investigation of HCl, DCl, and HBr on their surface. Also, since these clusters were formed at a higher temperature (nominally 90 K, and often annealed to an even higher temperature) they were free of

any thermal annealing upon deposition of the acid at 20K or upon warming the sample to 70 K. Finally, the setup of the experiment allowed for the collecting of a background spectrum, bare cluster spectrum, and then acid-coated cluster spectrum for each deposit at the time of the experiment. This was not possible with the amorphous thin-film deposits. For the thin-film deposits, the background and bare ice spectrum had to be collected prior to the experiment which allowed for slight mismatches to occur. These mismatches occurred due to slight changes in the alignment of the instrument and the inability to exactly reproduce identical thin-film deposits.

## HCl

The first attempts to deposit HCl molecularly onto a suspended cluster deposit was, for the most part, unsuccessful (see Fig. 49). Although a large "molecular complex" band was formed, there was also a large amount of reaction between the HCl and the cluster surface.

In another experiment, this time where the HCl was deposited onto the cluster surface in small aliquots, a pattern was observed similar to the deposition of HCl onto the LiF surface as was seen by Blass.<sup>29</sup> The molecular complex, when very first formed, has a band center at  $2480\text{ cm}^{-1}$  (see Fig. 50). This band center then shifts to higher frequency,  $2525\text{ cm}^{-1}$ , as more HCl aliquots are deposited and the intensity of the "molecular complex" band increases. This shifting in frequency is presumably due to changes in the way the HCl interacts with the surface as more acid is added, a crowding effect which will be discussed more later. However, as more HCl is deposited, the

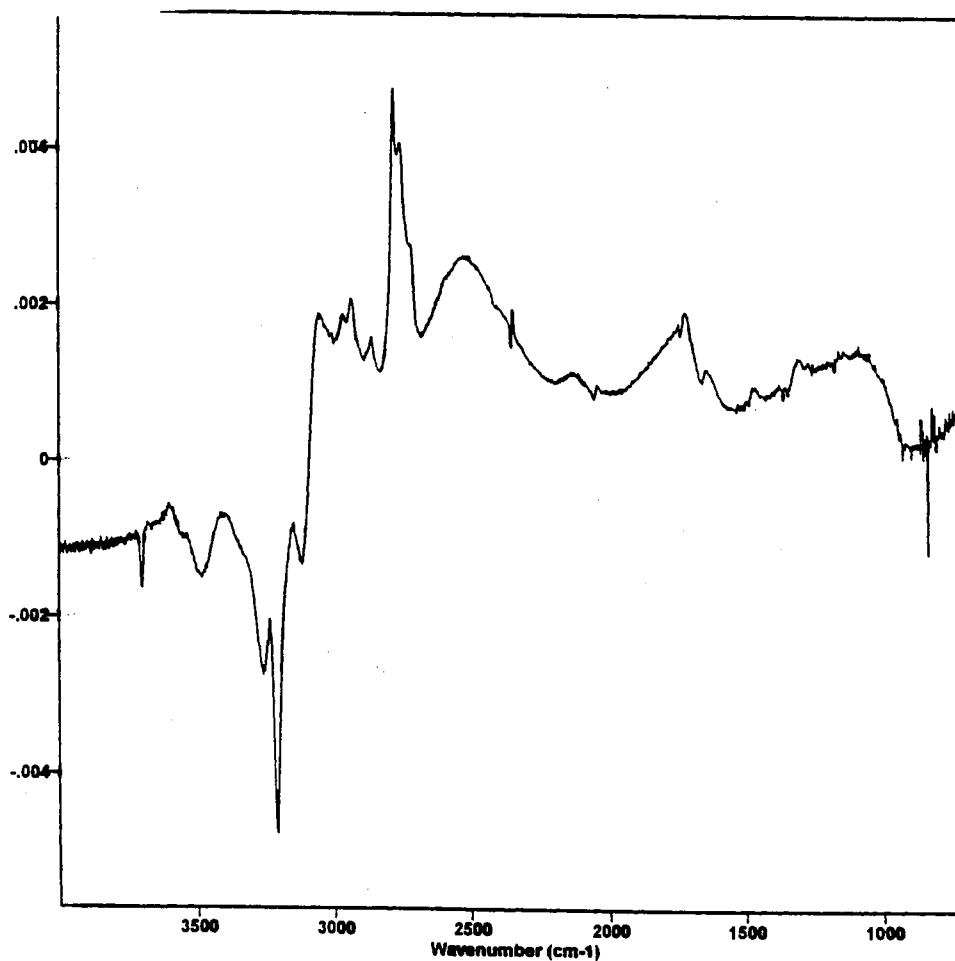


Fig. 49 Difference spectrum of the HCl coated minus bare clusters showing the reaction of the HCl with the ice surface to form the hydronium ion. The spectral features are: loss of the antisymmetric stretch of the d-H ( $3694\text{ cm}^{-1}$ ), d-O ( $3560\text{ cm}^{-1}$ ), and S-4 ( $3490\text{ cm}^{-1}$ ); loss of the symmetric stretch of the d-H, d-O, S-4, and interior ice ( $3400 - 3000\text{ cm}^{-1}$  region); and formation of the acid overlayer ( $2750\text{ cm}^{-1}$ ), "molecular complex" ( $2550\text{ cm}^{-1}$ ) and the hydronium ion ( $2100, 1700, \text{ and } 1100\text{ cm}^{-1}$ ).

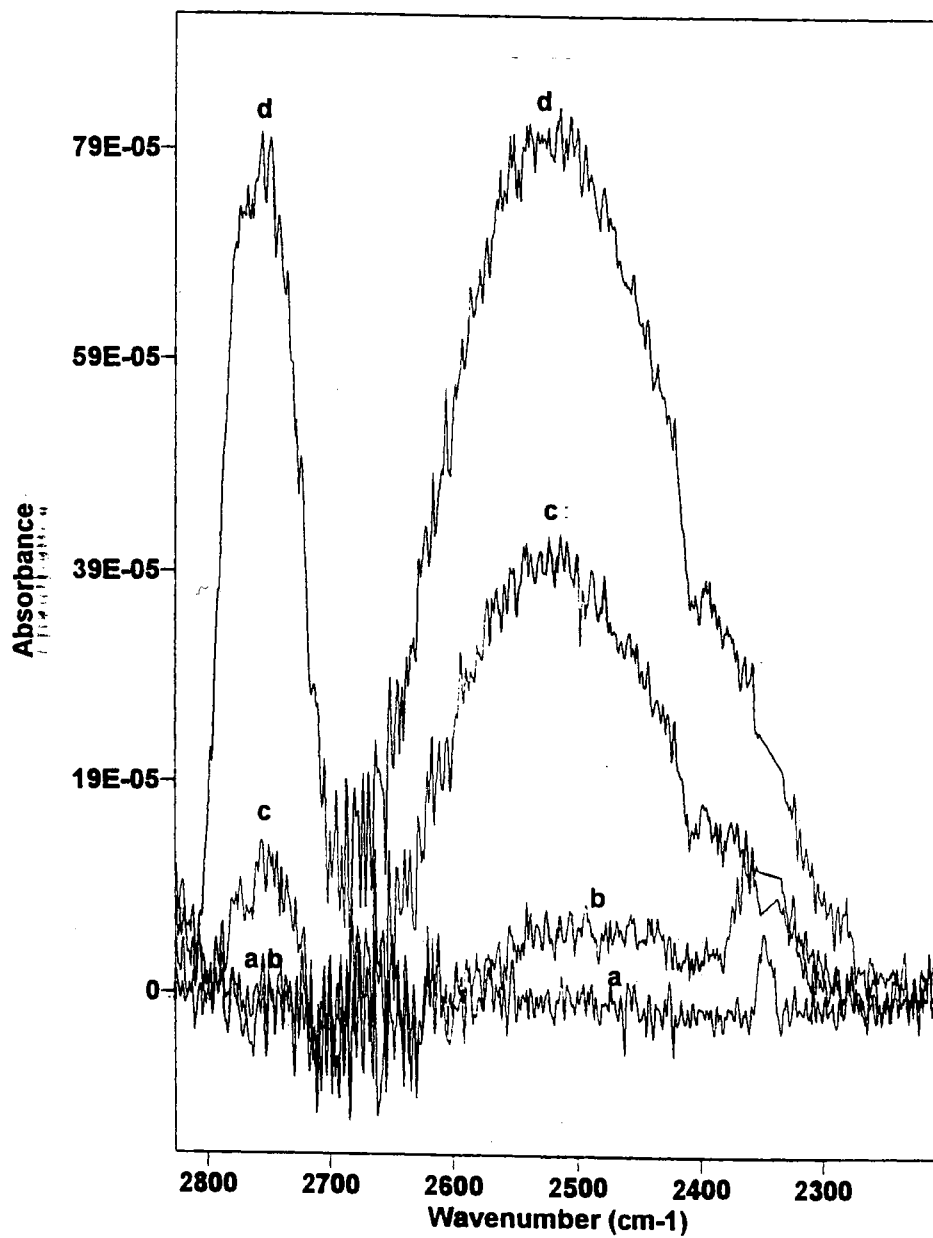


Fig. 50 Curves a - d show the formation of the molecular complex (first appearing at  $2480\text{ cm}^{-1}$  and then growing in at  $2525\text{ cm}^{-1}$ ) and acid overlayer ( $2750\text{ cm}^{-1}$ ) as successive aliquots of HCl are deposited on a cluster deposit.

2100  $\text{cm}^{-1}$  band of the hydronium ion also increases in intensity. Alternatively, this increase in frequency can also be due to the ionization of the acid on the cluster surface, thus changing the nature of the surface and the frequency of the molecular complex. This idea is discussed further below. Also, since the HCl has ionized on the cluster surface, this increase in intensity of the molecular complex could be due to the formation of one of the higher frequency hydronium ion bands. However, due to the lack of any other corresponding high frequency hydronium ion band, this shift in frequency of the molecular complex is believed to be due to one or both of the two previous possibilities.

The minimum temperature of this cluster cell was about 30 K. This was only 15 K below the temperature at which the HCl reacted with the amorphous ice surface. Therefore, the thermal energy contained within the HCl molecules must have been enough to warm the local area where the HCl molecule adsorbed, and cause reaction. This meant that the system needed to be redesigned in order to reduce the minimum temperature of the cluster cell. To this end, a radiation shield was installed. After the system was redesigned, the minimum temperature of the cluster cell became 20 K. This limited the amount of reaction which was taking place, however, it did not totally eliminate it.

Figure 51 shows data from the deposition of HCl on a cluster deposit at 20 K. The molecular complex first formed at 2505  $\text{cm}^{-1}$  and stayed at that frequency even upon warming to 30 K. When the deposit was warmed from 30 to 60 K, the frequency of the "molecular complex" increased. However, the 2100  $\text{cm}^{-1}$  band of the hydronium ion was present in all of the spectra and increased upon deposition of more HCl and upon



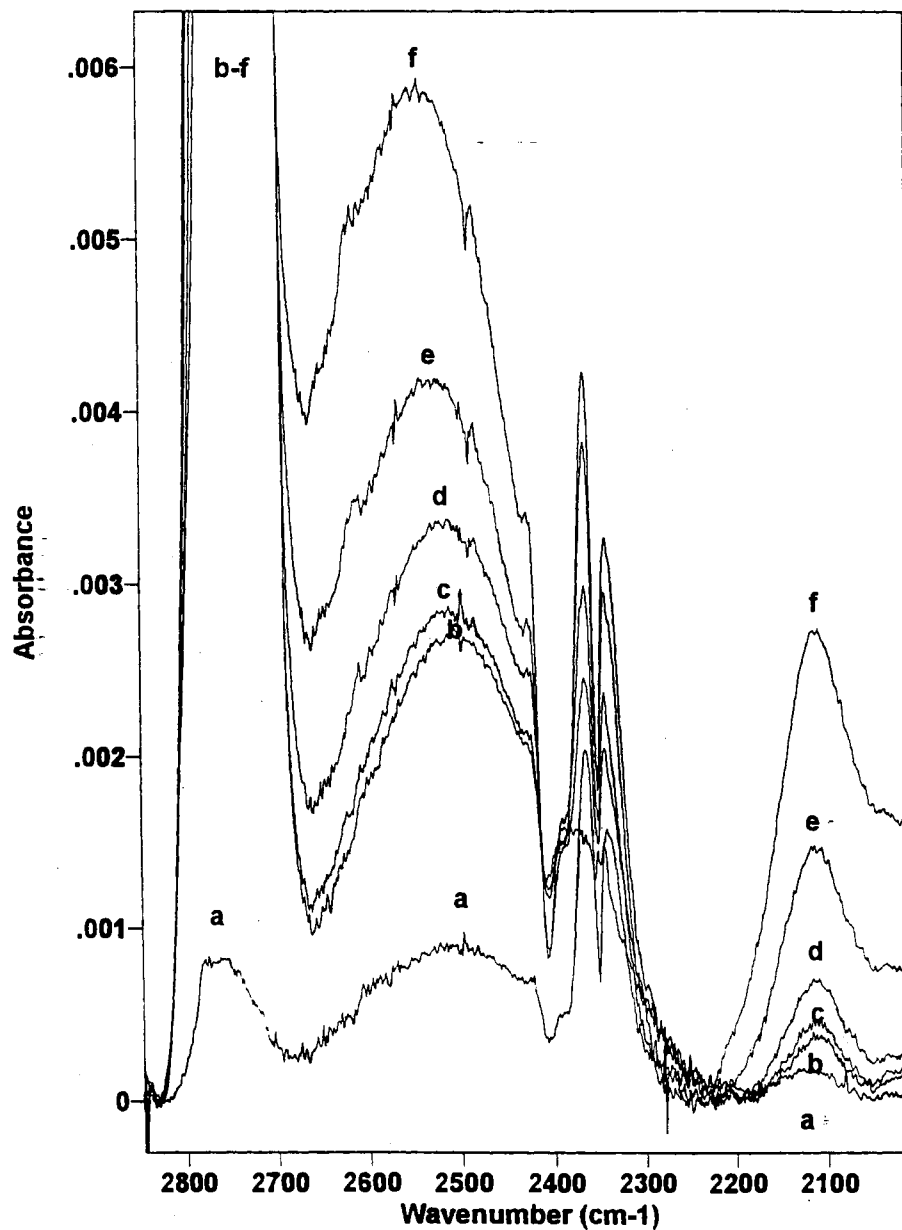


Fig. 51 Curves a - b show the continued formation of the acid overlayer, the "molecular complex", and the hydronium ion as more HCl is deposited onto the cluster surface at 20 K. Curves b - f show the increase in intensity and blueshifting in frequency of the "molecular complex" as the temperature is increased in 10 K steps from 20 to 60 K. Notice that the hydronium ion is present in all of the spectra.

increasing the temperature of the deposit.

Two different avenues to reduce the amount of reaction of the HCl with the cluster surface were apparent. The first possibility was to coadsorb the acid with a weak adsorbate (or else to deposit the acid on a cluster surface precoated with a weak adsorbate). This would mean that the HCl was not actually being deposited onto the cluster surface, but rather an adsorbate coated surface, a surface which could disperse the thermal energy released by the HCl before the HCl came into contact with the cluster surface. The second possibility was to highly anneal the clusters. This would increase the crystallinity of the cluster surface and, hence, decrease the amount of reaction of the acid with the surface.

To test the first possibility, the HCl was premixed with several different weak adsorbates and the mixture was deposited onto a cluster surface. Due to the design of the cell, the weak adsorbate was always deposited onto the cluster surface before the acid. This had the effect of depositing the acid onto an adsorbate coated surface. Several different weak adsorbates were used ( $N_2$ ,  $H_2$ , ethylene, and  $CH_4$ ), and they all worked to protect the surface from reaction with the HCl. Further, the molecular complex band was shifted to lower frequency in the presence of the weak adsorbate (see Fig. 52). The  $N_2$ ,  $H_2$ , ethylene, and  $CH_4$  shifted the molecular complex to 2490, 2480, 2480, 2460  $cm^{-1}$ , respectively. To check whether it was a complex between the acid and the weak adsorbate that was causing the lower frequency of the "molecular complex" band, the HCl: $CH_4$  premix was deposited on a cryogenic cold finger in the absence of an ice surface. The results showed that there was no interaction or complexation between the acid and the weak adsorbate. Thus, the lowering in the frequency of the molecular

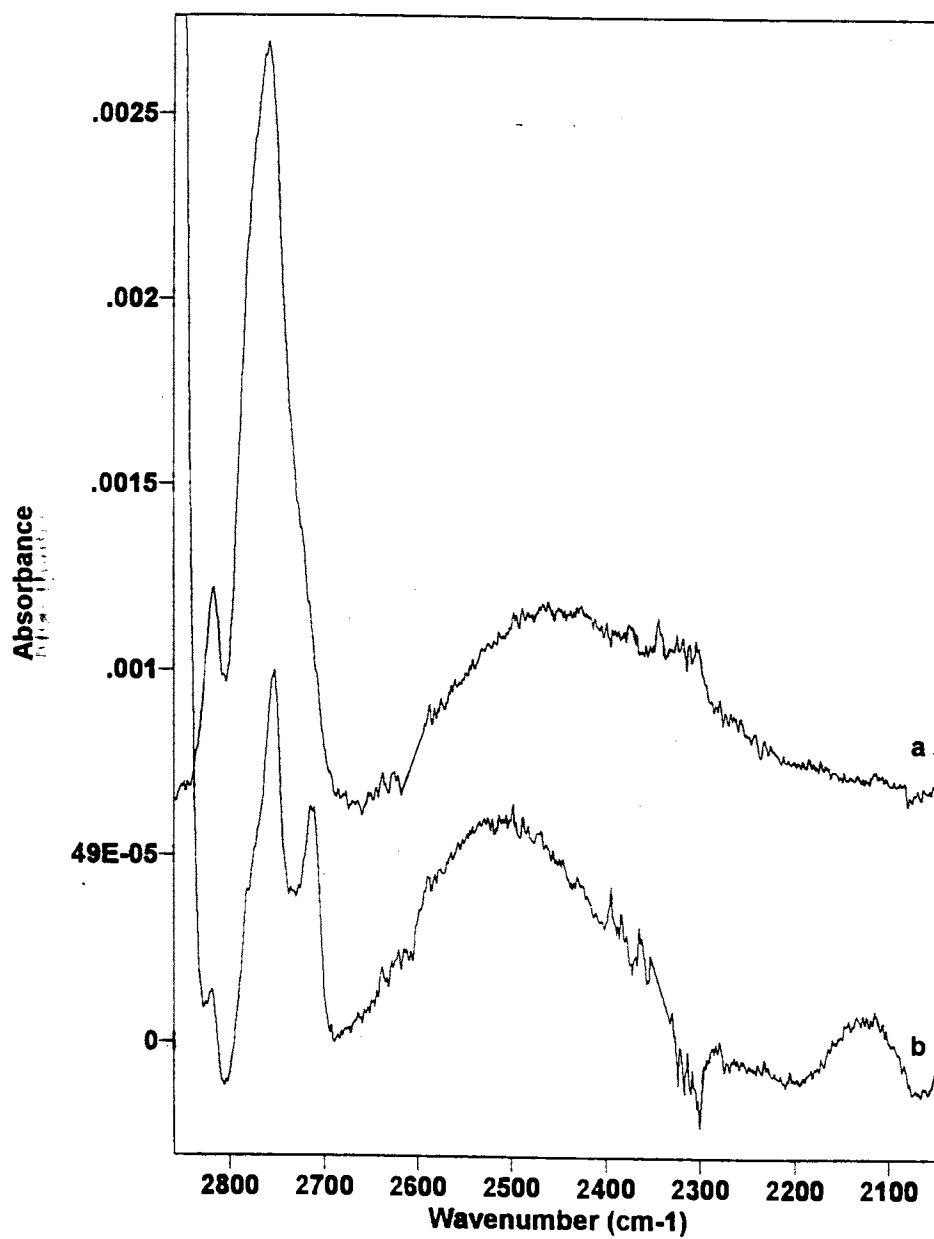


Fig. 52 Infrared spectra of crystalline nanoclusters coated with a premix of HCl:CH<sub>4</sub> both a) before and b) after the CH<sub>4</sub> has been pumped off.

complex was due to the weak adsorbate either: a) limiting the population of the acid on the cluster surface (crowding effect) or b) dispersing the thermal energy of the acid molecule before it contacted the cluster surface, thus limiting the ionization of the cluster surface by of the acid.

To test whether a highly annealed, more crystalline, cluster surface was more resistant to reaction with the HCl, a cluster deposit was annealed to 140 K. The cluster cell was then cooled to its minimum temperature and neat HCl deposited. Upon addition of the first HCl, the molecular complex appeared at  $2460\text{ cm}^{-1}$  with no sign of hydronium ion being formed (see Fig. 53a and b). This band then grew in upon deposition of more HCl with a band position of  $2500\text{ cm}^{-1}$ . There still was no sign of hydronium ion formation. Upon warming the sample to 30 K very little change takes place (see Fig. 53). Upon warming the sample in 10 K steps from 30 to 60 K, the band position of the "molecular complex" increased in frequency. Also, the  $2100\text{ cm}^{-1}$  band of the hydronium ion became detectable at 40 K. Therefore, the highly annealed surface was more resistant to reaction with the HCl.

## **DCI**

Deuterated hydrochloric acid was once again used to explore the reactivity of the acid with the surface. The deuterated hydronium ion has a very strong band which forms at  $\sim 2000\text{ cm}^{-1}$ , so it is a good probe to the reaction of the acid with the ice surface. As is seen in Fig. 54, when DCI was deposited onto a cluster surface, it formed the molecular

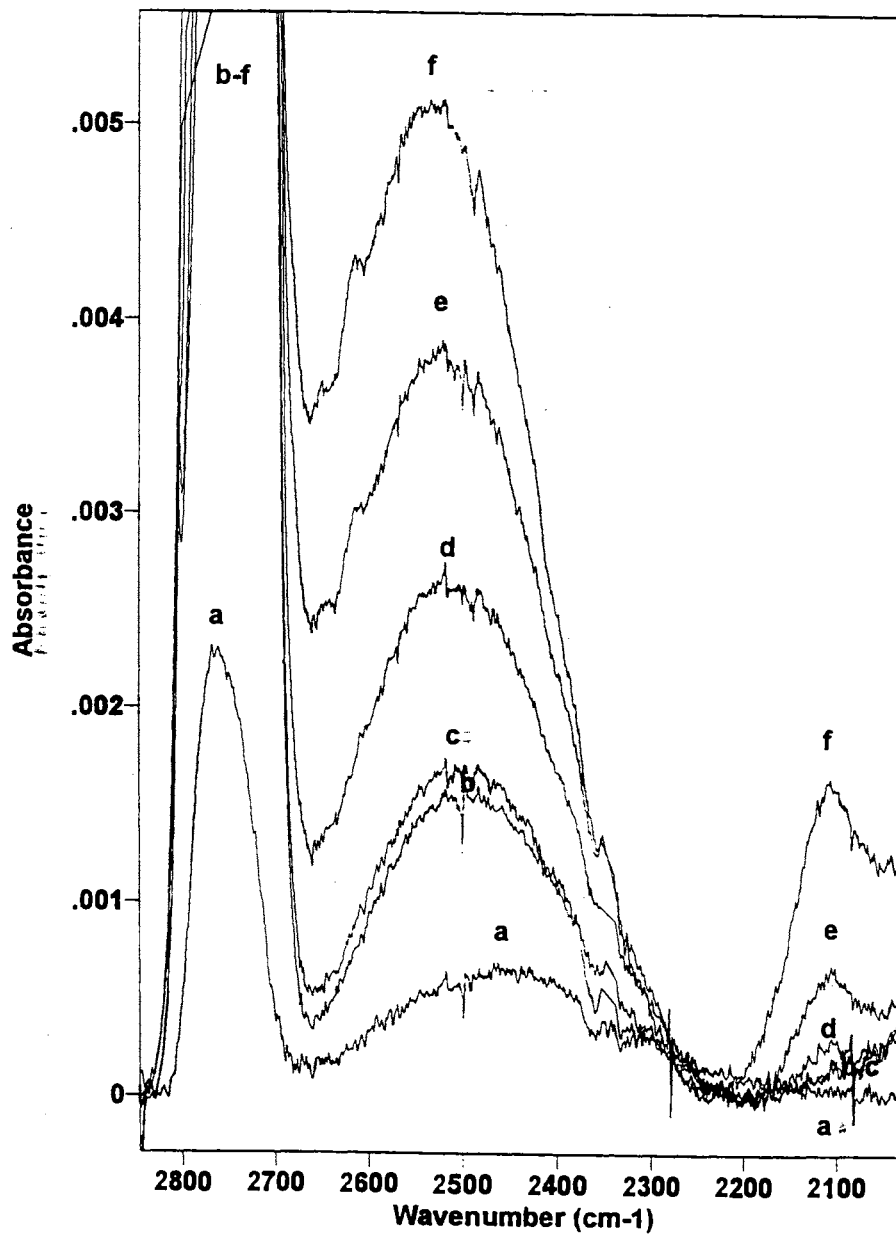


Fig. 53 Curves a - b show the continued formation of the acid overlayer, the "molecular complex", and the hydronium ion as more HCl is deposited onto a highly (140 K) anneal cluster surface at 20 K. Curves b - f show the increase in intensity and blueshifting in frequency of the "molecular complex" as the temperature is increased in 10 K steps from 20 to 60 K. Notice that the hydronium ion does not form until 40 K.

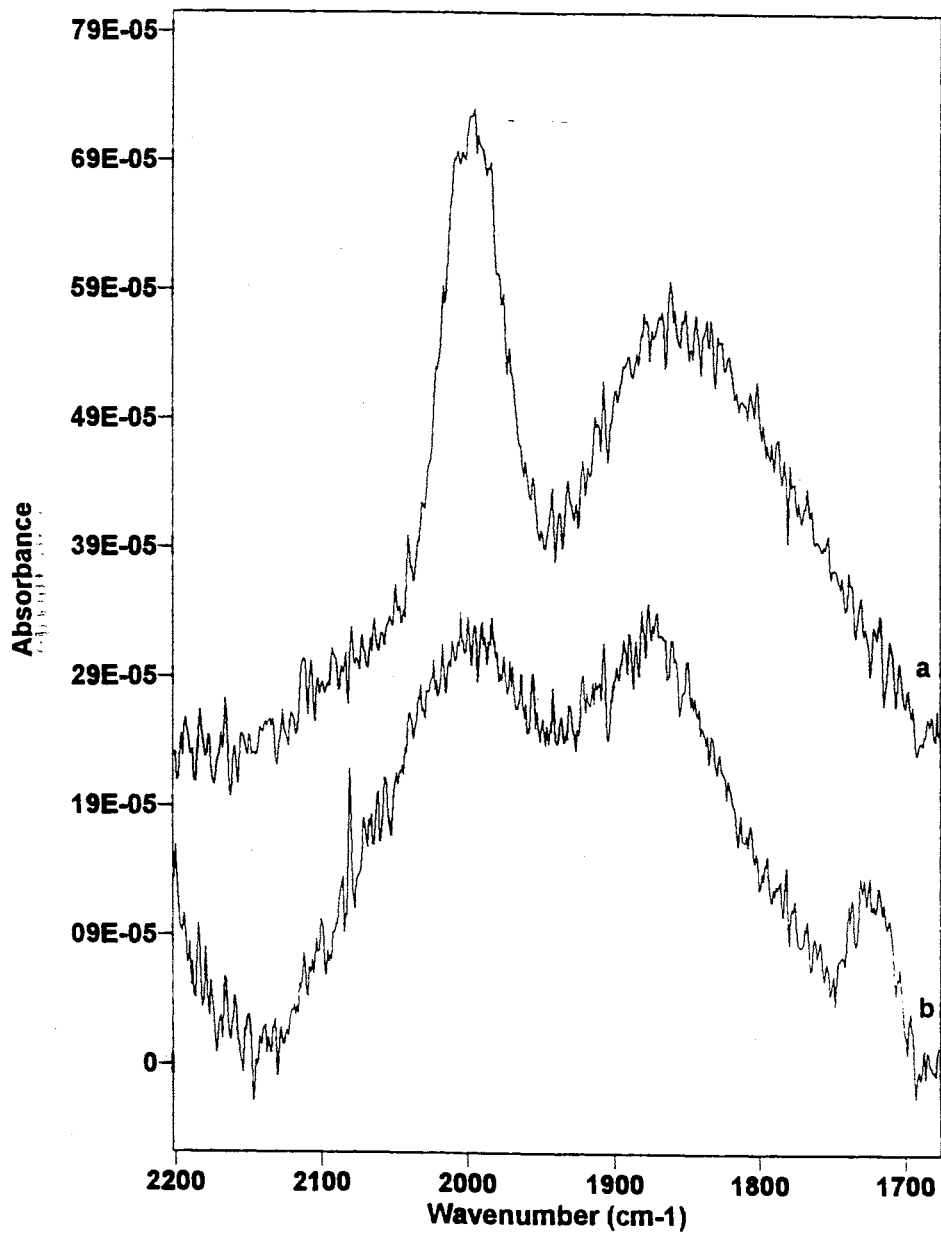


Fig. 54 Infrared spectra of DCl deposited onto D<sub>2</sub>O clusters. Spectrum (a) shows the DCl overlayer (1995 cm<sup>-1</sup>), the molecular complex (1860 cm<sup>-1</sup>), and the deuterated hydronium ion (2010 cm<sup>-1</sup>) at 20 K. Spectrum (b) shows the same sample warmed to 50 K.

complex at  $1860\text{ cm}^{-1}$ . However, the gentle increase in the intensity in the  $2100\text{ cm}^{-1}$  region is due to the formation of the deuterated hydronium ion. Therefore, when DCl was deposited onto a  $\text{D}_2\text{O}$  cluster surface at 20 K, it both adsorbed molecularly and, to a limited extent, reacted with that ice surface. Upon increasing the temperature to 50 K, the deuterated hydronium ion continued to increase in intensity. The molecular complex, although decreased in intensity, still remained.

If a premix of DCl with a weak adsorbate is deposited onto an ice cluster surface, it eliminates the reaction of the DCl with that surface. This can be seen by the comparison made in Fig. 55, in which there is intensity (increase in the baseline) in the  $2000\text{ cm}^{-1}$ , hydronium ion, region, but only a flat baseline for the premixed deposit. Further, the molecular complex for the premixed deposit is redshifted  $40\text{ cm}^{-1}$ .

## **HBr**

The deposition of HBr at 20 K onto an ice cluster surface follows the pattern which has already been developed (see Fig. 56). Upon deposition of the HBr, the molecular complex is observed at  $2240\text{ cm}^{-1}$ . There is also a band at  $\sim 2550\text{ cm}^{-1}$  which could either be due to the molecular complex of HCl or the hydronium ion due to the ionization of the acid. There is also a low frequency wing on the molecular complex band of the HBr which could be covering up the  $2100\text{ cm}^{-1}$  band of the hydronium ion.

Upon warming the sample to 50 K, the  $2550\text{ cm}^{-1}$  band increases in intensity as would be expected for either of the two possibilities for this band. However, at 50 K the molecular complex of the HBr lost intensity, leaving the  $2100\text{ cm}^{-1}$  band visible.

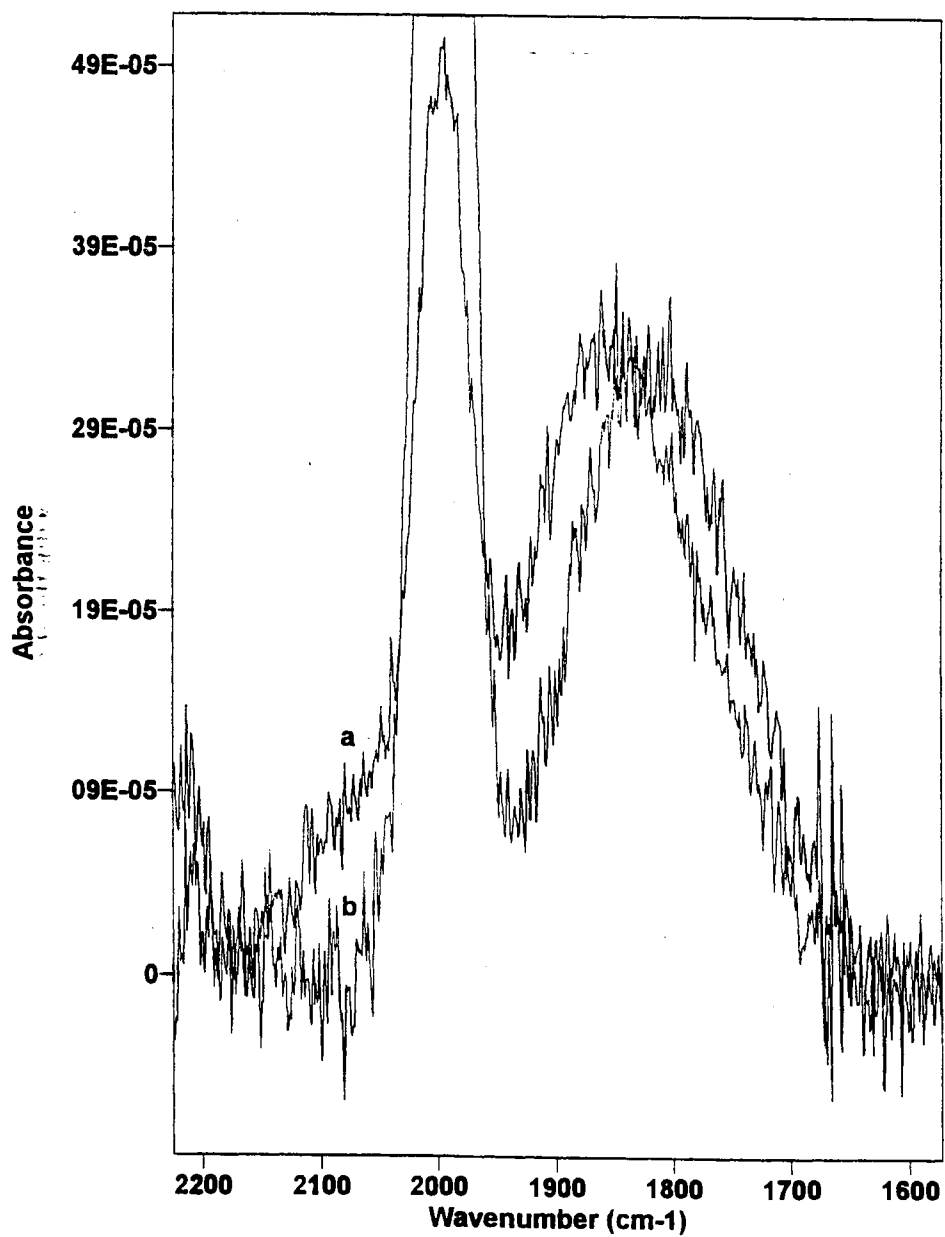


Fig. 55 Comparison of the overlayer deposits of (a) neat DCl to (b) a 1:1 premix of DCl:N<sub>2</sub>. Notice the absence of deuterated hydronium (2010 cm<sup>-1</sup>) ion in the premixed deposit.



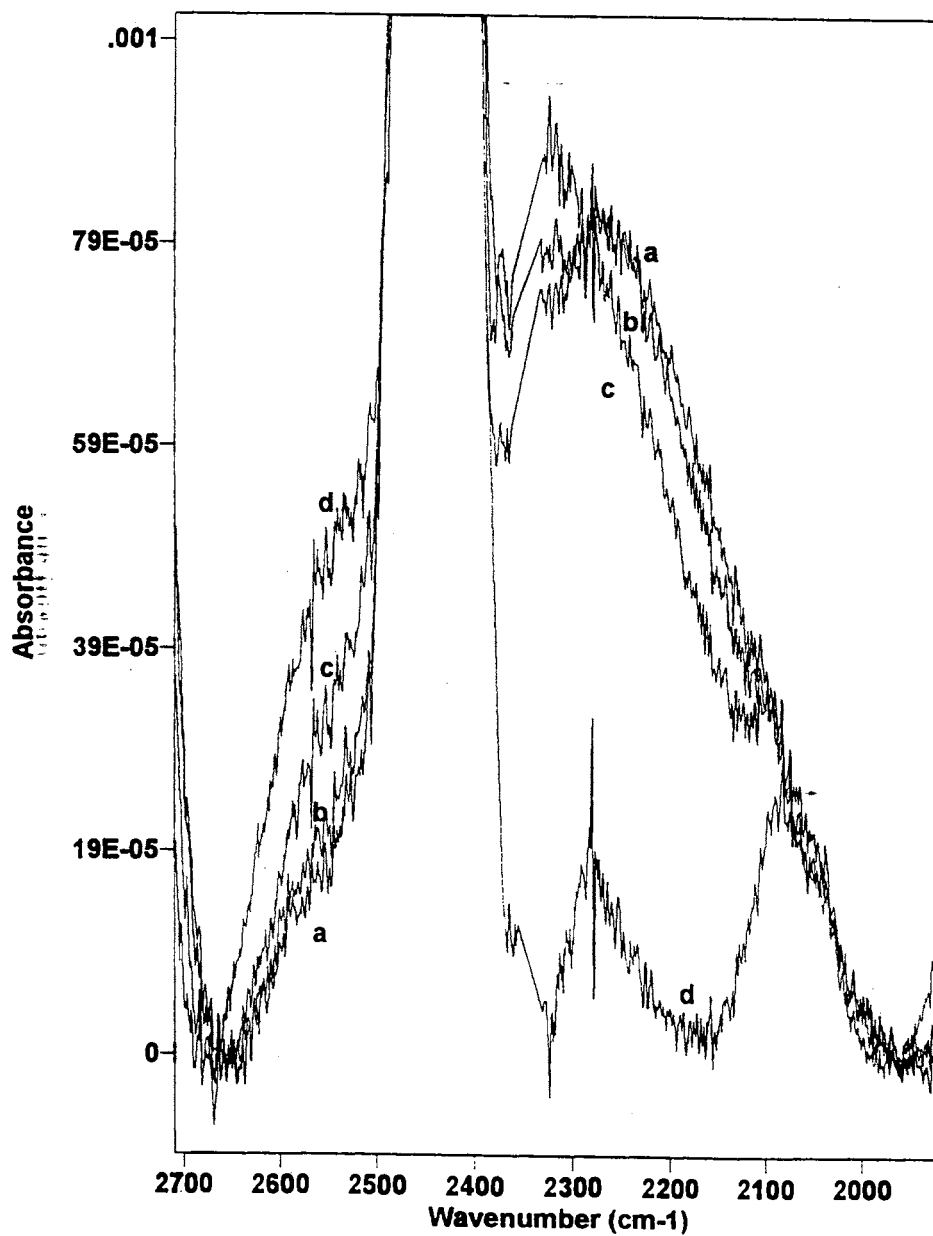


Fig. 56 Infrared spectra of HBr coated clusters at (a) 20, (b) 30, (c) 40, and (d) 50 K showing the formation of the hydronium ion ( $2550\text{ cm}^{-1}$ ) and the ultimate elimination of the HBr molecular complex ( $2240\text{ cm}^{-1}$ ).

If the HBr is premixed with a weak adsorbate and then deposited, the resulting molecular complex is redshifted to  $2220\text{ cm}^{-1}$  and the reaction of the acid with the ice surface is limited (see Fig. 57).

### Conclusions

The formation of the molecular complex is observed for the deposition of HCl, DCl, and HBr on both an amorphous thin film and a suspended cluster deposit. This complex varies in frequency depending on the exact conditions in which the acid is deposited. When HCl, DCl, or HBr is deposited onto a thin-film amorphous deposit, the molecular complex band that forms is found at  $2540$ ,  $1820$ , and  $2240\text{ cm}^{-1}$ , respectively.

If the acid is deposited neat onto an unannealed crystalline cluster deposit, the frequency of the molecular complex band is observed at  $2525$ ,  $1860$ , and  $2240\text{ cm}^{-1}$ , respectively. However, if the acid is deposited as a premix or on a highly annealed cluster surface, the band position of the molecular complex shifts to lower frequency. This lowering in frequency for the premixed or highly annealed deposit is presumably due to cooperative effects of the water surface, the HCl interacting with multiple sites on the cluster surface (see Table 6), thus lowering the frequency of the molecular complex. The higher frequency of the molecular complex for the deposits which are not premixed nor deposited onto highly annealed cluster surfaces can be due to one of two possibilities. First, the reaction (ionization) of the acid with the surface, this reaction (ionization) produces hydronium ions which then changes the nature of the surface. Thus, when the first molecules are deposited, they are deposited on an  $\text{H}_2\text{O}$  surface. However, the later

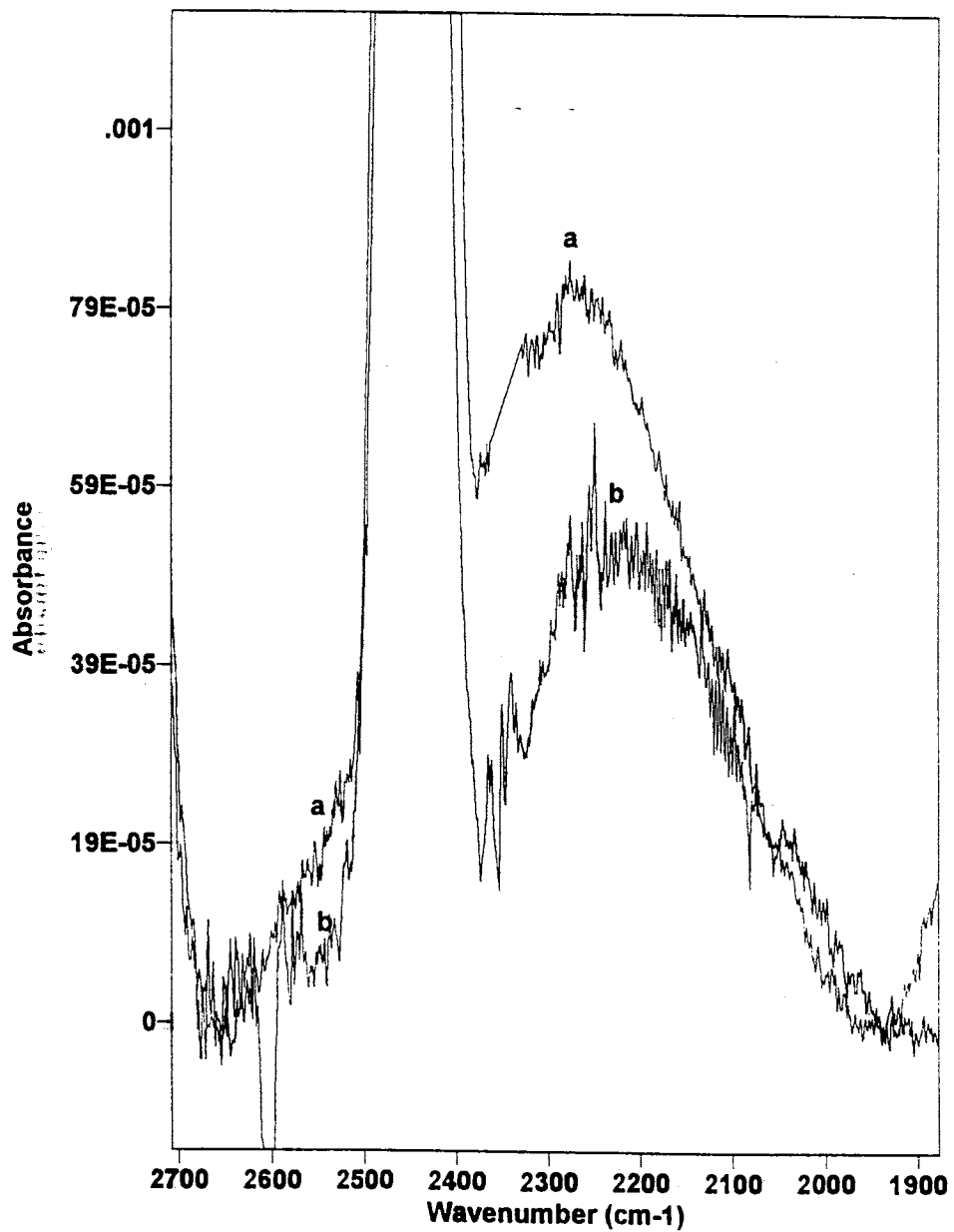


Fig. 57 Comparison of the overlayer deposits of (a) neat HBr to (b) a 1:1 premix of HBr:CH<sub>4</sub>. Notice the absence of hydronium ion (2550 cm<sup>-1</sup>) in the premixed deposit.

molecules are actually deposited onto a partially ionized  $\text{H}_3\text{O}^+(\text{H}_2\text{O})_n$  surface. This increased acidity of the surface weakens the interaction between the acid and the surface, shifting the molecular complex band to higher frequency. Second, as more adsorbate is deposited, it becomes crowded on the surface. This crowding changes the geometry of the adsorbate on the surface, thus changing the frequency of the molecular complex.

The molecular complex band also exists at temperatures up to 70 K. It does not lose intensity for temperatures lower than 40 K, but once above 50 K, the intensity of the molecular complex band decreases as the acid reacts with the ice.

## CHAPTER IV

### STRONG HYDROGEN-BONDING ADSORBATES

#### General

The initial classification of adsorbates on an ice surface was either as strong or weak hydrogen-bonding adsorbates, with the majority of the work, to this point in time, being done with the weak adsorbates. The weak adsorbates are generally classified as those molecules which will shift the surface modes a few to a few tens of wavenumbers. This shift is for the most part in a single step upon adsorption of the adsorbate. There are a few cases, however, that are the exception to this rule.  $N_2$ , for example, when fully coating a surface will shift the d-H from 3694 to 3677  $cm^{-1}$ . However, when the surface is only partially coated with  $N_2$ , the d-H is shifted to an intermediate value in a broad band. Strong adsorbates, on the other hand, general shift the surface modes several tens to several hundreds of wavenumbers. They also tend to shift the d-H in a fashion similar to  $N_2$ . When the strong adsorbate first starts to coat the surface, it shifts the d-H to some broad banded intermediate value which then shifts to its fully-shifted value after the surface is over half coated with the strong adsorbate.

An explanation for this half-shifted and then fully-shifted d-H comes from a "crowding" effect of the adsorbate on the surface. As the adsorbate first starts to adsorb onto the cluster surface, there are few adsorbed molecules on the surface for the adsorbate to interact with or push up against. Thus, when they adsorb onto the surface, they are able to "lay down" on the surface. This means that the adsorbate is able to

interact with several surface sites, but interacts with them less strongly than if it is interacting with only a single surface site. As the surface becomes more highly coated by the adsorbate, the adsorbate becomes "crowded" on the surface. This causes the adsorbate to "stand up" on the surface, to interact with fewer surface sites, but to interact more strongly with those few sites with which it does interact. Therefore, as the surface becomes more "crowded" and the adsorbates interact more strongly with the surface sites, the frequency of the surface groups with which they are interacting show a greater shift.

Strong hydrogen-bonding adsorbates have also, for the first time, shown the unambiguous presence of the symmetric stretch of the surface d-H molecules, referred to from now on as the sym d-H. As is expected, this mode is found in the lower part of the OH-stretching region at  $3110\text{ cm}^{-1}$ . This mode is not readily observable upon the adsorption of weak adsorbates due to the nature of this mode. Even though the sym d-H mode is produced from a surface molecule, this mode is not actually a surface mode. It would more accurately be described as a subsurface mode. This is because an adsorbate can not actually directly influence this mode. It can not interact with either of the atoms (H or O) which are responsible for this mode, nor is the coupling between this mode and any of the modes with which an adsorbate can interact with strong enough to cause any observable effect upon the sym d-H. Even if a molecule adsorbs to the free hydrogen of the d-H molecule, this will have little effect on the sym d-H mode because this mode could as easily be called the OH-stretch of the bonded-OH of the d-H molecule, with little coupling between the free and the bonded OH-stretches. Thus, there is little affect on this mode due to the adsorption of a weak adsorbate. However, when strong

adsorbates are adsorbed onto the surface of the ice clusters, and the subsurface of the cluster is now being affected, the sym d-H is also observable.

Due to the way in which the strong hydrogen-bonding adsorbates affect the cluster, their classification needs to be derived even further. There have been found to be at least three different classifications for strong hydrogen-bonding adsorbates. These classifications are nonordering, ordering, and ordering and reactive.

The ordering and nonordering adsorbates are named such in order to contrast between the way in which they each affect the cluster surface and subsurface as seen by their infrared difference spectrum. The band structure in the infrared difference spectrum for an ordering adsorbate resembles the band structure of crystalline ice. This can be contrasted to that of a nonordering adsorbate which produces a band structure in the infrared difference spectrum which resembles amorphous ice. Each of these classifications will be discussed in further detail throughout the rest of this chapter.

### **Nonordering**

The only nonordering strong hydrogen-bonding adsorbate which has been found is HCN. This does not make it any less valuable than any of the other strong adsorbate, rather, just unique and, to a large degree, much more interesting. Figure 58 shows the changes which take place as more and more HCN is adsorbed onto the surface of a 135 K annealed cluster at 120 K. What is seen is that as the first 20% of the HCN is adsorbed, 40% of the d-H is lost (shifted), but only shifted to its half-shifted position. (The percentage change is given as the percent of the maximum gain or loss of the

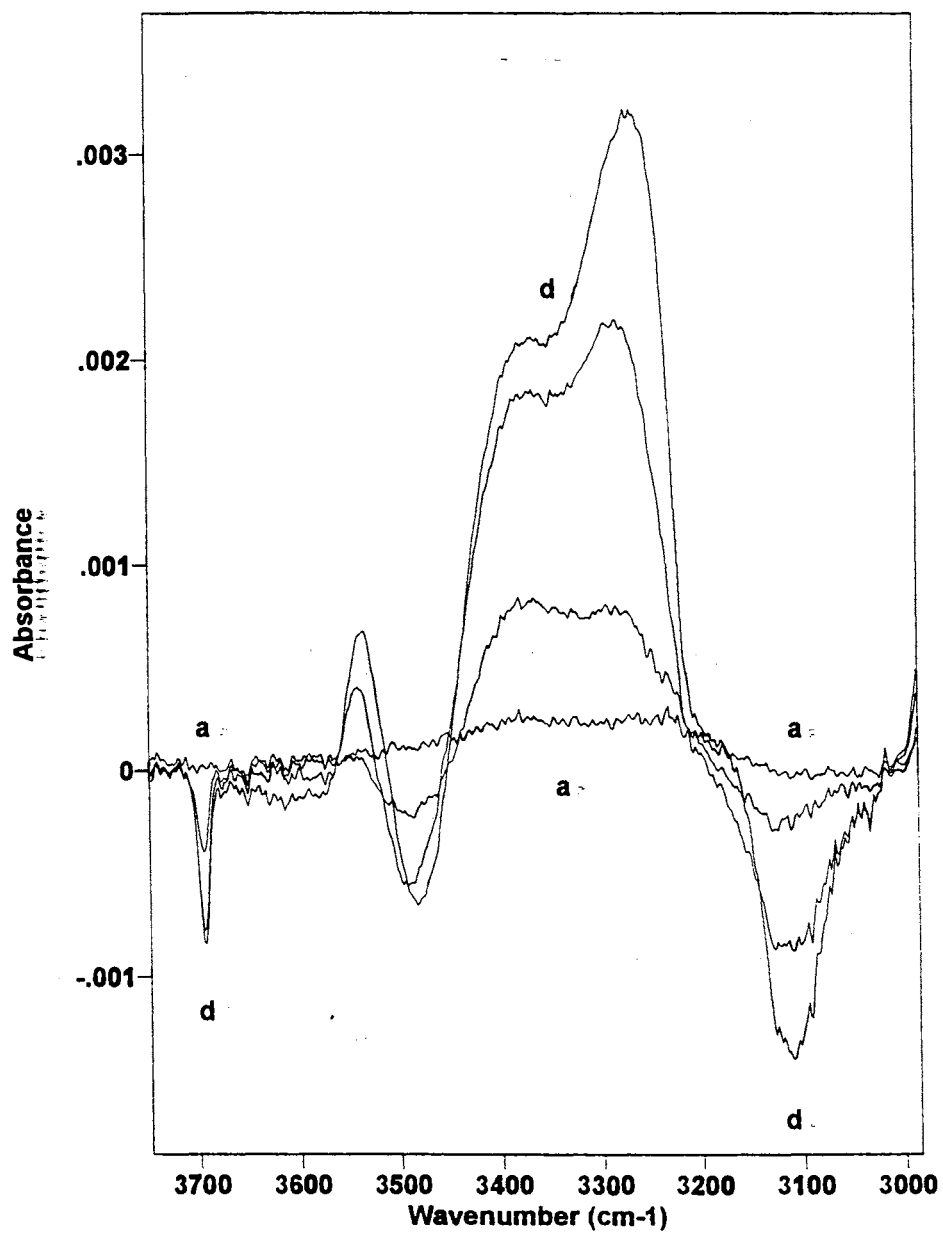


Fig. 58 Curves a - d show the loss of the cluster surface and the formation of new interior as more and more HCN is deposited onto the cluster surface.



appropriate band). The S-4 also loses 40% of its intensity. Simultaneously, the first 25% of a large growth in intensity forms in the 3400 to 3200  $\text{cm}^{-1}$  region (to be explained below). Also, a sym d-H band at 3110  $\text{cm}^{-1}$  loses 10% of its intensity.

As 75% of the total HCN is adsorbed onto the cluster, nearly 90% of the d-H and S-4 has been lost. The originally half-shifted d-H is now being shifted to its fully-shifted value of 3535  $\text{cm}^{-1}$  and is about half way to its maximum intensity. The growth in intensity in the 3400 to 3200  $\text{cm}^{-1}$  has reached 70% of its maximum intensity. However, the sym d-H has only lost just over 50% of its intensity.

As more HCN is adsorbed and the cluster surface became fully coated with HCN, the d-H finishes shifting to its fully-shifted value of 3535  $\text{cm}^{-1}$ . This band, although broader than the bare d-H band, is much sharper and more intense than the half-shifted d-H. The S-4 also continues to decrease. It is not as intense as would be expected, even for a weak adsorbate, but is having its loss of intensity filled in by the shifted d-H band. For this same reason, the lost d-O band intensity is not observable. Further, the intensity of the shifted d-H is larger than what it appears because it is actually filling in the loss of the d-O and S-4. The intensity in the 3400 - 3200  $\text{cm}^{-1}$  region continues to increase. Finally, the loss of the sym d-H also increases to the same intensity as the d-H, except with a breadth which is about ten times greater.

The percentage loss of the surface modes, d-H and S-4, both lead the percentage gain of the HCN as measured using the  $\text{C}\equiv\text{N}$  stretch band at  $\sim 2100 \text{ cm}^{-1}$ . This means that as the first HCN is adsorbed onto the cluster surface, it influences several surface modes. This can be explained by the HCN "laying down" on the surface and interacting with several sites. This is verified by the half-shifting of the d-H in which the adsorbate

interacts "weakly" with a multitude of sites. Then, when the surface is about half coated with HCN, the HCN becomes "crowded" and "stands up" on the surface. When this happens, the strength of the hydrogen-bonding between the adsorbate and the surface increases and the d-H is shifted to its fully-shifted value. This is exemplified by the d-H being ~50% lost at ~25% HCN coating and the fully-shifted d-H reaching half of its maximum value when the HCN is at 75% of its maximum coating.

Further, if we look at the sym d-H we can follow what is happening to the subsurface of the cluster. At 20% HCN coating, 10% of the sym d-H has been lost. At 75% HCN coverage, only 50% of the sym d-H is lost. This shows that as the surface becomes more fully coated, and the adsorbate becomes "crowded" causing the interaction between the adsorbate and the surface to increase, the adsorbate can more strongly influence the subsurface of the cluster. This in turn is reflected in the increase in intensity of the 3400 - 3200  $\text{cm}^{-1}$  region.

As was mentioned above, the strong hydrogen-bonding adsorbates should not only affect the surface of the cluster, but due to the strength of their interaction, they should also affect the subsurface as well. The question now becomes, what kind of an affect will the strong hydrogen-bonding adsorbate have on the subsurface. The answer is not immediately obvious, but does become apparent after comparing HCN coated clusters to  $\text{H}_2\text{S}$  coated clusters, and the answer is as follows.

When the HCN is adsorbed onto the cluster surface, it forms strong hydrogen-bonds with that surface. This will, to some degree, remove some of the asymmetry of the surface and put the surface molecules into an environment which will be more "bulk" like in nature. Thus, by adding a strong hydrogen-bonding adsorbate to

the surface, we have effectively added an extra "ice-like" layer to the surface of the cluster. This will consequently put each of the layers of water molecules in the surface and subsurface in an environment which is effectively one layer deeper than it actually is. Thus, the adsorbate has effectively eliminated the surface of the cluster and formed a new layer which is more "bulk-like" in nature. The question becomes what will this new "bulk layer" look like. We have to this point said nothing about adding any order (crystallinity) to the surface, as will be seen for H<sub>2</sub>S, so that this would describe an amorphous ice. If we compare the intensity gained in the bulk region of the HCN coated cluster to an amorphous thin film deposit, we will see an amazing similarity (see Fig. 59). The band center for the center peak is coincident in both cases. They also both have a high frequency wing of slightly different shape but same frequency and relative intensity. The amorphous film also has a weak, low frequency wing which is not reproduced very well, but the overall match between the two is still quite good.

## **Ordering**

### **Introduction**

The second class of strong hydrogen-bonding adsorbates are those which order the surface and subsurface. These adsorbates include H<sub>2</sub>S, SO<sub>2</sub>, and acetylene. The affects of adsorbing H<sub>2</sub>S onto an ice cluster surface will be described in detail, with the adsorbates SO<sub>2</sub> and acetylene simply being added to show support and the general nature of the hypothesis proposed for H<sub>2</sub>S.

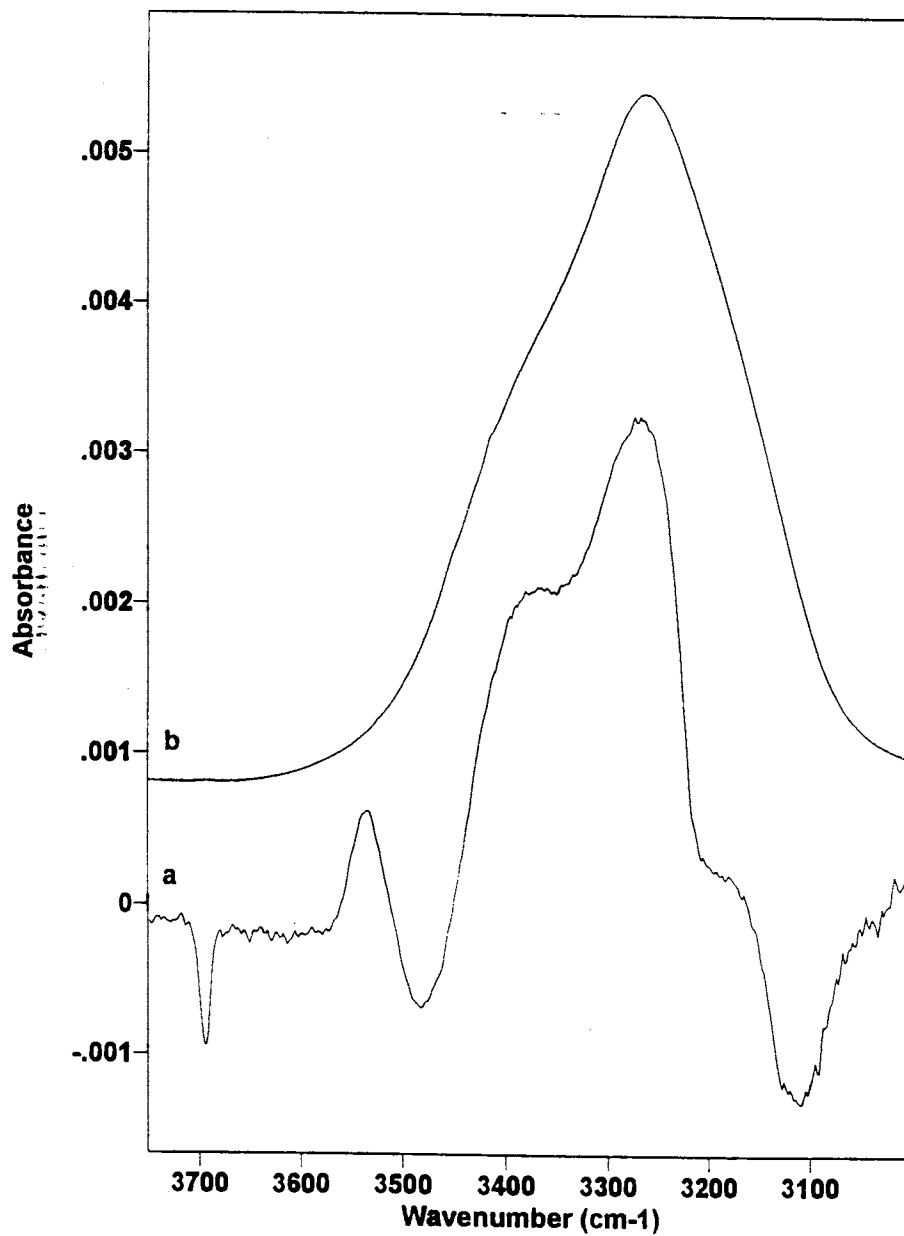


Fig. 59 Comparison of the difference spectrum for (a) fully HCN coated clusters to (b) thin film amorphous deposit.

## H<sub>2</sub>S

When H<sub>2</sub>S is adsorbed onto an annealed ice cluster deposit at 100 K, the effects are very similar to those observed with the adsorption of HCN (see Fig. 60). When the first 30% of the H<sub>2</sub>S is adsorbed, 50% of the d-H band intensity is shifted. It is again not shifted to its fully-shifted value, but rather is only half-shifted, as in the case of HCN. The d-O and S-4 both show a distinct loss, equal in intensity to the loss of d-H. There is an increase in intensity in the 3400 - 3100 cm<sup>-1</sup> region, and the sym d-H shows a weak loss.

As the cluster is fully coated with H<sub>2</sub>S, there is the continued loss of d-H and S-4. The d-H band is first shifted to its half-shifted position and then fully-shifted position of 3525 cm<sup>-1</sup>. The intensity in the 3400 - 3100 cm<sup>-1</sup> region continues to increase, and the sym d-H appears at 3090 cm<sup>-1</sup>.

To this point the H<sub>2</sub>S and the HCN sound identical in their behavior and as far as they have been described, they are. The difference between them comes from the structure of the intensity which was gained in the 3400 - 3100 cm<sup>-1</sup> region. The HCN formed two broad peaks which overlapped, the H<sub>2</sub>S forms three narrower bands at lower frequency (see Fig. 61). The question now is how to explain this difference.

The answer first came from realizing that the H<sub>2</sub>S is isoelectronic to H<sub>2</sub>O. Therefore, it is easily imagined that the H<sub>2</sub>S can "mimic" a water molecule when it adsorbed onto the cluster surface. Since this will effectively add an extra "ice like" layer to the surface of the ice cluster, it is imagined that the original bare surface was now in an environment which is very similar to the second bilayer of the cluster surface (the first

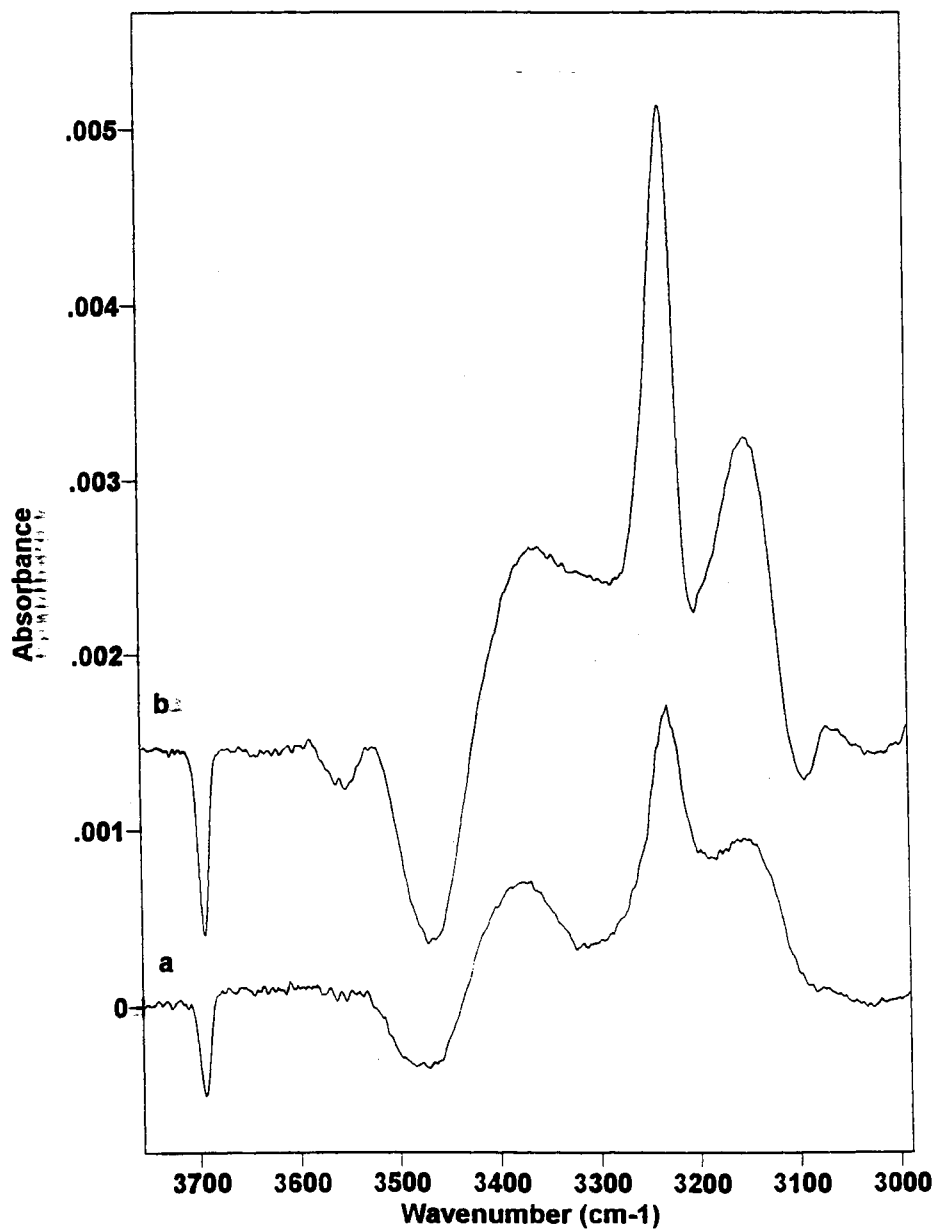


Fig. 60 Curves a and b show the loss of the cluster surface and the formation of new interior as more and more  $H_2S$  is deposited onto the cluster surface.

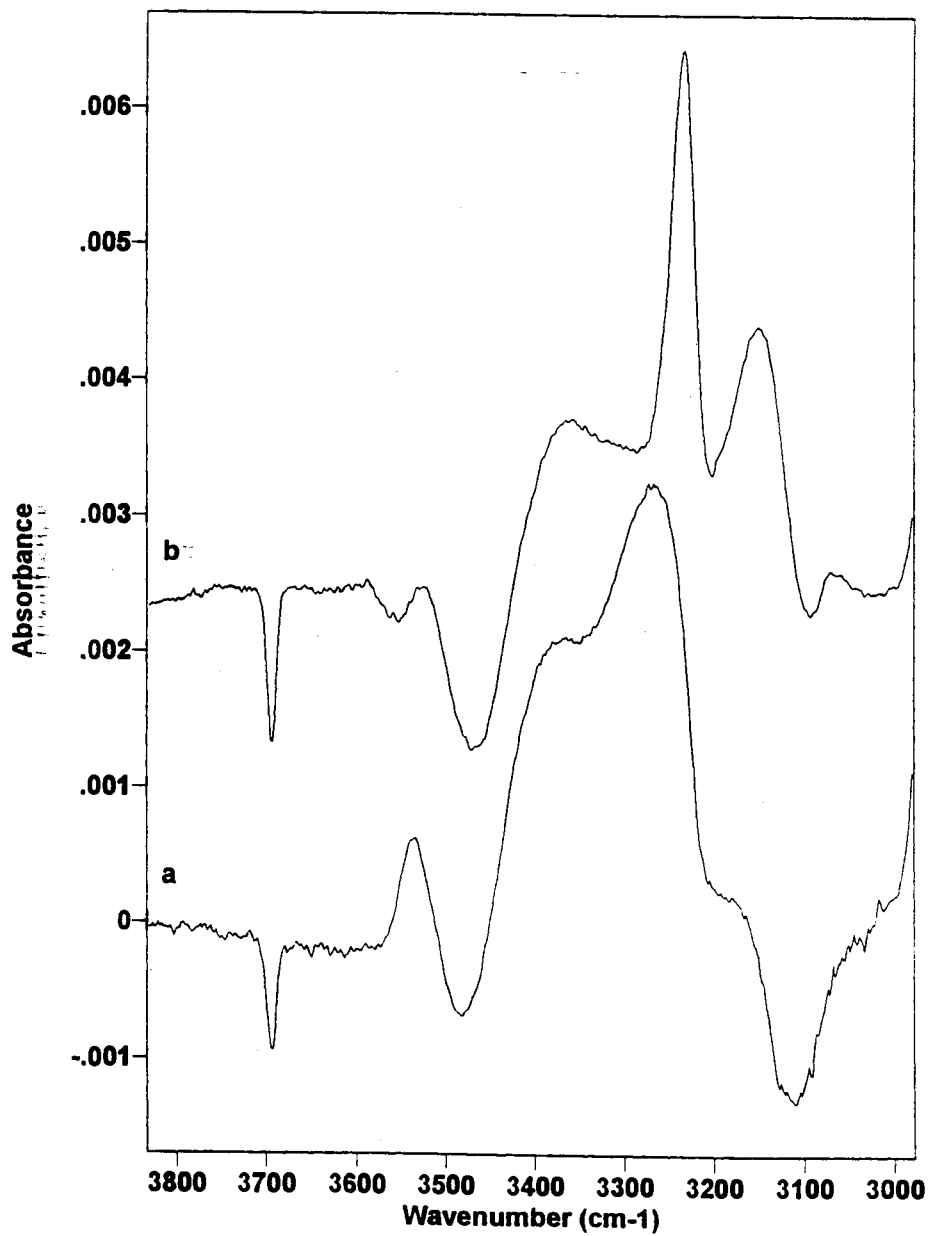


Fig. 61 Comparison of the difference spectra of (a) HCN and (b) H<sub>2</sub>S coated clusters.

subsurface bilayer). Then in turn, the first subsurface bilayer will be in an environment which will resemble that of the second subsurface bilayer. This will continue until the final subsurface layer is converted to "bulk". Therefore, what will be seen in the difference spectra shall be the loss of the surface and the formation of a "bulk" layer. When a comparison is made between the three peaks of the H<sub>2</sub>S coated clusters and the spectrum of a crystalline cluster deposit, the resemblance is amazing (see Fig. 62). The comparison shows that in both cases there are three peaks with the same relative band position and intensity.

### **Acetylene and SO<sub>2</sub>**

Acetylene and SO<sub>2</sub> were also investigated as strong hydrogen-bonding adsorbates. They both produce a difference spectrum which is very similar to that of H<sub>2</sub>S (see Fig. 63). This however does not fit into the picture which has been developed. Neither acetylene nor SO<sub>2</sub> are isoelectronic to H<sub>2</sub>O, so how could they "mimic" a water molecule.

The explanation comes from simply taking what has already been developed and making it more general. If we look at a water molecule as having an electron donating site (oxygen atom) and an electron accepting site (hydrogen atom) separated by ~1 Å, then we can see how they fit. Both acetylene and SO<sub>2</sub> have electron donating (C=C and oxygen atoms, respectively) and electron accepting (hydrogen atoms and sulfur atom, respectively) groups separated by ~1 Å.



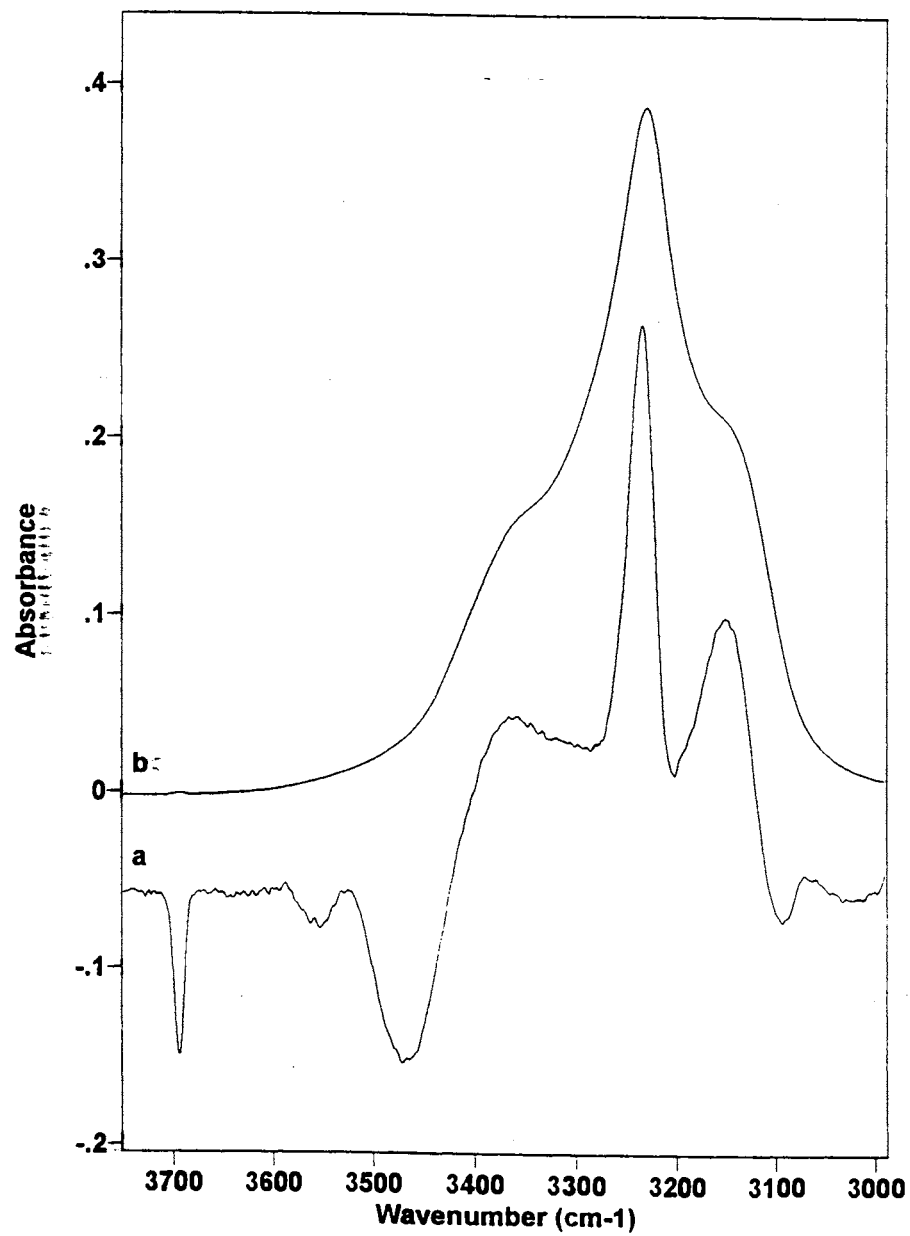


Fig. 62 Comparison of the difference spectrum for (a) fully H<sub>2</sub>S coated clusters to (b) crystalline cluster deposit.

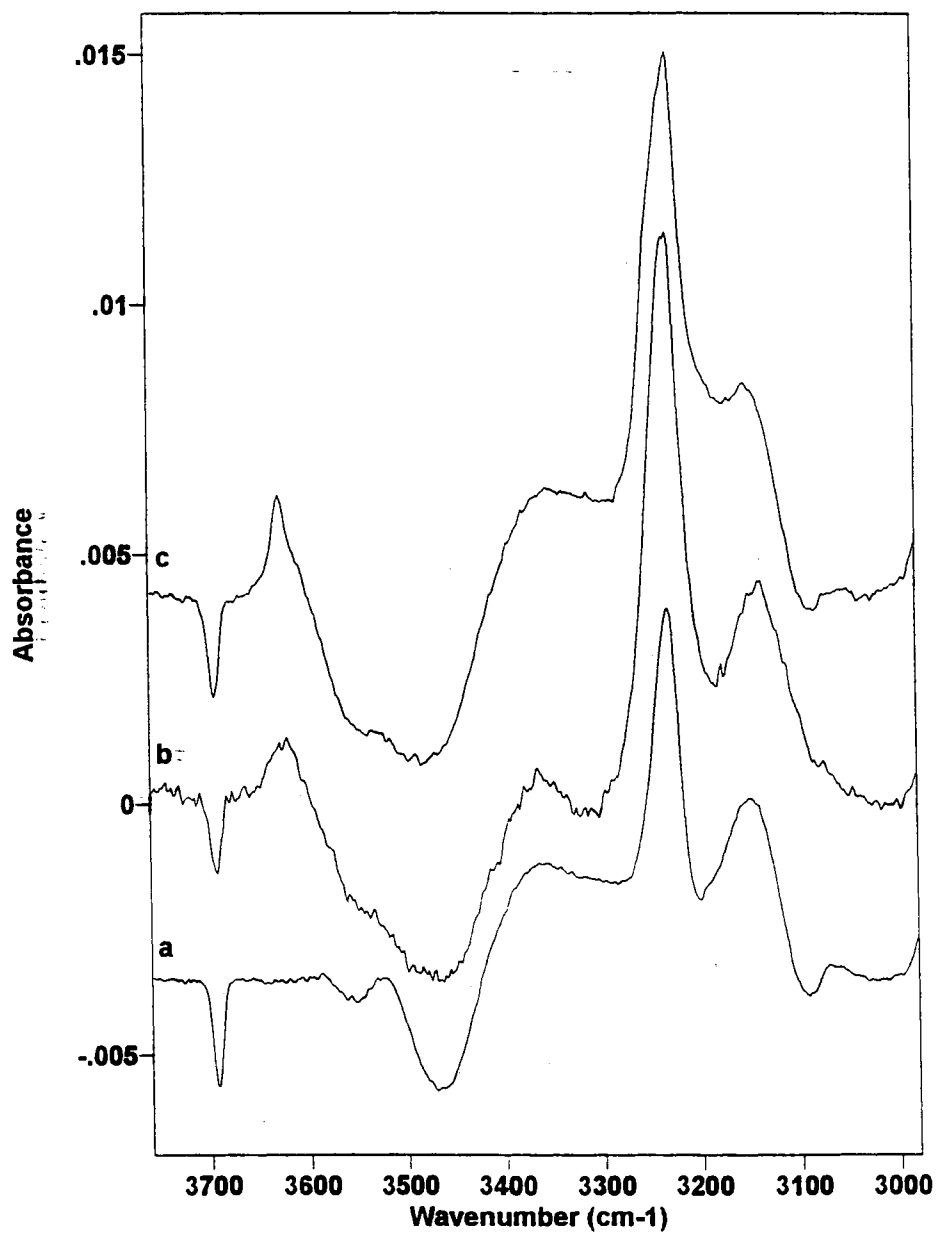


Fig. 63 Comparison of the difference spectra of (a) H<sub>2</sub>S, (b) SO<sub>2</sub>, and (c) acetylene coated clusters.

## Ordering and Reactive

### Introduction

The final classification is for those molecules which not only have the ability to induce order within the surface and subsurface of the ice cluster, but also have a tendency to react with that surface. This category contains the molecules  $\text{NH}_3$ , TMA, and HCl (and DCl and HBr). The trick to investigating these molecules is to find the conditions in which the reaction is limited enough to observe the ordering which is taking place and then to understand the changes which are taking place due to the reaction.

### $\text{NH}_3$

When  $\text{NH}_3$  is adsorbed onto an  $\text{H}_2\text{O}$  cluster deposit, it readily reacts with that surface upon adsorption (even at the minimum temperature at which it will adsorb, 110K).<sup>57</sup> As is seen in Fig. 64, the first  $\text{NH}_3$  which is adsorbed does actually interact with the cluster surface to give a loss of the surface features and an enhancement in the intensity in the  $3400 - 3200 \text{ cm}^{-1}$  region. However, the  $\text{NH}_3$  quickly attacks the cluster surface forming the monohydrate, accompanied by the loss of intensity in the  $3400 - 3200 \text{ cm}^{-1}$  (bulk) region and the gain of intensity in the  $3000 \text{ cm}^{-1}$  (monohydrate) region.

In an attempt to limit this reaction,  $\text{NH}_3$  was also adsorbed onto a  $\text{D}_2\text{O}$  cluster deposit. In this case, due to the isotopic effects of the deuterium, the reactivity of the cluster surface to the  $\text{NH}_3$  is reduced enough to observe the ordering of the cluster surface and subsurface which is taking place.

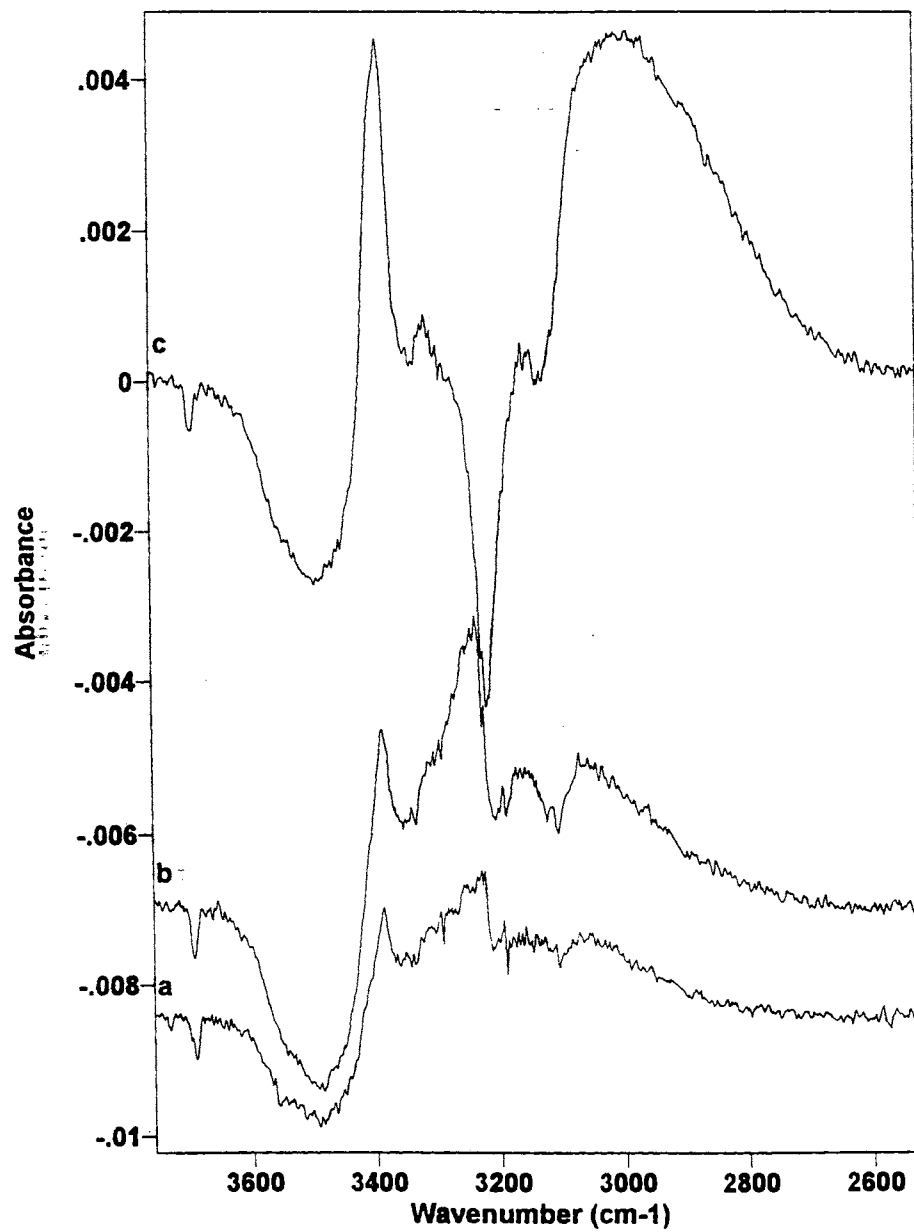


Fig. 64 Curves a - c show the adsorption of NH<sub>3</sub> onto the surface of H<sub>2</sub>O crystalline nanoclusters.

As is seen in Fig. 65, when the  $\text{NH}_3$  is adsorbed, the surface features are affected first and most strongly. It is not until additional  $\text{NH}_3$  is adsorbed that the loss of the sym d-D is observed at  $2300\text{ cm}^{-1}$ . However, upon adsorption of still more  $\text{NH}_3$ , a broad band starts to form in the  $2200\text{ cm}^{-1}$  region along with a decrease in intensity in the  $2500 - 2300\text{ cm}^{-1}$  region due to reaction of the  $\text{NH}_3$  with the surface. The shifting of intensity from the  $2400$  to the  $2200\text{ cm}^{-1}$  regions is due to the conversion of the "bulk" into the ammonia monohydrate.

If one compares the intensity lost in the d-H band to the total amount of d-H in the cluster deposit, one would notice that only a few percent of the total amount of d-H is actually coated by  $\text{NH}_3$  when the  $\text{NH}_3$  is adsorbed onto the cluster surface at  $110\text{ K}$ . This is contrary to what is seen for the other strong hydrogen-bonding adsorbates. They tend to coat all of the d-H. This means that when the  $\text{NH}_3$  adsorbs onto the cluster surface, it does not migrate into the interior of the cluster deposit. Instead, it remains at the exterior of the deposit and reacts with the clusters. This is contrary to the results of other  $\text{NH}_3$  experiments but is a result of the method in which the  $\text{NH}_3$  is adsorbed. It is adsorbed into the cluster cell in small aliquots causing a competition between the  $\text{NH}_3$  diffusing deeper into the cluster deposit and the reacting with the outer clusters of the cluster deposit. As is clearly seen from Fig. 65, the  $\text{NH}_3$  is much more prevalent to react with the outer clusters of the cluster deposit rather than to diffuse into the deposit upon the addition small aliquots of  $\text{NH}_3$ . A similar effect will be seen in the deposition of  $\text{HCl}$  ( $\text{DCl}$ , and  $\text{HBr}$ ) onto a cluster deposit.

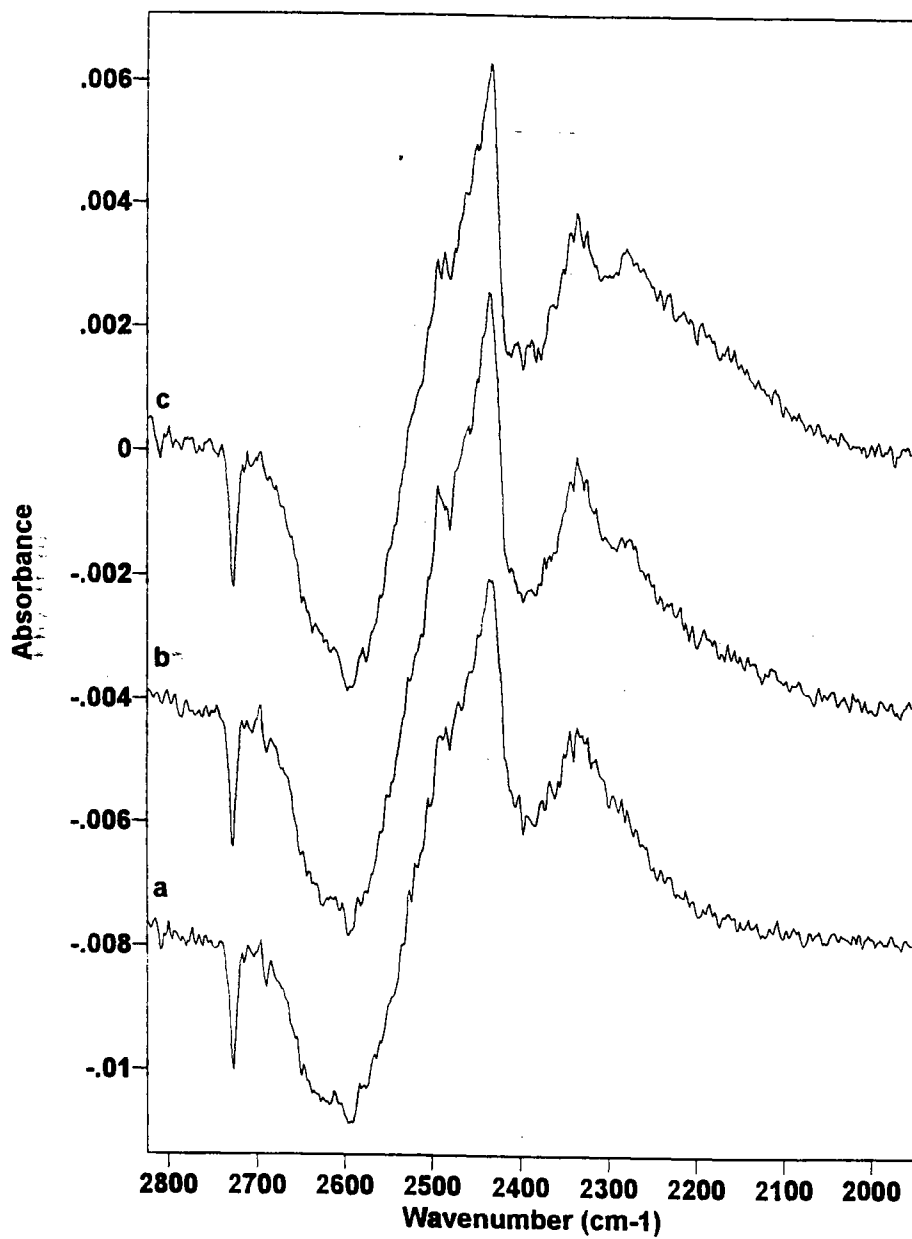


Fig. 65 Curves a - c show the adsorption of NH<sub>3</sub> onto the surface of D<sub>2</sub>O crystalline nanoclusters.

### Tri-Methyl Amine (TMA)

In an attempt to reduce the reactivity of the  $\text{NH}_3$ , the tri-methyl substituted amine, TMA, was tried as an adsorbate. It was hoped that the three large bulky methyl groups would limit the reactivity of the amine by: 1) replacing the electron accepting hydrogen groups, which would reduce the interaction between the amine and the surface, and 2) the bulky nature of the methyl groups would keep the amine from being able to penetrate the ice surface, thus limiting the reaction.

The TMA did appear to be less reactive with the  $\text{H}_2\text{O}$  cluster surface, however, it was still much more reactive than was hoped. This did however provide us with an intermediate case between that of the nonreactive adsorbates and  $\text{NH}_3$ .

If the adsorption of TMA (before the reaction of TMA with the cluster surface becomes predominant) is examined (see Fig. 66), it is seen that the TMA interacts with the cluster surface very similarly to the  $\text{H}_2\text{S}$  or  $\text{HCN}$ . The first 25% of the TMA adsorbed (as measured by the band at  $2800\text{ cm}^{-1}$ ) shifts 50% of the d-H. The d-O and S-4 are also shifted with equal relative intensity. When 75% of the TMA is adsorbed 90% of the d-H is shifted and the sym d-H has lost about half of its maximum intensity.

### $\text{SO}_3$

$\text{SO}_3$  is included here simply for completeness.  $\text{SO}_3$  will not diffuse into the cluster cell below a cell temperature of 140 K. Unfortunately, at this temperature the  $\text{SO}_3$  is too reactive with the ice cluster surface and simply reacts with the cluster surface to form  $\text{H}_2\text{SO}_4$ . At lower temperatures, the  $\text{SO}_3$  reacts with the rubber inlet hose and

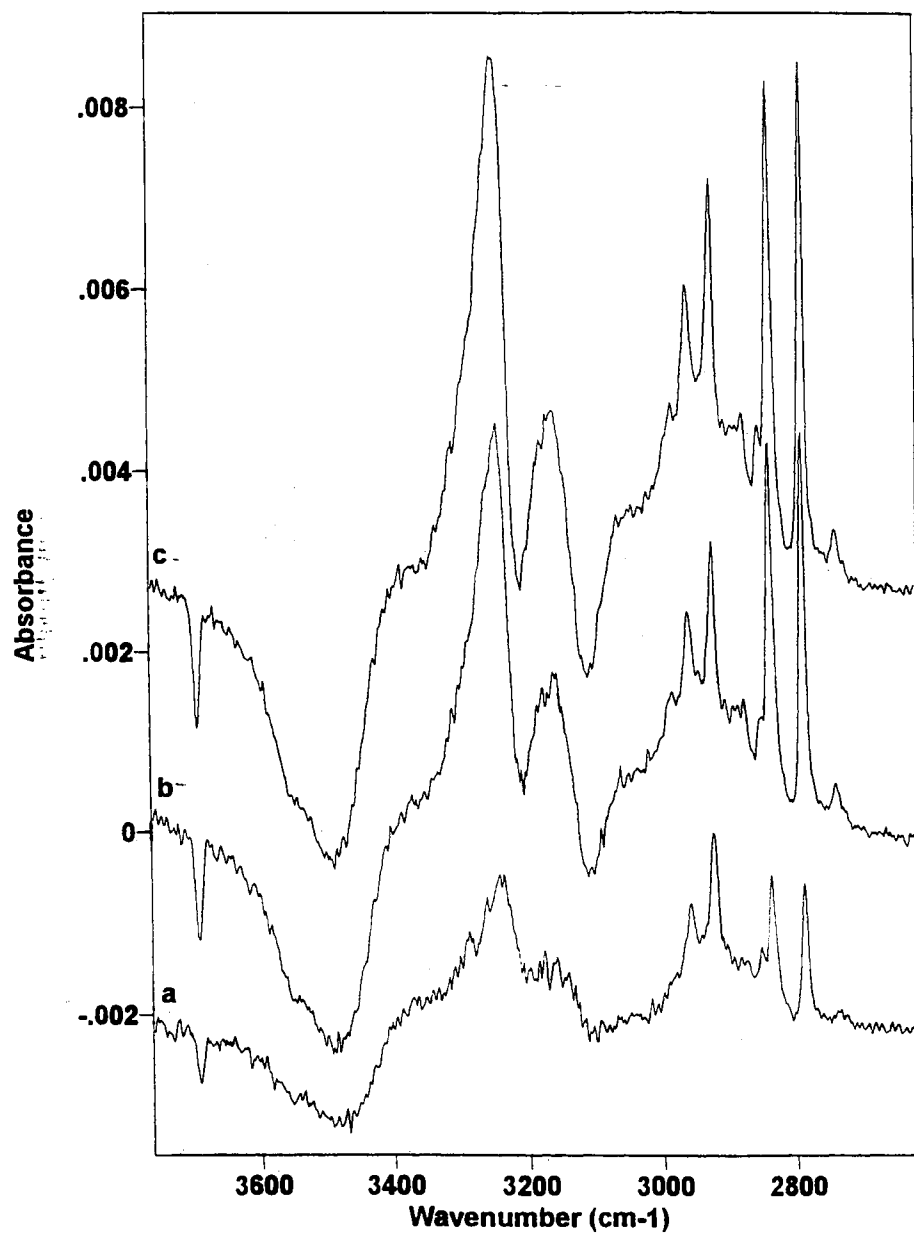


Fig. 66 Curves a - c show the adsorption of TMA onto the surface of H<sub>2</sub>O crystalline nanoclusters.



the grease in the system and converted to SO<sub>2</sub>. No further work was done with SO<sub>3</sub> although it could be a viable adsorbate with a redesigned system.

### **HCl, DCl, and HBr**

As has already been shown for gas phase clusters exposed to low levels of HCl, the first hydrate to form, for an HCl exposed ice surface, is the dihydrate.<sup>25</sup> The same is true for a suspended ice cluster deposit with an HCl overlayer. When a suspended cluster deposit with an HCl overlayer is warmed, the acid hydrate which is formed is the amorphous dihydrate. This can be seen by comparison of Fig. 67 with Fig. 16c.<sup>25</sup>

If we look at how the spectra are changing as the temperature is increased (see Fig. 68), it is seen that the acid attacks the cluster in three different steps as the sample is warmed. The first step is the attack of the cluster surface. This happens upon deposition of the acid onto the cluster surface at 20 K and is seen by the loss in intensity in the surface bands above 3400 cm<sup>-1</sup>, the region of the spectrum which is dominated by the surface. Once the temperature is increased to 50 K, the second step is seen. It is accompanied by: a) the loss of intensity in the 3400 - 3000 cm<sup>-1</sup> region of the ice spectra and in the spectrum of the acid overlayer at 2750 cm<sup>-1</sup>, b) the gain in intensity in the 3000 cm<sup>-1</sup> region and at 2100 cm<sup>-1</sup> due to the formation of the amorphous dihydrate, and c) the increase in intensity and blue-shifting in frequency of the "molecular complex" band. This second step reflects the reaction of the HCl with the subsurface of the clusters. Finally, when the temperature is increased to 70 K, the acid attacks the bulk of the cluster. This is accompanied by the loss in intensity in the "bulk" region, the gain in

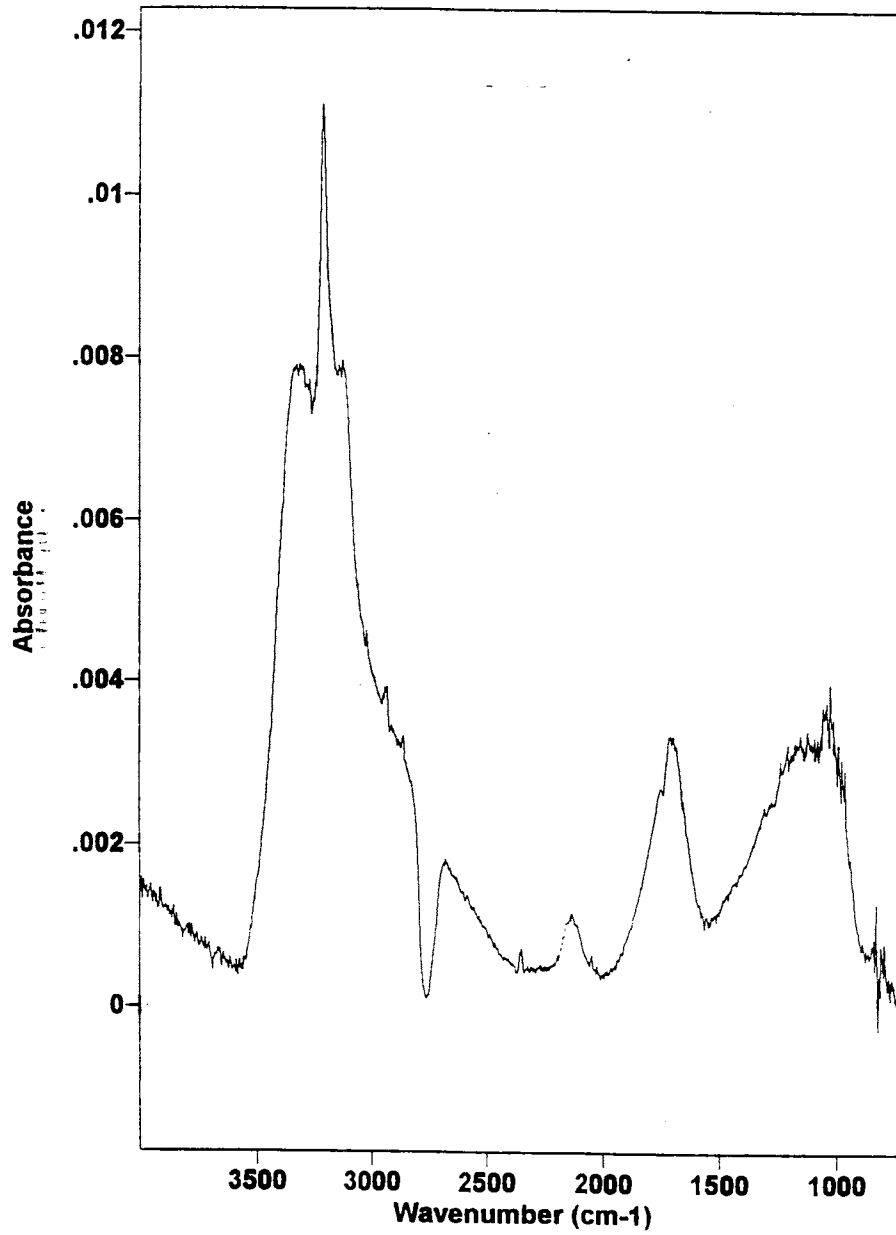


Fig. 67 The infrared difference spectrum for an HCl coated cluster with 4% interior ice added back in showing the formation of the HCl dihydrate.

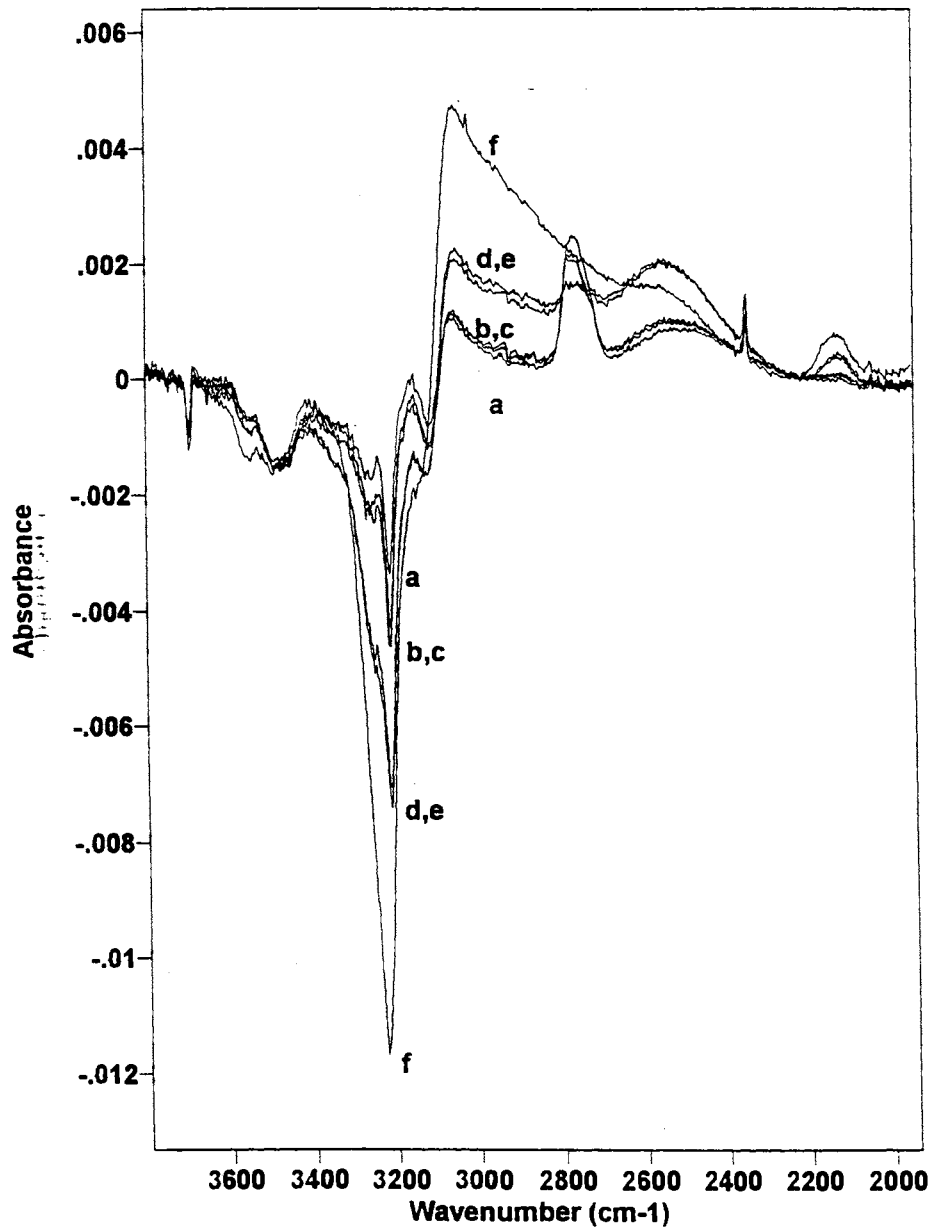


Fig. 68 Curves a - f show the changes in the infrared difference spectra for an HCl coated cluster deposit as the temperature is increased in 10 K steps from 20 to 70 K.

intensity of the dihydrate band, and the loss of the molecular complex adsorption intensity.

If we now examine another experiment, a deposit of a 1:1 HCl:N<sub>2</sub> premix onto a cluster deposit (see Fig. 69), it is seen that the changes which occur above 3000 cm<sup>-1</sup> look very similar to the adsorption of a weak adsorbate. This should not be surprising since N<sub>2</sub> is in fact a weak adsorbate and enters the cell and coats the clusters before the HCl is deposited, as has been described above. The interesting part is that the HCl does penetrate the N<sub>2</sub> to reach the surface. This is seen by the formation of the molecular complex and the loss of the sym d-H band intensity at 3110 cm<sup>-1</sup> (an effect not seen with weak adsorbates). Also, positive bands form at 3230 and 3155 cm<sup>-1</sup>. These are approximately the same frequencies as the bands observed after the adsorption of C<sub>2</sub>H<sub>2</sub>, SO<sub>2</sub>, TMA, and H<sub>2</sub>S onto the cluster surface. If the HCl is interacting with the d-H, this effect can not be identified in this experiment. The derivative shape around 3700 cm<sup>-1</sup> and the positive band at 3550 cm<sup>-1</sup> is a result of shifting of the d-H and the d-O through interaction of N<sub>2</sub> with each of these groups, respectively. When the temperature is increased to 60 K, the acid attacks the subsurface as was seen above. This results in the loss in the "bulk" region and the formation of the amorphous dihydrate.

The question is now, does the HCl affect the d-H, and if so, how. If we look at the neat acid being deposited onto the clusters surface, we will see a shifting of the d-H (see Fig. 70). This shifting could be the result of a small amount of N<sub>2</sub> contaminant present in the acid. However, because of the care taken to avoid N<sub>2</sub> contamination, this shifting is believed to be caused by the acid. So, why is the shifting so small, more like a

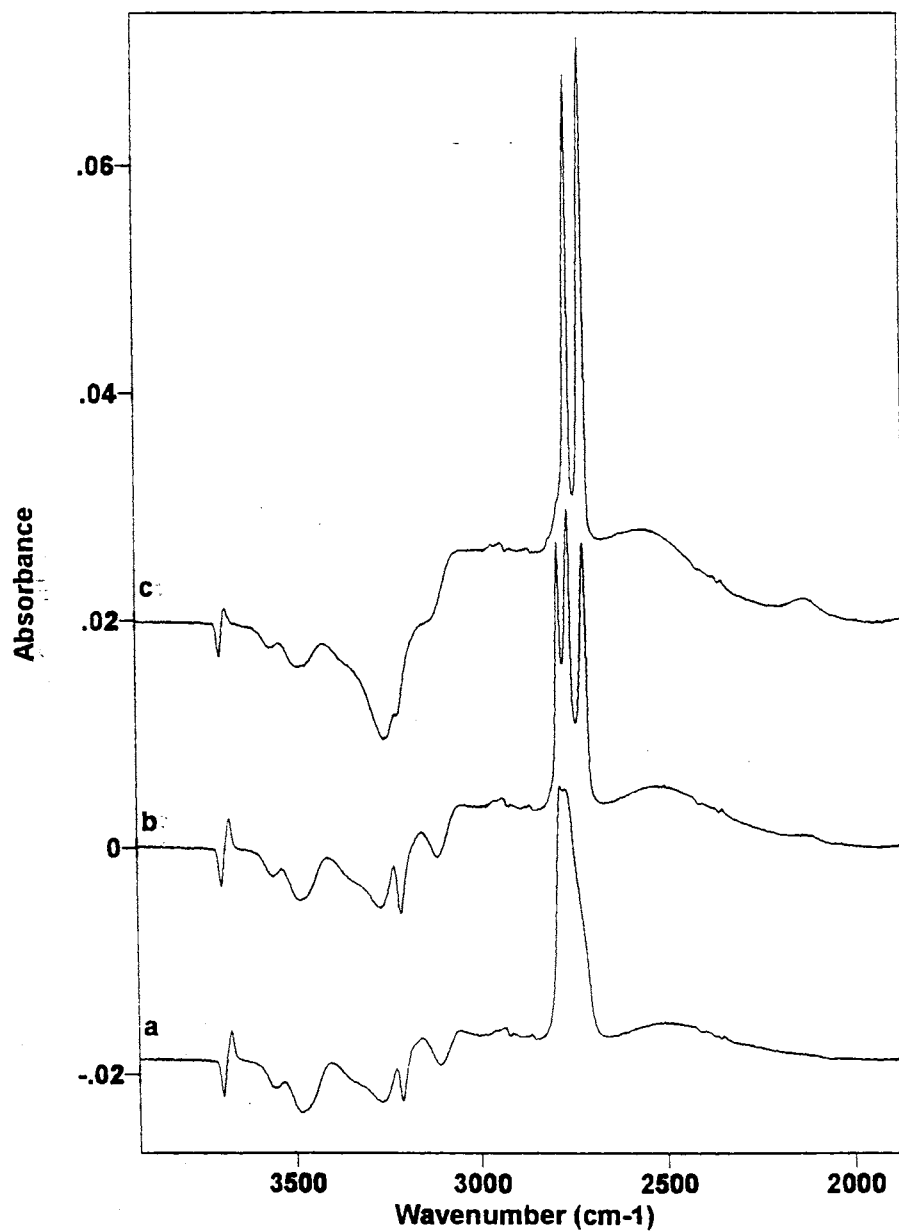


Fig. 69 Curves a - c show the changes in the infrared difference spectra for an HCl:N<sub>2</sub> coated cluster deposit as the temperature is increased in 20 K steps from 20 to 60 K.

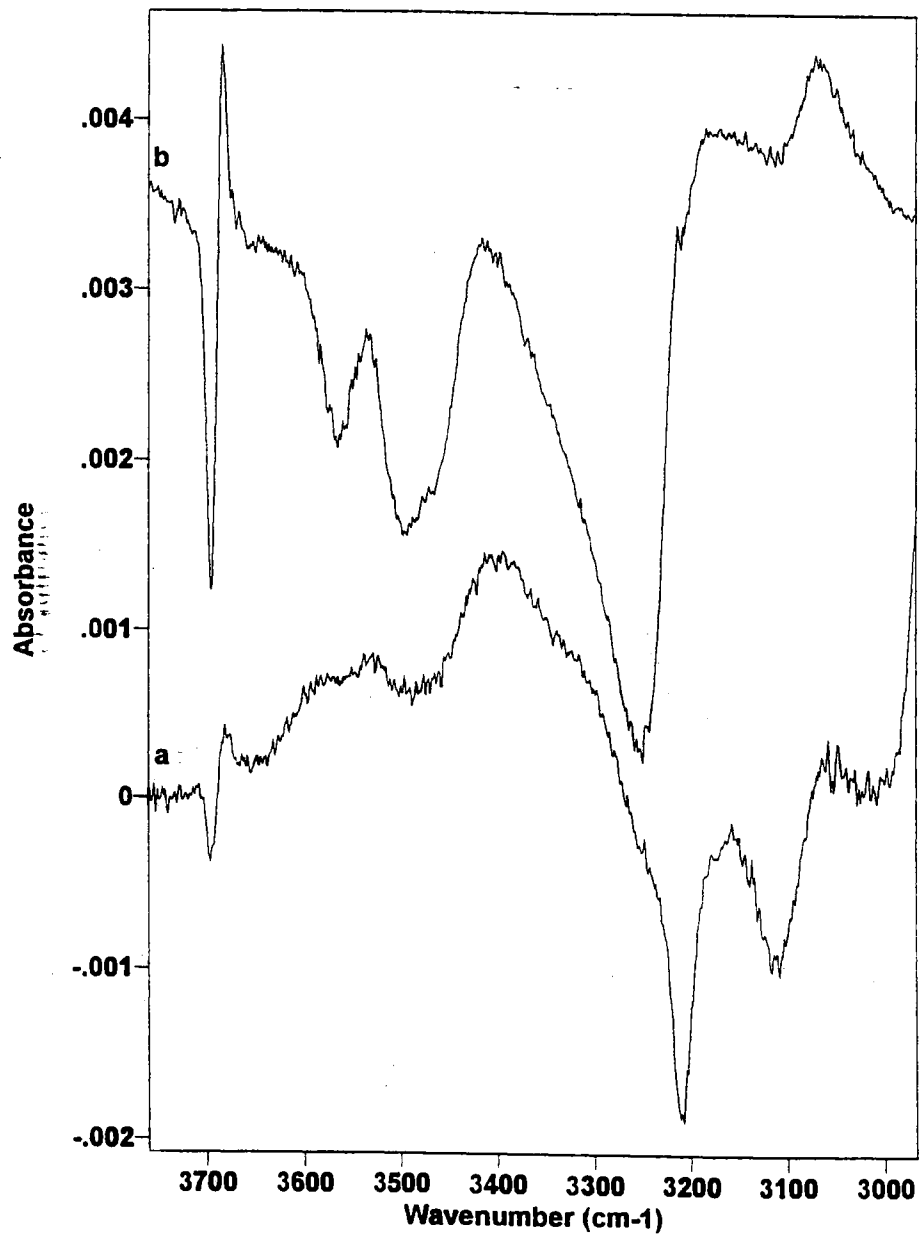


Fig. 70 Infrared spectra of (a) HCl and (b) HBr coated cluster showing the effects on the surface modes of the cluster. Particularly notice the weak shifting of the d-H by the strong hydrogen-bonding adsorbates.

weak adsorbate rather than large as for other strong hydrogen-bonding molecules. A possible answer to this question comes from the theoretical work which has been performed on the  $\text{HCl}(\text{H}_2\text{O})_n$  system.<sup>35</sup> In this system, the acid and the water form a hydrogen-bonded ring system. However, the interaction between the hydrogen of the water and the chloride of the acid is found not to be a hydrogen-bond. Instead, they simply form a weak interaction, an interaction which is not strong enough to be considered a hydrogen-bond, but which is strong enough to stabilize the system into a ring. If we use this as the model for the interaction of the chloride and the d-H, it is expected that the acid would affect the d-H as if it is a weak adsorbate. Further, from Kroes and Clary's model<sup>34</sup> for the acid adsorbed onto an ice surface, it can be seen that the chloride of the HCl is positioned in the middle of a hexagonal ring and interacts with multiple d-H, thus further weakening the interaction between the chloride and the individual d-H.

## Conclusions

The interaction of strong hydrogen-bonding adsorbates with the surface of ice nanocrystals can be divided into three classes. These classes are nonordering, ordering, and reactive.

The nonordering class has only one example at this time. It is HCN. When HCN is adsorbed onto the surface of a cluster deposit, it strongly affects the surface and subsurface of the ice clusters. The corresponding OH-stretch modes are shifted and

enhanced in such a manner that a gain in intensity results which closely resembles amorphous ice.

The second class is the ordering adsorbates. They include  $\text{H}_2\text{S}$ ,  $\text{SO}_2$ , and  $\text{C}_2\text{H}_2$ . These adsorbates affect the surface of the clusters in a manner similar to HCN with the exception that the resulting increase in intensity in the "bulk" region resembles crystalline ice. This is thought to be a result of these adsorbates being able to "mimic" a water molecule on the cluster surface and effectively add an additional layer to the surface. These adsorbates differ from HCN in that their structure is closer to that of  $\text{H}_2\text{O}$  so that they are also able to induce order into the surface.

The third class of adsorbates are those molecules which are reactive with the cluster surface. They include  $\text{NH}_3$ , TMA, and the hydrogen halides. These adsorbates have a tendency to react with the cluster surface at increased exposures and temperatures. However, under strictly controlled conditions, the interaction of these adsorbates with the surface, in the absence of significant reaction, can be seen. They tend to interact only with the outer clusters of the cluster assembly due to their tendency to react rather than diffuse into the deposit. Other than this, they tend to order the surface of the clusters in a manner similar to the ordering strong hydrogen-bonding adsorbates.



## CHAPTER V

### COMPARISON OF C<sub>2</sub>H<sub>6</sub>, C<sub>2</sub>H<sub>4</sub>, AND C<sub>2</sub>H<sub>2</sub>

Up to this point, most of the work done with adsorbates in an attempt to understand the surface of ice has been done with weak adsorbates. Now, with this work, strong hydrogen-bonding adsorbates have been investigated. This chapter is included in order to show the changes which occur as one goes from a weak to a strong adsorbate with the least number a variables changing. To this end C<sub>2</sub>H<sub>6</sub>, C<sub>2</sub>H<sub>4</sub>, and C<sub>2</sub>H<sub>2</sub> have been investigated. C<sub>2</sub>H<sub>6</sub> is a weak adsorbate with neither a good electron donating nor electron accepting group. In C<sub>2</sub>H<sub>4</sub>, the double bond introduces an electron donating group into the molecule, while the hydrogens still do not make very good electron acceptors. Finally, C<sub>2</sub>H<sub>2</sub> is a strong hydrogen bonding adsorbate with both electron donating (the triple bond) and electron accepting (the protic hydrogens) groups.

Figure 71 shows the changes which occur in the spectra as the adsorbate goes from a weak to a strong hydrogen-bonding adsorbate. The C<sub>2</sub>H<sub>6</sub> is a typical weak adsorbate. The d-H is shifted only a few tens of wave numbers producing a derivative shape in the difference spectrum. Also, the intensity of the shifted d-H is one of the strongest features in the difference spectrum. The intensity of the other surface modes are of approximately the same intensity as the d-H. Finally, there is no obvious sign of the shifted sym d-H.

The C<sub>2</sub>H<sub>4</sub>, which now has an electron donating group, has a little stronger effect on the difference spectrum. The d-H is now shifted several tens of wave numbers, which is more indicative of a strong adsorbate, with most of the other surface effects closely

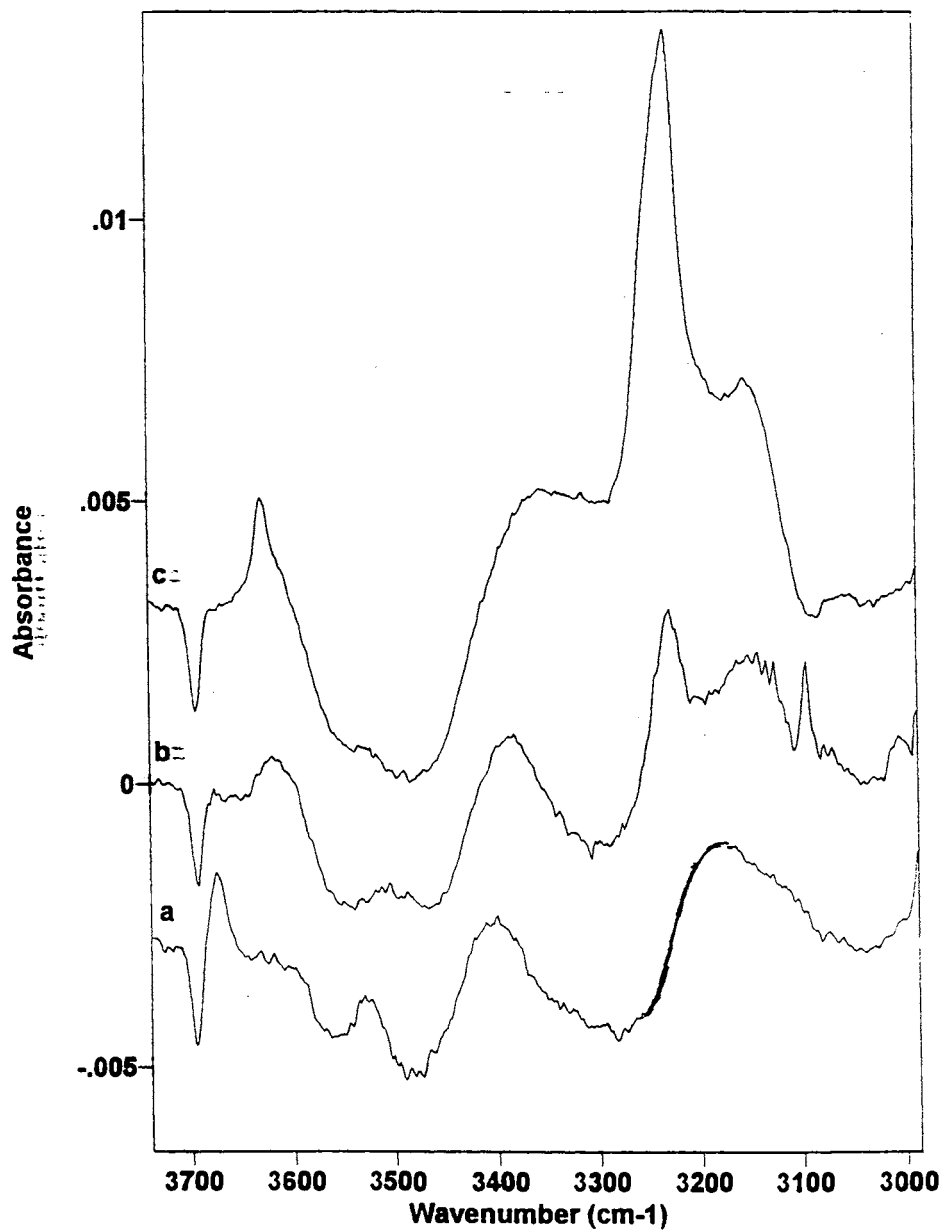


Fig. 71 Comparison of the difference spectra from going from (a) the weak hydrogen-bonding adsorbate  $C_2H_2$  to (b) the intermediate adsorbate  $C_2H_4$ , to (c) the strong hydrogen-bonding adsorbate acetylene.

resembling those of a weak adsorbate. The only exception is that there is a little structure starting to form in the "bulk" region of the difference spectrum. This structure is similar to the structure which is produced by an ordering strong hydrogen-bonding adsorbate, although its intensity much more resembles a weak adsorbate.

Finally,  $C_2H_2$  has both an electron donating and an electron accepting group, which, as state earlier, will allow it to "mimic" a water molecule. Therefore this adsorbate, as has been seen, is an ordering strong hydrogen-bonding adsorbate. Its basic structure is very similar to that produced by  $C_2H_4$  although its effects on the cluster surface and subsurface are much stronger. The d-H is shifted the same distance as it was for the  $C_2H_4$  although now it is much sharper. The d-H is also no longer one of the strongest features of the difference spectrum, in fact, it is now one of the weakest. The intensity of the loss of d-O and S-4 has increased and is now about twice that of the d-H. Also, the sym d-H is now observable for the first time. Its intensity seems to be weak, but this is most likely due to being on the edge of an intense "bulk" band, which tends to make it appear weaker. The structure in the "bulk" region also increases in intensity by a factor of five.

Unfortunately a similar molecule with only an electron accepting group (no electron donating group) is not available. This would of presented an interesting look at the effects of having only one of the two groups. However, this series still presented an interesting and valuable insight into the need for a molecule to have both an electron donating and an electron accepting group to order the surface of an ice cluster.

## CHAPTER VI

### DISCUSSION AND CONCLUSIONS

#### Literature Review

As has been shown in the literature review, the surface of ice clusters are disordered. This disorder extends a finite distance into the interior of the cluster as is demonstrated by both experimental<sup>8-10</sup> and theoretical<sup>11-17</sup> work. This disorder, as shown by Torchet *et al.*, extends somewhere between 8 and 13 Å into the interior of the ice surface. If a bilayer is assumed to be 3.7 Å thick, then this means that the disorder extends between 2 and 3.5 bilayers into the surface. If one of these is considered to be the surface bilayer, this leaves between 1 and 2.5 bilayers to compose the subsurface of the cluster. The subsurface is that region of the cluster which is spectroscopically identifiable as being different from both the surface and the interior of the cluster. It is not part of the surface because it is not affected by weak hydrogen-bonding adsorbates, yet it is not part of the interior of the cluster due to the fact that its infrared spectrum is different from that of the interior. Thus, the subsurface is defined on a phenomenological basis as can be seen spectroscopically (see Appendix A).

In theoretical computations by both Kroes<sup>13</sup> and Buch *et al.*,<sup>14-17</sup> they show that the surface of a slab of ice is indeed disordered, and that this disorder extends into the subsurface of the cluster. However, due to the manner in which the theoretical calculations are performed, it is not possible to assign a spectroscopically identifiable

depth to the subsurface of the slab, only that this disorder is present and diminishes as one looks deeper into the slab.

In experiments performed with long chain aliphatic alcohols,<sup>18-20</sup> the 2-dimensional self-assembled monolayers (SAMs) induce order into the liquid water layer directly in contact with the SAM. This order is also carried over to the surface of the ice which is formed when this assembly is cooled, thus indicating that the disorder normally found within the surface of ice can be reduced if not eliminated due to the presence of the right adsorbate on its surface. This idea is further substantiated in a molecular dynamics simulation<sup>21</sup> where long chain aliphatic acid molecules show an epitaxial relationship between the overlayer which they form and the rigid hexagonal ice surface on which they order.

### **Strong Hydrogen-Bonding Adsorbates**

Since SAMs are able to reduce the degree of disorder found within the surface of ice, it is not too presumptuous to assume that other molecules will be able to produce a similar effect. It is to this end, along with a desire to understand the OH-stretching region for clusters with adsorbed HCl, that strong hydrogen-bonding molecules are studied.

It is found that strong hydrogen-bonding molecules can be divided into three classes: a) nonordering, b) ordering, and c) ordering and reactive. This classification is derived from the manner in which the different strong hydrogen-bonding adsorbates interact with the ice cluster surface.

The "nonordering" strong hydrogen-bonding adsorbates when adsorbed onto an ice cluster surface do not induce any ordering into that surface. This "nonordering" is determined spectroscopically by the band structure which is obtained in the difference spectra of the adsorbate coated minus bare cluster spectra. The band structure obtained in the difference spectra for the nonordering adsorbates is the composite of the loss of the cluster surface due to the adsorption of the adsorbate and the gain of new "interior" ice due to the interaction of the adsorbate with the surface. It is the band structure of this new "interior" ice which determine if the adsorbate is ordering or nonordering. For a nonordering adsorbate, this band structure closely resembles the band structure for a thin film amorphous ice, thus the nonordering terminology.

However, this nonordering [as well as the classification of the a) ordering and b) ordering and reactive cases] is determined by the adsorption of the adsorbate at the minimum temperature at which it will adsorb. Therefore, it says nothing about the behavior of these adsorbates at higher temperatures (see Appendix A).

"Ordering" strong hydrogen-bonding adsorbates, on the other hand, produce a band structure for the gain of "interior" ice in the difference spectra which closely resemble the spectra of a crystalline cluster deposit. Therefore, when these adsorbates adsorb onto the cluster surface, they tend to restructure the cluster surface in such a fashion as to create, as determined spectroscopically, new crystalline interior ice. Thus the terminology of ordering.

The final classification is the "ordering and reactive" adsorbates. They tend to order the cluster surface just as the "ordering" adsorbates do, but they also have a tendency to also react with that ice surface. Therefore, great care is needed in order to

observe the effects which they have on the cluster surface. However, once the right "nonreactive" conditions are found, they tend to behave just the same as the "ordering" adsorbates.

The ability of the adsorbate to "mimic" a water molecule on the cluster surface is apparently what determines if the adsorbate is "ordering" or "nonordering". If the adsorbate has an electron donating and an electron accepting group separated by  $\sim 1$  Å, then it will be able to "mimic" a water molecule and will induce order into the surface of the ice cluster.

When a strong hydrogen-bonding adsorbate adsorbs onto the surface of an ice cluster, it affects the surface in two steps. The first step is when the adsorbate first starts to adsorb and continues until the surface is about 50% coated. During this time, the adsorbate affects primarily just the surface of the cluster. The d-H is shifted to a half-shifted position, and the d-O and S-4 of the bare ice have lost approximately the same intensity as the d-H. There is an increase in the intensity in the "bulk" region of the spectrum and the sym d-H is only starting to lose intensity. During this period, the adsorbate is believed to be "laying down" on the surface and interacting with several surface groups at the same time.

As the surface become greater than 50% coated, the second step takes place. During this step, due to the number of adsorbed molecules on the surface of the cluster, the adsorbate molecules begin to become "crowded" on the surface. As they become "crowded", they tend to "stand up" on the surface and interact with fewer surface groups. However, they interact more strongly with the surface groups with which they do interact. This is demonstrated by the half-shifted d-H band shifting to its fully-shifted

position. Also, the intensity of the loss in the d-O and S-4 bands increases until the intensity of the loss of the S-4 is about twice that of the d-H. The intensity gained in the "bulk" region of the difference spectrum continues to increase and the sym d-H appears quite strongly. In fact, the sym d-H band intensity loss at  $3100\text{ cm}^{-1}$  goes from almost nonexistent at 50% coverage to approximately the same intensity loss as the d-H band, thus signifying a much stronger interaction between the adsorbate and the surface.

### HCl Coated Clusters

As was stated earlier, one of the reasons for investigating strong hydrogen-bonding adsorbates is to understand the changes which occur in the OH-stretching region when HCl is deposited onto the cluster surface. It is found that even though the HCl is deposited onto the cluster surface at a temperature much lower than that of the other adsorbates, the HCl produces the same effects as is found for the other ordering and reactive adsorbates. That is, when the HCl is deposited, the vibrational frequency of the surface modes are strongly shifted, and there is a gain in intensity in the "bulk" region of the difference spectrum which is representative of ordering of the cluster surface and subsurface.

As has been stated, the HCl is an ordering and reactive adsorbate. It reacts readily with the cluster surface except under very strict conditions. These conditions are: a) if the clusters have been highly (140 K) annealed, or b) if the clusters have been precoated with an adsorbate. Under both of these conditions, the HCl still has to be deposited onto the clusters at 20 K and with a very slow deposition rate, otherwise



reaction will take place. If any other conditions are used, then the HCl reacts with the cluster surface forming the amorphous dihydrate.

### **Comparison of $C_2H_6$ , $C_2H_4$ , and $C_2H_2$**

The comparison of  $C_2H_6$ ,  $C_2H_4$ , and  $C_2H_2$  shows the effects of increasing the strength of the interaction between the adsorbate and the cluster surface. What is seen is that when ethane is adsorbed onto the cluster surface, the surface modes of the cluster are the only vibrations which are affected due to the presence of the adsorbate. Thus, ethane behaves as a typical weak adsorbate. If we now look at acetylene, we see that the surface is strongly affected, but so is the subsurface. Thus, acetylene is a strong hydrogen-bonding adsorbate. Now, if ethylene is examined, it has an effect somewhere in between that of a weak and a strong adsorbate. It affects the surface modes fairly strongly, especially the d-H, but the "bulk" region of the difference spectrum is not affected very strongly. The band structure which forms in the "bulk" region resembles the band structure for the "ordering" adsorbates, however, its intensity is nowhere near as intense as that produced by the strong hydrogen-bonding adsorbates. In fact, the intensity of the effects are more closely related to the intensities of a weak adsorbate. Thus, ethylene shows the possibility of maybe an intermediate hydrogen-bonding adsorbate, between the effects of strong and weak. This intermediate effect may be, at least in part, due to the ethylene only have an electron donating site, and no specific electron accepting site. The implication of this result shows a need for further studies

into adsorbates which contain either an electron donating or an electron accepting group, but not both.

## REFERENCES

1. Wofsy, S. C., Molina, M. J., Salawitch, L. E., and McElroy, M. B., "Interactions Between HCl, NO<sub>x</sub>, and H<sub>2</sub>O Ice in the Antarctic Stratosphere: Implications for Ozone." Journal of Geophysical Research, Vol. 93, p. 2442, 1988.
2. Chu, Liang T., Leu, Ming-Taun, and Keyser, Leon F., "Uptake of HCl in Water Ice and Nitric Acid Ice Films." J. Phys. Chem., Vol. 97, p. 7779, 1993.
3. Abbatt, J. P. D., Beyer, K. D., Fucaloro, A. F., McMahon, J. R., Wooldridge, P. J., Zhang, R., and Molina, M. J., "Interaction of HCl Vapor with Water-Ice: Implications for the Stratosphere." Journal of Geophysical Research, Vol. 97, p. 15819, 1992.
4. Hanson, D. R. and Ravishankara, A. R., "The Reaction Probabilities of ClONO<sub>2</sub> and N<sub>2</sub>O<sub>5</sub> on Polar Stratospheric Cloud Materials." Journal of Geophysical Research, Vol. 96, p. 5081, 1991.
5. Hanson, D. R. and Ravishankara, A. R., "Investigation of the Reactive and Nonreactive Processes Involving ClONO<sub>2</sub> and HCl on Water and Nitric Acid Doped Ice." J. Phys. Chem., Vol. 96, p. 2682, 1992.
6. Molina, M. J., Tso, Tai-Ly, Molina, L. T., and Wang, F. C-Y., "Antarctic Stratospheric Chemistry of Chlorine Nitrate, Hydrogen Chloride, and Ice: Release of Active Chlorine." Science, Vol. 238, p. 1253, 1987.
7. Robertson, S. H. and Clary, D. C., "Solvation of Hydrogen Halides on the Surface of Ice." Faraday Discussion, Vol. 100, p. 309, 1995.
8. Torchet, G., Schwartz, P., Farges, J., de Feraudy, M. F., and Raoult, B., "Structure of Solid Water Clusters Formed in a Free Jet Expansion." J. Chem. Phys., Vol. 79, p. 6193, 1983.
9. Huang, J. and Bartell, S., "Kinetics of Homogeneous Nucleation in the Freezing of Large Water Clusters." J. Phys. Chem., Vol. 99, p. 3942, 1995.
10. a) Dosch, H., Lied, A., and Bilgram, J. H., "Glancing-Angle X-Ray Scattering Studies of the Premelting of Ice Surfaces." Surface Science, Vol. 327, p. 145, 1995.

- b) Materer, N., Starke, U., Barbieri, A., Van Hove, M. A., Somorjai, G. A., Kroes, G. J., and Minot, C., "Molecular Structure of a Low-Temperature Ice Ih (0001) Crystal." J. Phys. Chem., Vol. 99, p. 6267, 1995.
11. Zhang, Q. and Buch, V., "Computational Study of Formation Dynamics and Structure of Amorphous Ice Condensates." J. Chem. Phys., Vol. 92, p. 5004, 1990.
12. Buch, V., "Growth and Structure of Amorphous Ice Condensates: A Computational Study. II." J. Chem. Phys., Vol. 96, p. 3814, 1992.
13. Kroes, G.-J., "Surface Melting of the (0001) Face of TIP4P Ice." Surface Science, Vol. 275, p. 365, 1992.
14. Devlin, J. P. and Buch, V., "Surface of Ice as Viewed from Combined Spectroscopic and Computer Modeling Studies." J. Phys. Chem., Vol. 99, p. 16534, 1995.
15. Rowland, B., Kadagathur, N. S., Devlin, J. P., Buch, V., Feldman, T., and Wojcik, M. J., "Infrared Spectra of Ice Surfaces and Assignment of Surface-Localized Modes from Simulated Spectra of Cubic Ice." J. Chem. Phys., Vol. 102, p. 8328, 1995.
16. Buch, V., Delzeit, L., Blackledge, C., and Devlin, J. P., "Structure of the Ice Nanocrystal Surface from Simulated versus Experimental Spectra of Adsorbed CF<sub>4</sub>." J. Phys. Chem., Vol. 100, p. 3732, 1996.
17. Buch, V., Delzeit, L., Devlin, M. S., Rowland, B., and Devlin, J. P., "Adsorbate-Induced Partial Ordering of the Irregular Surface and Subsurface of Crystalline Ice." J. Phys. Chem., Vol. 100, p. 10076, 1996.
18. Gavish, M., Popovitz-Biro, R., Lahav, M., and Liserovitz, L., "Ice Nucleation By Alcohols Arranged in Monolayers at the Surface of Water Drops." Science, Vol. 250, p. 973, 1990.
19. Majewski, J., Margulis, L., Jacquemain, D., Leveiller, F., Böhm, C., Arad, T., Talmon, Y., Lahav, M., and Leiserowitz, "Electron Diffraction and Imaging of Uncompressed Monolayers of Amphiphilic Molecules on Vitreous and Hexagonal Ice." Science, Vol. 261, p. 899, 1993.
20. Majewski, J., Popovitz-Biro, R., Kjaer, K., Als-Nielsen, J., Lahav, M., and Leiserowitz, L., "Toward a Determination of the Critical Size of Ice Nuclei. A Demonstration by Grazing Incidence X-ray Diffraction of Epitaxial Growth of Ice under the C<sub>31</sub>H<sub>64</sub>OH Alcohol Monolayer." J. Phys. Chem., Vol. 98, p. 4087, 1994.

21. Bell, K-P and Rice, S. A., "Structure and Equation of State of a Long Chain Amphiphile Monolayer Adsorbed on Ice Ih: A Molecular Dynamics Study." J. Chem. Phys., Vol. 104, p. 1684, 1996.
22. Engquist, I., Lundström, I., and Liedberg, B., "Temperature-Programmed Desorption and Infrared Studies of D<sub>2</sub>O Ice on Self-Assembled Alkanethiolate Monolayers: Influence of Substrate Wettability." J. Phys. Chem., Vol. 99, p. 12257, 1995.
23. Popovitz-Biro, R., Wang, J. L., Majewski, J., Shavit, E., Leiserowitz, L., and Lahav, M., "Induced Freezing of Supercooled Water into Ice by Self-Assembled Crystalline Monolayers of Amphiphilic Alcohols at the Air-Water Interface." J. Am. Chem. Soc., Vol. 116, p. 1179, 1994.
24. a) Ferriso, C. C. and Hornig, D. F., J. Am. Chem. Soc., Vol. 75, p. 4113, 1953.,  
b) Ferriso, C. C. and Hornig, D. F., "Infrared Spectra of Oxonium Halides and the Structure of the Oxonium Ion." J. Chem. Phys., Vol. 23, p. 1464, 1955.
25. Delzeit, L., Rowland, B., and Devlin, J. P., "Infrared Spectra of HCl Complexed/ionized in Amorphous Hydrates and at Ice Surfaces in the 15-90 K Range." J. Phys. Chem., Vol. 97, p. 10312, 1993.
26. a) Graham, J. D. and Roberts, J. T., "Interaction of Hydrogen Chloride with an Ultrathin Ice Film: Observation of Adsorbed and Absorbed States." J. Phys. Chem., Vol. 98, p. 5974, 1994.  
b) Horn, A. B., Chesters, M. A., McCoustra, M. R. S., and Sodeau, J. R., "Adsorption of Stratospherically Important Molecules on Thin D<sub>2</sub>O Ice Films using reflection Absorption Infrared Spectroscopy." J. Chem. Soc. Faraday Trans., Vol. 88, p. 1077, 1992.
27. Graham, J. D. and Roberts, J. T., "Interaction of HCl with Crystalline and Amorphous Ice: Implications for the Mechanisms of Ice-Catalyzed Reactions." Geophysical Research Letters, Vol. 22, p. 251, 1995.
28. Smart, R. St. C. and Sheppard, F. R. S., "Infrared Spectroscopic Studies of Adsorption on Alkali Halide Surfaces: I. HCl, HBr, and HI on Fluorides, Chlorides, Bromides, and Iodides." Proc. Roy. Soc. Lond. A, Vol. 320, p. 417, 1971.
29. Blass, P. M., Jackson, R. C., Polanyi, J. C., and Weiss, H., "Infrared Spectroscopy of HX (X=Br,Cl) Adsorbed on LiF (001): Alignment and orientation." J. Chem. Phys., Vol. 94, p. 7003, 1991.
30. Ault, B. S. and Pimentel, G. C., "Infrared Spectrum of the Water-Hydrochloric Acid Complex in Solid Nitrogen." J. Phys. Chem., Vol. 77, p. 47, 1973.

31. Ayers, G. P. and Pullin, A. D. E., "The I.R. Spectra of Matrix Isolated Water Species-II. The Characterization of Non-Rotating monomer Water Species in an Argon Matrix by Xenon Doping: The Matrix Isolated Spectra of  $\text{H}_2\text{O}\cdot\text{HCl}$  and  $(\text{CH}_3)_2\text{O}\cdot\text{H}_2\text{O}$  as Model Compounds for Water Dimer Spectra." Spectrochimica Acta., Vol. 32A, p. 1641, 1976.
32. Schriver, A., Silvi, B., Maillard, D., and Perchard, J. P., "Structure of Water-Hydrochloric Acid Complexes in Argon and Nitrogen Matrices From Infrared Spectra." J. Phys. Chem., Vol. 81, p. 2095, 1977.
33. Amirand, C. and Maillard, D., "Spectrum and Structure of Water-Rich Water-Hydracid Complexes from Matrix Isolation Spectroscopy: Evidence for Proton Transfer." Journal of Molecular Structure, Vol. 176, p. 181, 1988.
34. Kroes, Geert-Jan and Clary, D. C., "Sticking of HCl and ClOH to Ice: A Computational Study." J. Phys. Chem., Vol. 96, p. 7079, 1995.
35. Packer, M. J. and Clary, D. C., "Interaction of HCl with Water Clusters:  $(\text{H}_2\text{O})_n\text{HCl}$ ,  $n = 1-3$ ." J. Phys. Chem., Vol. 99, p. 14323, 1995.
36. Robertson, S. H. and Clary, D. C., "Solvation of Hydrogen Halides on the Surface of Ice." Faraday Discussion, Vol. 100, p. 309, 1995.
37. Gutowsky, H. S., Germann, T. C., Augspurger, J. D., and Dykstra, C. E. "Structure and Dynamics of the  $\text{H}_2\text{O}\text{-HCN}$  Dimer." J. Chem. Phys., Vol. 96, p. 5808, 1992.
38. Knözinger, E., Kollhoff, H., Schrems, O., and Langel, W., "Intermolecular Interactions and Dynamics of Molecules and Clusters Isolated in Solid Argon and  $\text{CCl}_4$  Matrices." J. Mol. Struct., Vol. 141, p. 399, 1986.
39. Maroncelli, M., Hopkins, G. A., Nibler, J. W., and Dyke, T. R., "Coherent Raman and Infrared Spectroscopy of HCN Complexes in Free Jet Expansions and in Equilibrium Samples." J. Chem. Phys., Vol. 83, p. 2129, 1985,
40. Walsh, B., Barnes, A. J., Suzuki, S., and Orville-Thomas, W. J., "Studies of Intermolecular Interactions by Matrix Isolation Vibrational Spectroscopy an Normal Coordinate Analysis." J. Mol. Spec., Vol. 72, p. 44, 1978.
41. Johnson, G. L. and Andrews, L., "Infrared Spectra of Two 1:1 Complexes between HCN and HF in Solid Argon at 12 K." J. Am. Chem. Soc., Vol. 105, p. 163, 1983.
42. Pacansky, J., "The Infrared Spectrum of a Molecular Aggregate. The HCN Dimer Isolated in an Argon Matrix." J. Phys. Chem., Vol. 81, p. 2240, 1977.

43. Kozirovski, Y. and Folman, M., "Infra-red Spectrum and Spectral Shifts of HCN Adsorbed on Evaporated Alkali Halides." Trans. Faraday Soc., Vol. 62, p. 808, 1966.
44. Cruz, M., Kaiser, A., Rouxhet, P. G., and Fripiat, J. J., "Adsorption and Transformation of HCN on the Surface of Copper and Calcium Montmorillonite." Clays and Clay Minerals, Vol. 22, p. 417, 1974.
45. Amos, R. D., "Structures, Harmonic Frequencies and Infrared Intensities of the Dimers of H<sub>2</sub>O and H<sub>2</sub>S." Chemical Physics, Vol. 104, p. 145, 1986.
46. Datta, A. and Cavell, R. G., "Claus Catalysis. 2. An FTIR Study of the Adsorption of H<sub>2</sub>S on the Alumina Catalyst." J. Phys. Chem., Vol. 89, p. 450, 1985.
47. Phillips, J. A., Canagaratna, M., Goodfriend, H., and Leopold, K. R., "Microwave Detection of a Key Intermediate in the Formation of Atmospheric sulfuric Acid: The Structure of H<sub>2</sub>O-SO<sub>3</sub>." J. Phys. Chem., Vol. 99, p. 501, 1995.
48. Tso, T.-L. and Lee, K. C., "Formation of Sulfuric Acid and Sulfur Trioxide/Water Complex from Photooxidation of Hydrogen Sulfide in O<sub>2</sub> at 15 K." J. Phys. Chem., Vol. 88, p. 2776, 1984.
49. Bondybey, V. E. and English, J. H., "Infrared Spectra of SO<sub>3</sub> Polymers and Complexes in Rare Gas Matrices." J. Mol. Spec., Vol. 109, p. 221, 1985.
50. Schriver, L., Carrere, D., Schriver, A., and Jaeger, K., "Matrix-isolation photolysis of SO<sub>2</sub>, O<sub>3</sub>, and H<sub>2</sub>O: Evidence for the H<sub>2</sub>O:SO<sub>3</sub> Complex." Chem. Phys. Lett., Vol. 181, p. 505, 1991.
51. Chen, T. S. and Plummer, P. L. M., "Ab Initio MO Investigation of the Gas-Phase Reaction SO<sub>3</sub> + H<sub>2</sub>O - H<sub>2</sub>SO<sub>4</sub>." J. Phys. Chem., Vol. 89, p. 3689, 1985.
52. Hofmann, M. and Schleyer, Paul von Rague, "Acid Rain: Ab Initio Investigation of the H<sub>2</sub>O-SO<sub>3</sub> Complex and Its Conversion into H<sub>2</sub>SO<sub>4</sub>." J. Am. Chem. Soc., Vol. 116, p. 4947, 1994.
53. Reiner, T. and Arnold, F., "Laboratory Investigations of Gaseous Sulfuric Acid Formation via SO<sub>3</sub> + H<sub>2</sub>O + M - H<sub>2</sub>SO<sub>4</sub> + M: Measurement of the Rate Constant and Product Identification." J. Chem. Phys., Vol. 101, p. 7399, 1994.
54. Morokuma, K. and Muguruma, C., "Ab Initio Molecular Orbital Study of the Mechanism of the Gas Phase Reaction SO<sub>3</sub> + H<sub>2</sub>O: Importance of the Second Water Molecule." J. Am. Chem. Soc., Vol. 116, p. 10316, 1994.
55. Matsumura, K., Lovas, F. J., and Suenram, R. D., "The Microwave spectrum and Structure of the H<sub>2</sub>O-SO<sub>2</sub> Complex." J. Chem. Phys., Vol. 91, p. 5887, 1989.

56. Fleyfel, F., Richardson, H. H., and Devlin, J. P., "Comparative SO<sub>2</sub> Infrared Spectra: Type I and II Clathrate Hydrate Films, Large Gas-Phase Clusters, and Anhydrous Crystalline Films." J. Phys. Chem., Vol. 94, p. 7032, 1990.
57. Bertie, John E. and Shehata, Mohamed R., "The Infrared spectra of NH<sub>3</sub>·H<sub>2</sub>O and ND<sub>3</sub>·D<sub>2</sub>O at 100 K." J. Chem. Phys., Vol. 83, p. 1449, 1985.



## BIBLIOGRAPHY

- Abbatt, J. P. D., Beyer, K. D., Fucaloro, A. F., McMahon, J. R., Wooldridge, P. J., Zhang, R., and Molina, M. J., "Interaction of HCl Vapor with Water-Ice: Implications for the Stratosphere." Journal of Geophysical Research, Vol. 97, p. 15819, 1992.
- Amirand, C. and Maillard, D., "Spectrum and Structure of Water-Rich Water-Hydracid Complexes from Matrix Isolation Spectroscopy: Evidence for Proton Transfer." Journal of Molecular Structure, Vol. 176, p. 181, 1988.
- Amos, R. D., "Structures, Harmonic Frequencies and Infrared Intensities of the Dimers of H<sub>2</sub>O and H<sub>2</sub>S." Chemical Physics, Vol. 104, p. 145, 1986.
- Ault, B. S. and Pimentel, G. C., "Infrared Spectrum of the Water-Hydrochloric Acid Complex in Solid Nitrogen." J. Phys. Chem., Vol. 77, p. 47, 1973.
- Ayers, G. P. and Pullin, A. D. E., "The I.R. Spectra of Matrix Isolated Water Species-II. The Characterization of Non-Rotating monomer Water Species in an Argon Matrix by Xenon Doping: The Matrix Isolated Spectra of H<sub>2</sub>O·HCl and (CH<sub>3</sub>)<sub>2</sub>O·H<sub>2</sub>O as Model Compounds for Water Dimer Spectra." Spectrochimica Acta., Vol. 32A, p. 1641, 1976.
- Bell, K-P and Rice, S. A., "Structure and Equation of State of a Long Chain Amphiphile Monolayer Adsorbed on Ice Ih: A Molecular Dynamics Study." J. Chem. Phys., Vol. 104, p. 1684, 1996.
- Bertie, John E. and Shehata, Mohamed R., "The Infrared spectra of NH<sub>3</sub>·H<sub>2</sub>O and ND<sub>3</sub>·D<sub>2</sub>O at 100 K." J. Chem. Phys., Vol. 83, p. 1449, 1985.
- Blass, P. M., Jackson, R. C., Polanyi, J. C., and Weiss, H., "Infrared Spectroscopy of HX (X=Br,Cl) Adsorbed on LiF (001): Alignment and orientation." J. Chem. Phys., Vol. 94, p. 7003, 1991.
- Bondybey, V. E. and English, J. H., "Infrared Spectra of SO<sub>3</sub> Polymers and Complexes in Rare Gas Matrices." J. Mol. Spec., Vol. 109, p. 221, 1985.
- Buch, V., "Growth and Structure of Amorphous Ice Condensates: A Computational Study. II." J. Chem. Phys., Vol. 96, p. 3814, 1992.

- Buch, V., Delzeit, L., Blackledge, C., and Devlin, J. P., "Structure of the Ice Nanocrystal Surface from Simulated versus Experimental Spectra of Adsorbed CF<sub>4</sub>." J. Phys. Chem., Vol. 100, p. 3732, 1996.
- Buch, V., Delzeit, L., Devlin, M. S., Rowland, B., and Devlin, J. P., "Adsorbate-Induced Partial Ordering of the Irregular Surface and Subsurface of Crystalline Ice." J. Phys. Chem., Vol. 100, p. 10076, 1996.
- Chen, T. S. and Plummer, P. L. M., "*Ab Initio* MO Investigation of the Gas-Phase Reaction SO<sub>3</sub> + H<sub>2</sub>O - H<sub>2</sub>SO<sub>4</sub>." J. Phys. Chem., Vol. 89, p. 3689, 1985.
- Chu, Liang T., Leu, Ming-Taun, and Keyser, Leon F., "Uptake of HCl in Water Ice and Nitric Acid Ice Films." J. Phys. Chem., Vol. 97, p. 7779, 1993.
- Cruz, M., Kaiser, A., Rouxhet, P. G., and Fripiat, J. J., "Adsorption and Transformation of HCN on the Surface of Copper and Calcium Montmorillonite." Clays and Clay Minerals, Vol. 22, p. 417, 1974.
- Datta, A. and Cavell, R. G., "Claus Catalysis. 2. An FTIR Study of the Adsorption of H<sub>2</sub>S on the Alumina Catalyst." J. Phys. Chem., Vol. 89, p. 450, 1985.
- Delzeit, L., Rowland, B., and Devlin, J. P., "Infrared Spectra of HCl Complexed/ionized in Amorphous Hydrates and at Ice Surfaces in the 15-90 K Range." J. Phys. Chem., Vol. 97, p. 10312, 1993.
- Devlin, J. P. and Buch, V., "Surface of Ice as Viewed from Combined Spectroscopic and Computer Modeling Studies." J. Phys. Chem., Vol. 99, p. 16534, 1995.
- Engquist, I., Lundström, I., and Liedberg, B., "Temperature-Programmed Desorption and Infrared Studies of D<sub>2</sub>O Ice on Self-Assembled Alkanethiolate Monolayers: Influence of Substrate Wettability." J. Phys. Chem., Vol. 99, p. 12257, 1995.
- Ferriso, C. C. and Hornig, D. F., J. Am. Chem. Soc., Vol. 75, p. 4113, 1953.,
- Ferriso, C. C. and Hornig, D. F., "Infrared Spectra of Oxonium Halides and the Structure of the Oxonium Ion." J. Chem. Phys., Vol. 23, p. 1464, 1955.
- Fleyfel, F., Richardson, H. H., and Devlin, J. P., "Comparative SO<sub>2</sub> Infrared Spectra: Type I and II Clathrate Hydrate Films, Large Gas-Phase Clusters, and Anhydrous Crystalline Films." J. Phys. Chem., Vol. 94, p. 7032, 1990.
- Gavish, M., Popovitz-Biro, R., Lahav, M., and Liserovitz, L., "Ice Nucleation By Alcohols Arranged in Monolayers at the Surface of Water Drops." Science, Vol. 250, p. 973, 1990.

- Graham, J. D. and Roberts, J. T., "Interaction of Hydrogen Chloride with an Ultrathin Ice Film: Observation of Adsorbed and Absorbed States." J. Phys. Chem., Vol. 98, p. 5974, 1994.
- Graham, J. D. and Roberts, J. T., "Interaction of HCl with Crystalline and Amorphous Ice: Implications for the Mechanisms of Ice-Catalyzed Reactions." Geophysical Research Letters, Vol. 22, p. 251, 1995.
- Gutowsky, H. S., Germann, T. C., Augspurger, J. D., and Dykstra, C. E. "Structure and Dynamics of the H<sub>2</sub>O-HCN Dimer." J. Chem. Phys., Vol. 96, p. 5808, 1992.
- Hofmann, M. and Schleyer, Paul von Rague, "Acid Rain: *Ab Initio* Investigation of the H<sub>2</sub>O-SO<sub>3</sub> Complex and Its Conversion into H<sub>2</sub>SO<sub>4</sub>." J. Am. Chem. Soc., Vol. 116, p. 4947, 1994.
- Hanson, D. R. and Ravishankara, A. R., "The Reaction Probabilities of ClONO<sub>2</sub> and N<sub>2</sub>O<sub>5</sub> on Polar Stratospheric Cloud Materials." Journal of Geophysical Research, Vol. 96, p. 5081, 1991.
- Hanson, D. R. and Ravishankara, A. R., "Investigation of the Reactive and Nonreactive Processes Involving ClONO<sub>2</sub> and HCl on Water and Nitric Acid Doped Ice." J. Phys. Chem., Vol. 96, p. 2682, 1992.
- Huang, J. and Bartell, S., "Kinetics of Homogeneous Nucleation in the Freezing of Large Water Clusters." J. Phys. Chem., Vol. 99, p. 3942, 1995.
- Johnson, G. L. and Andrews, L., "Infrared Spectra of Two 1:1 Complexes between HCN and HF in Solid Argon at 12 K." J. Am. Chem. Soc., Vol. 105, p. 163, 1983.
- Knözinger, E., Kollhoff, H., Schrems, O., and Langel, W., "Intermolecular Interactions and Dynamics of Molecules and Clusters Isolated in Solid Argon and CCl<sub>4</sub> Matrices." J. Mol. Struct., Vol. 141, p. 399, 1986.
- Kozirovski, Y. and Folman, M., "Infra-red Spectrum and Spectral Shifts of HCN Adsorbed on Evaporated Alkali Halides." Trans. Faraday Soc., Vol. 62, p. 808, 1966.
- Kroes, G.-J., "Surface Melting of the (0001) Face of TIP4P Ice." Surface Science, Vol. 275, p. 365, 1992.
- Kroes, Geert-Jan and Clary, D. C., "Sticking of HCl and ClOH to Ice: A Computational Study." J. Phys. Chem., Vol. 96, p. 7079, 1995.

- Majewski, J., Margulis, L., Jacquemain, D., Leveiller, F., Böhm, C., Arad, T., Talmon, Y., Lahav, M., and Leiserowitz, "Electron Diffraction and Imaging of Uncompressed Monolayers of Amphiphilic Molecules on Vitreous and Hexagonal Ice." Science, Vol. 261, p. 899, 1993.
- Majewski, J., Popovitz-Biro, R., Kjaer, K., Als-Nielsen, J., Lahav, M., and Leiserowitz, L., "Toward a Determination of the Critical Size of Ice Nuclei. A Demonstration by Grazing Incidence X-ray Diffraction of Epitaxial Growth of Ice under the C<sub>31</sub>H<sub>64</sub>OH Alcohol Monolayer." J. Phys. Chem., Vol. 98, p. 4087, 1994.
- Maroncelli, M., Hopkins, G. A., Nibler, J. W., and Dyke, T. R., "Coherent Raman and Infrared Spectroscopy of HCN Complexes in Free Jet Expansions and in Equilibrium Samples." J. Chem. Phys., Vol. 83, p. 2129, 1985.
- Materer, N., Starke, U., Barbieri, A., Van Hove, M. A., Somorjai, G. A., Kroes, G. J., and Minot, C., "Molecular Structure of a Low-Temperature Ice Ih (0001) Crystal." J. Phys. Chem., Vol. 99, p. 6267, 1995.
- Matsumura, K., Lovas, F. J., and Suenram, R. D., "The Microwave spectrum and Structure of the H<sub>2</sub>O-SO<sub>2</sub> Complex." J. Chem. Phys., Vol. 91, p. 5887, 1989.
- Molina, M. J., Tso, Tai-Ly, Molina, L. T., and Wang, F. C-Y., "Antarctic Stratospheric Chemistry of Chlorine Nitrate, Hydrogen Chloride, and Ice: Release of Active Chlorine." Science, Vol. 238, p. 1253, 1987.
- Morokuma, K. and Muguruma, C., "Ab Initio Molecular Orbital Study of the Mechanism of the Gas Phase Reaction SO<sub>3</sub> + H<sub>2</sub>O: Importance of the Second Water Molecule." J. Am. Chem. Soc., Vol. 116, p. 10316, 1994.
- Pacansky, J., "The Infrared Spectrum of a Molecular Aggregate. The HCN Dimer Isolated in an Argon Matrix." J. Phys. Chem., Vol. 81, p. 2240, 1977.
- Packer, M. J. and Clary, D. C., "Interaction of HCl with Water Clusters: (H<sub>2</sub>O)<sub>n</sub>HCl, n = 1-3." J. Phys. Chem., Vol. 99, p. 14323, 1995.
- Phillips, J. A., Canagaratna, M., Goodfriend, H., and Leopold, K. R., "Microwave Detection of a Key Intermediate in the Formation of Atmospheric sulfuric Acid: The Structure of H<sub>2</sub>O-SO<sub>3</sub>." J. Phys. Chem., Vol. 99, p. 501, 1995.
- Popovitz-Biro, R., Wang, J. L., Majewski, J., Shavit, E., Leiserowitz, L., and Lahav, M., "Induced Freezing of Supercooled Water into Ice by Self-Assembled Crystalline Monolayers of Amphiphilic Alcohols at the Air-Water Interface." J. Am. Chem. Soc., Vol. 116, p. 1179, 1994.

- Reiner, T. and Arnold, F., "Laboratory Investigations of Gaseous Sulfuric Acid Formation via  $\text{SO}_3 + \text{H}_2\text{O} + \text{M} \rightarrow \text{H}_2\text{SO}_4 + \text{M}$ : Measurement of the Rate Constant and Product Identification." J. Chem. Phys., Vol. 101, p. 7399, 1994.
- Robertson, S. H. and Clary, D. C., "Solvation of Hydrogen Halides on the Surface of Ice." Faraday Discussion, Vol. 100, p. 309, 1995.
- Rowland, B., Kadagathur, N. S., Devlin, J. P., Buch, V., Feldman, T., and Wojcik, M. J., "Infrared Spectra of Ice Surfaces and Assignment of Surface-Localized Modes from Simulated Spectra of Cubic Ice." J. Chem. Phys., Vol. 102, p. 8328, 1995.
- Schriver, L., Carrere, D., Schriver, A., and Jaeger, K., "Matrix-isolation photolysis of  $\text{SO}_2$ ,  $\text{O}_3$ , and  $\text{H}_2\text{O}$ : Evidence for the  $\text{H}_2\text{O}:\text{SO}_3$  Complex." Chem. Phys. Lett., Vol. 181, p. 505, 1991.
- Schriver, A., Silvi, B., Maillard, D., and Perchard, J. P., "Structure of Water-Hydrochloric Acid Complexes in Argon and Nitrogen Matrices From Infrared Spectra." J. Phys. Chem., Vol. 81, p. 2095, 1977.
- Smart, R. St. C. and Sheppard, F. R. S., "Infrared Spectroscopic Studies of Adsorption on Alkali Halide Surfaces: I. HCl, HBr, and HI on Fluorides, Chlorides, Bromides, and Iodides." Proc. Roy. Soc. Lond. A, Vol. 320, p. 417, 1971.
- Torchet, G., Schwartz, P., Farges, J., de Feraudy, M. F., and Raoult, B., "Structure of Solid Water Clusters Formed in a Free Jet Expansion." J. Chem. Phys., Vol. 79, p. 6193, 1983.
- Tso, T.-L. and Lee, K. C., "Formation of Sulfuric Acid and Sulfur Trioxide/Water Complex from Photooxidation of Hydrogen Sulfide in  $\text{O}_2$  at 15 K." J. Phys. Chem., Vol. 88, p. 2776, 1984.
- Walsh, B., Barnes, A. J., Suzuki, S., and Orville-Thomas, W. J., "Studies of Intermolecular Interactions by Matrix Isolation Vibrational Spectroscopy and Normal Coordinate Analysis." J. Mol. Spec., Vol. 72, p. 44, 1978.
- Wofsy, S. C., Molina, M. J., Salawitch, L. E., and McElroy, M. B., "Interactions Between HCl,  $\text{NO}_x$ , and  $\text{H}_2\text{O}$  Ice in the Antarctic Stratosphere: Implications for Ozone." Journal of Geophysical Research, Vol. 93, p. 2442, 1988.
- Zhang, Q. and Buch, V., "Computational Study of Formation Dynamics and Structure of Amorphous Ice Condensates." J. Chem. Phys., Vol. 92, p. 5004, 1990.

## APPENDIX A

### THE SUBSURFACE

This section has had contributions from several people, including: Dr. Devlin, Brad Rowland, Nevin Uras, and myself. It is included here in order to complete the description of what happens when a strong hydrogen-bonding adsorbate adsorbs to the ice surface.

Ice clusters are composed of three regions: the surface, the subsurface, and the interior. The spectrum of the interior is easy enough to see, for it is the dominating spectrum of the annealed cluster deposit itself (the surface and subsurface have only a minimal contribution). The surface is also fairly easy to identify from the band shifts which follow from the addition of most any weak adsorbate to a cluster deposit. This leaves only the subsurface left to be characterized.

The subsurface is the transition region that connects the surface to the interior of the cluster, so it should have a spectrum which has a band shape somewhere in between that of the surface and the interior. The difficulty in obtaining its spectrum is that a simple subtraction factor of one, which has been used for both the weak and strong adsorbates in order to see the changes which have occurred in their difference spectra upon their adsorption, will no longer be valid to use. This is because, up to this point, we have only been looking at the net composite of the changes which have been occurring, but now we are actually trying to obtain the actual spectra of one of the components (the subsurface) without any contribution from either the surface or interior of the ice cluster. In the method to be used to identify the subsurface spectrum, the surface of the ice

clusters will remain invariant and the subsurface will be converted into interior ice. This newly created interior ice then has to be subtracted out in order to reveal the composite subsurface spectrum. A more detailed description follows.

A cluster deposit is made and then highly annealed. HCN is then deposited onto this annealed cluster surface and a spectrum obtained. This HCN coated cluster is then annealed, but to a temperature less than that to which the clusters were originally annealed. Thus, any changes which occur are due to annealing of the cluster in the presence of the HCN on the surface and not the thermal annealing of the clusters themselves. After the HCN coated clusters have been annealed, a second spectrum is obtained. The difference between these two HCN coated spectra is then obtained using a subtraction factor of one (see Fig. 72b). This shows the loss of the subsurface and the formation of new interior ice (relaxation of the subsurface to interior). No surface is involved since it has been preshifted by the original HCN coating and is stable during the annealing phase. If we now subtract out the newly formed interior ice using the spectrum for the annealed cluster deposit, we can obtain a spectrum for the subsurface of the clusters (see Fig. 72c). This is the spectrum for the subsurface lost during annealing in the presence of HCN on the cluster surface.

Similar spectra can also be obtained for SO<sub>2</sub> adsorbed on the cluster surface. However, in this case, annealing the clusters after the adsorbate have been adsorbed is not necessary. Instead, a spectrum is obtain immediately after adsorption of the adsorbate and then a second spectrum is obtained a few hours later. Then a similar procedure is followed just as was done for the HCN coated clusters to monitor the subsurface relaxation to interior ice.

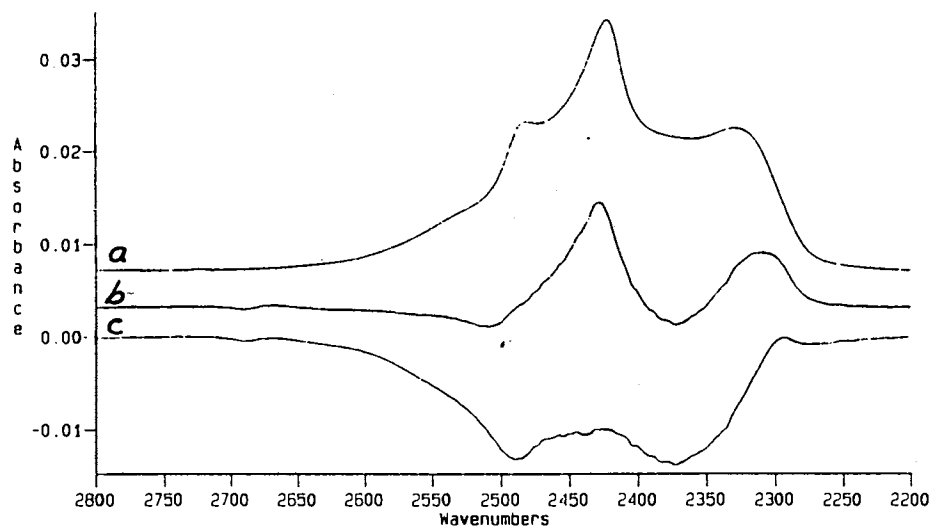


Fig. 72 Spectra of a) a crystalline nanocluster deposit, b) the difference between the annealed and unannealed HCN coated clusters, and c) spectrum b) with the newly formed interior ice subtracted out revealing the subsurface spectrum



In order to check whether these similar spectra were indeed the spectra of the subsurface, a second separate approach to obtaining the spectrum of the subsurface spectrum was needed. To do this, a cluster deposit was made and a spectrum obtained. The deposit was then annealed and a second spectrum obtained. If a difference spectrum is obtained between the annealed and unannealed clusters (see Fig. 73c), what is seen is the loss of the surface and subsurface and the formation of interior ice due to the increase in the average cluster size due to annealing. Now, if we once again subtract out the newly formed interior ice, we obtain a difference spectrum showing the surface and subsurface modes (see Fig. 73b). If we use the difference spectrum for a weak adsorbate, we can identify the bands which are due to surface features. We can then compare the subsurface spectrum obtained from the adsorption of an adsorbate onto the cluster surface with that obtained by annealing the cluster deposit (after mentally subtracting out the surface features with the aid of the weak adsorbate difference spectrum), and what is seen is very similar (see Fig. 74).

The next question is, how many bilayers thick is the subsurface. Again, the subsurface is determined by its spectroscopic band structure and not by any actual structure whether crystalline or amorphous. According to the work by Torchet *et al.* the surface and subsurface is between 8 and 13 Å (2 to 3.5 bilayers) thick. If we assume sort of an average and say that the surface and subsurface is 10 Å thick and then apply this to our clusters (20 nm diameter), we would find that ~30 % of our water molecules were in the surface and subsurface. If we compare this to our experimental data, we find that it is in very good agreement.

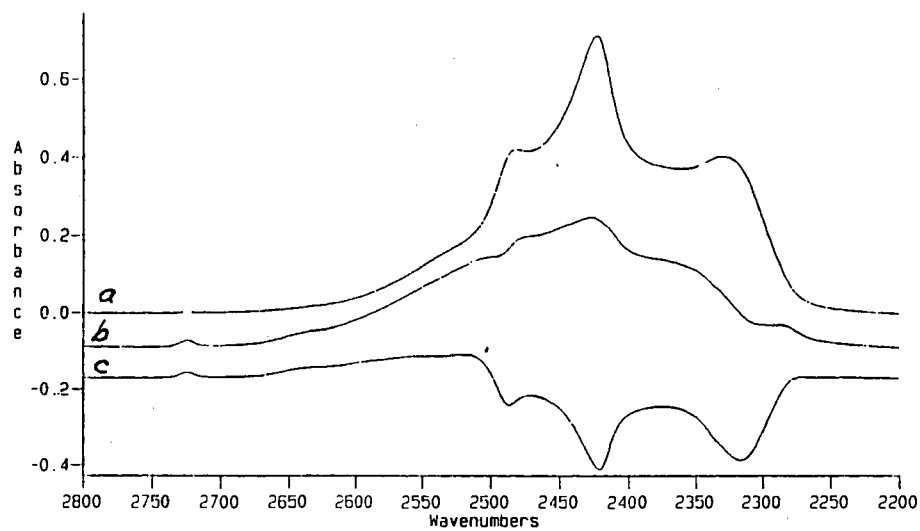


Fig. 73 Spectra of a) a crystalline nanocluster deposit, b) spectrum c) with the newly formed interior ice added back in, showing the composite surface and subsurface, and c) the difference between the annealed and unannealed clusters

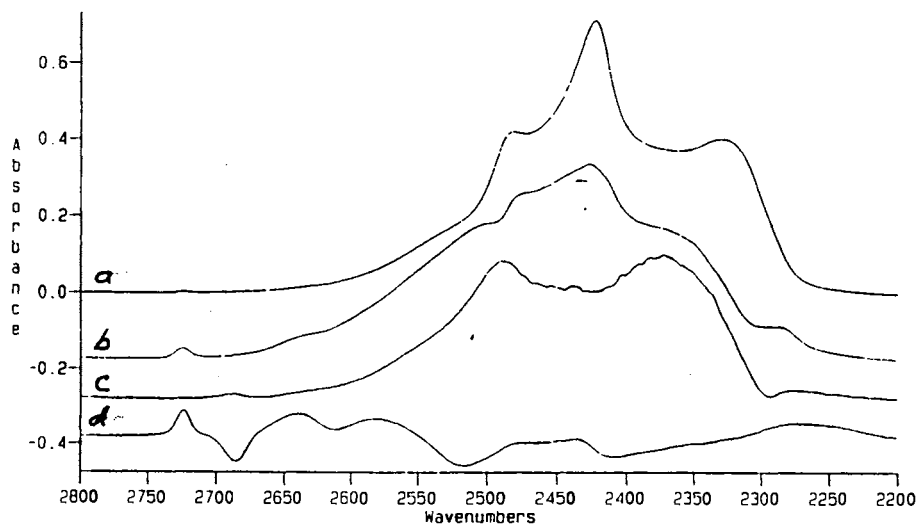


Fig. 74 Spectra of a) a crystalline nanocluster deposit, b) the composite of the surface and subsurface obtained from the difference between annealed and unannealed clusters, c) the subsurface obtained from the difference between the annealed and unannealed HCN coated clusters, and d) a weak hydrogen-bonding adsorbate.

The experimental value was determined by correcting the amount of interior which was added to eliminate the newly formed interior, obtained from Ostwald ripening, by the percentage of the cluster surface that was eliminated, as determined by the lost intensity of the d-H band. This assumes that when the surface is annealed, the population density of the d-H on the surface remains constant. The actual validity of this assumption is not known, although, no better assumption is possible at this time. Therefore, if 50% of the surface is eliminated by annealing the clusters, and 15% of the cluster deposit needs to be added back in order to eliminate the newly formed interior, then this means that 30% of the molecules belong to the surface and subsurface and is consistent with ~20 nm diameter clusters having 2 - 3 bilayers of surface and subsurface molecules.

2

VITA

Lance Delzeit

Candidate for the degree of

Doctor of Philosophy

Thesis: THE INTERACTION OF STRONG HYDROGEN-BONDING  
MOLECULES WITH THE SURFACE OF ICE NANOCRYSTALS

Major Field: Chemistry

Biographical:

Personal Data: Born in Oakley, Kansas, on August 14, 1968, the son of  
Clem and Ann Delzeit.

Education: Graduated salutatorian from Dodge City Senior High, Dodge City  
Kansas; received Bachelor of Science degree in Chemistry and a Bachelor  
of Science degree in Applied Mathematics from St. Mary of the Plains  
College, Dodge City, Kansas in May 1991. Completed the requirements  
for the Doctor of Philosophy degree with a major in Chemistry at  
Oklahoma State University in May 1997.

Memberships: Phi Lambda Upsilon